STERILE FILTRATION OF THERAPEUTIC VIRUS SURROGATES

THE USE OF FLUORESCENTLY LABELED NANOPARTICLES AS THERAPEUTIC VIRUS SURROGATES IN STERILE FILTRATION STUDIES

By

MOHAMMADREZA PAZOUKI, B.Sc.

A Thesis Submitted to the School of Graduate Studies in
Partial Fulfilment of the Requirements for the Degree
Master of Applied Science

MASTER OF APPLIED SCIENCE (2018) McMaster University

(Chemical Engineering) Hamilton, Ontario

TITLE: The use of fluorescently labeled nanoparticles as therapeutic virus surrogates in sterile filtration studies

AUTHOR: Mohammadreza Pazouki, B. Sc. (University of Tehran)

SUPERVISOR: Dr. David R. Latulippe

NUMBER OF PAGES: xvii, 120

Lay Abstract

Nanoparticles (NPs) has been employed enormously in various applications for a variety of purposes. One of the areas that have been greatly influenced by NPs, is the field of separation science. In the pharmaceutical industry, purification of therapeutics involves a sequence of filtration and in this step, therapeutic virus filtration, sterile filtration, in particular, have been poorly studied. There is also a growing interest in the use of engineered viruses for cancer treatment due to its magnificent implication on human health. However, there are significant challenges in running filtration experiments with pathogenic substances. Therefore it has been determined that a detailed and comprehensive study of sterile filtration of virus-size NPs can benefit this area. In this work, fluorescently-labeled NPs has been used as surrogates of oncolytic viruses to extract fundamental aspects affecting the transmission of virus-sized particles through commercial microfiltration sterilizing grade membranes.

Abstract

Nanoparticles (NPs) have attracted considerable attention in the field of separation science, especially in filtration studies for direct membrane integrity tests, investigating pore-size distribution, and their potential to be used as surrogates for various types of viruses encountered in water treatment and bioprocessing applications. Although the effect of adding surfactants to stabilize NP suspension have been explored for a number of different applications, there is significant variation in the amounts and types of surfactants used in filtration studies. This study used three different sizes (59, 188, and 490 nm) of fluorescent polystyrene nanoparticles (PNPs) to mimic the length, width, and aggregates of Rhabdovirus Maraba, a bullet-shape envelope virus. The PNPs were suspended in solutions with varying concentrations of the nonionic surfactant Tween 20 (0.0005% to 0.1% (v/v) in the carbonate buffer feed solution) and were tested in constant-flux filtration studies using two commercial microfiltration (MF) membranes (Durapore PVDF and MiniSart PES) with 0.22 micron pore size ratings. Results clearly demonstrate that adding a nonionic surfactant to a PNP solution will cause a shift from full retention to complete transmission during the dead-end MF of PNPs that are smaller than the pore size of an MF membrane. In a separate study, in order to have a better resemblance of virus particles in terms of surface properties, 188 nm PNPs were coated with different (lysozyme, α -lactalbumin and bovine serum albumin) proteins in order to gain similar surface properties to actual virus particles. Filtration results with one type of commercial MF membranes (Durapore PVDF) 0.22 μm pore size, clearly indicate that the transmission behavior of PNPs strongly depends on their surface properties. PNPs fully covered with BSA and α–lactalbumin could completely pass through the membranes while uncovered or partially covered PNPs resulted in no transmission or partial transmission.

Acknowledgments

I would like to express my sincere appreciation to my supervisor, Dr. David Latulippe, for his constant support, guidance, patience, and encouragement throughout my study. I am truly honored and humbled by the chance that David gave me to pursue graduate studies at McMaster University. It was a great privilege for me to work and complete this project under his supervision and share of his scientific knowledge. David's continuous support and advice in this path not just helped me to complete this project and overcome different challenges but also assisted me to employ that guidance in my personal life which all turns to a life-changing experience for me in these two years. I'm thankful for everything.

I would like to thank Dr. Robert Pelton for his valuable guidance and fruitful discussions in the course of my project. I would like to thank my course instructors, Dr. Robert Pelton, Dr. Raja Ghosh, Dr. Tohid Didar and Dr. Zeinab Hosseini-Doust for their help and directions. I would like to extend my thanks to Dr. Philip Wood, which I had the great honor to be his assistant in his teaching course one year before his retirement.

I owe many thanks to my lab mates and friends through my study which I would like to mention everyone's name here; Indranil Sarkar, Karina Kawka, Amir Kazemi, Ryan LaRue, Evan Wright, Patrick Morkus, Shabnam Shoaebargh, Salman Alizadeh, Kurt Westhaver and special thanks to Kimia Aghasadeghi. I would like to thank undergraduate students, Noelle Wilton and Jillian Ma for their help, friendship, and patient in the completion of this project. All of the experiments and testing in this project would not have been possible without their help in our lab.

From the Department of Chemical Engineering, I would like to acknowledge all the administrative staff, especially Michelle Whalen, Linda Ellis and Kristina Trollip for their sincere

dedication and help from the very first day I applied to pursue graduate studies at McMaster University until now. I would like to thank Paul Gatt for his extraordinary expertise in fabricating and manufacturing the experimental setups in my research project that would have been difficult without his involvement. I am especially grateful to Marcia Reid from the Electron Microscopy Facility at the Department of Health Sciences and Travis Casagrande from the Canadian Centre for Electron Microscopy (CCEM) for their assistance. I would also like to thank Mark Mackenzie and John Colenbrander from the Department of Mechanical Engineering for their valuable advice, guidance, and assistance in building the automated sampling system. I would like to thank Jessica Kun from the Department of Biomedical Engineering for her valuable assistance over confocal laser scanning microscopy.

I would also like to thank my friends and housemates, Hossein Mohammadi and Amin Halali for their friendship, support, help and valuable advice in these years. They have been always by my side as my own brothers.

I am indebted to my parents, Vida and Mohammad and my dear sister and her wife, Hunaz and Sepehr for their immeasurable and unconditional love and care. They have always been beside me throughout my study and supported my every choice. The completion of this project and bigger projects in life would not have been and will not be possible without their support, help, and love.

To my love, the most important thing in my life, Elmira. Thank you for your patience in these years. I have been loved so much by you that I would say without this love I couldn't have taken even one step forward. Thank you for accompanying me on this pathway. I saw the lovely bright future with you and from now on the future is ours.

"Let yourself be silently drawn by the stronger pull of what you really love" - **Rumi**

Table of Contents

List of Figures

Chapter 1

Chapter 2

Chapter 3

Appendix B

List of Tables

List of Acronyms

BSA……..……..Bovine serum albumin

CLSM……..……..…Confocal laser scanning microscopy

DLS…….……..…….Dynamic light scattering

FDA…..…….……...……Food and Drug Administration

GMP……...……Good Manufacturing Practice

GNP……...…….……...Gold nanoparticle

HTAF…….….High throughput automated filtration

MF……..……Microfiltration

NF…….....Nanofiltration

NP……..……Nanoparticle

OV……...……..Oncolytic virus

PBS……...Phosphate-buffered saline

PEEK……..Polyether ether ketone

PES……..…….Polyethersulfone

PNP…….……..……..Polystyrene nanoparticle

PSD…….…….Pore size distribution

PVDF……..……...…..…….Polyvinylidene fluoride

SEM……...…..…..Scanning electron microscopy

SDS……..Sodium dodecyl sulfate

TMP……..…….Transmembrane pressure

UF……...….Ultrafiltration

VF…….……..Virus filtration

Chapter 1: Nanoparticles as therapeutic virus surrogates

1.1. Introduction to nanoparticles

In the field of nanotechnology, solid colloidal particles or structures of any shape with dimensions in the 1 to 100 nm range that behave as a whole unit in terms of transport and properties are considered as nanoparticles (NP) [1]. Although the first use of nano-sized materials is not clearly known, some discoveries have shown that in the fourth-century A.D. Roman glassmakers were fabricating glasses that nano-sized metals were used in their structure [2]. However, some of the remarkable properties of nano-sized materials were not discovered until the eighteenth and nineteenth centuries when Michael Faraday provided a scientific description of the optical properties of metals in the nanometer-scale [3]. The development of photography industry is indebted to the efforts that scientists have put, back in early days in order to produce silver NPs sensitive to light. Photographic film is a transparent plastic film that is coated with an emulsion containing light-sensitive silver halide crystals in the order of nanometers.

Since "Nanotechnology" was presented by Richard P. Feynman, the Nobel laureate in 1959 [4], significant developments have been made in the field of nanoscience. Synthesizing NPs from a variety of materials (e.g. silica, gold, and silver, polystyrene) with different functionalities (e.g. fluorescently labeled, magnetic properties) and various surface functional groups (e.g. carboxyl, amine, and amide), are just a short list of numerous developments in the field to nanotechnology and colloidal science. These outstanding developments have offered many technologies the opportunity to employ NPs in different experimental studies for a variety of purposes. Moreover, recent progress in the fabrication of NPs has given the possibility to precisely control the reaction

processes in order to produce the desired NP in terms of size and shape (e.g. spherical, rod-shaped, triangular) [5,6]. Figure 1.1 shows a summary of different NPs that have been fabricated in a variety of size ranges, surface properties, shapes, and materials. The use of NPs has been attracted considerable interest in various applications in the past few decades due to their numerous outstanding properties stemming by its nature or engineered and designed with special properties. Physicochemical properties such as larger surface area, chemically reactive and optically active, make NPs a unique and suitable candidate for different applications [8]. NPs have been used in biomedical applications [7–9], manufacturing and material [10,11], environment [12–14], electronics [15–17], energy harvesting [18–20] and separation sciences [21–23].

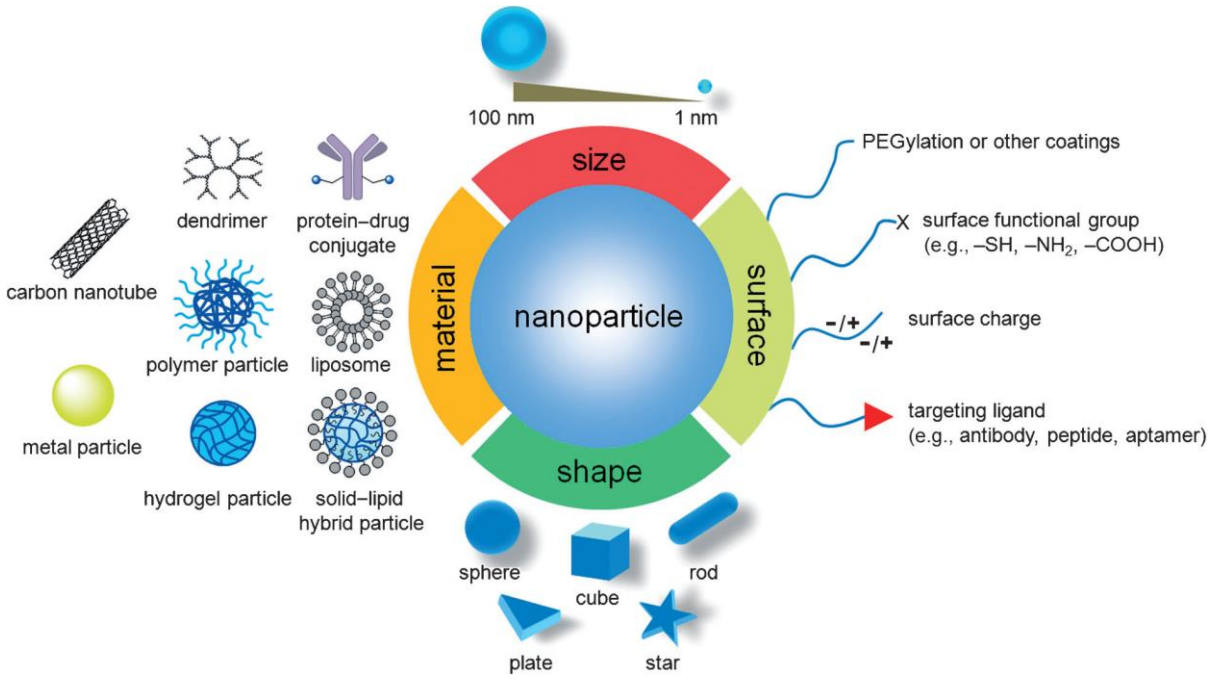

Figure 1.1 A summary of different NPs that have been explored and fabricated in terms of size, surface properties, shape and material (reprinted from [24]).

In recent years the manipulation of materials in the nano-scale and utilization of unique properties of NPs have been the main part of research and studies in the field of renewable energies.

For instance, titanium dioxide based nanomaterials have been proven to be a potential candidate for several applications including photo-catalysis in order to enhance the efficiency of solar cell devices [25–28]. Carbon nanotubes are another important example of nano-scale materials that are being used in a huge number of applications in nanotechnology, material science, electronics and environmental studies due to their extraordinary mechanical, electrical and thermal properties. NPs has also been used enormously in drug delivery studies and to date, a large number of NP-based products have been manufactured by the pharmaceutical industry and approved by regulatory agencies to be used for diagnostic or therapeutic purposes [29]. For example, the Food and Drug Administration (FDA) has nowadays commercialized new macromolecular drug-delivery formulations such as albumin-bound paclitaxel nanoparticles (ABI-007) and Doxil® in the market for cancer therapy [30–32]. Figure 1.2 shows other applications that NPs are currently being used for various reasons.

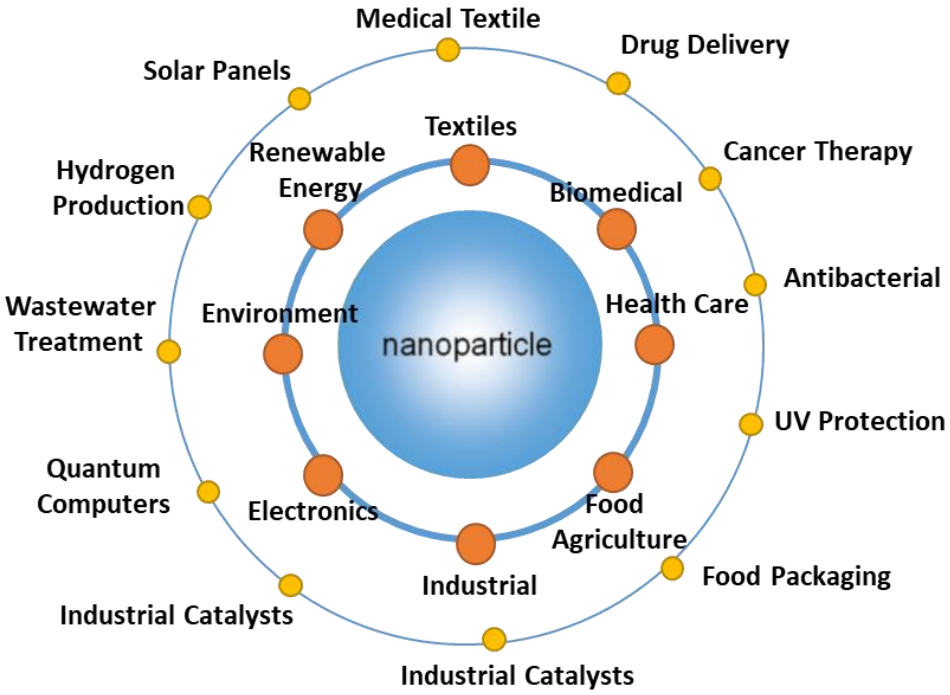

Figure 1.2 Applications that NPs are currently being used (adapted from [33]).

1.2. NPs in separation science

One of the areas that have been significantly influenced by NPs, is the separation science which will be discussed profoundly in this thesis. NPs has attracted widespread interest and has been used with great success in the entire field of separation sciences for a variety of reasons in order to benefit from their extraordinary physicochemical properties. However, there are three common motivations to employ NPs in separation studies which cover the majority of researches and published works in this field.

First, NPs have been used in many studies in order to increase the efficiency or enhancing the properties of current separation techniques. As mentioned earlier, NPs have a large surface area, meaning that the percentage of their surface in relation to the volume is significant. This is the most important characteristic of materials in the nano-scale range which makes NPs suitable to employ for specific separation techniques. The large surface area of NPs gives the opportunity to use them as an excellent nano-adsorbent for separation of desired compounds from the bulk in different applications. For example in the field of water/wastewater treatment, the use of magnetic oxide and carbon-based nano-adsorbents are considered as a cost-effective approach for rapid removal and recovery of metal ions from wastewater with the aid of magnetic field [34–37]. NPs are also being used in many studies related to desalination processes and manufacturing of novel membranes [38–40]. For instance, Lee et al. [41] have fabricated a polyamide (in forms of NPs) thin-film nanofiltration (NF) membrane which contains high loading of titanium dioxide NPs via in-situ interfacial polymerization. The advantage of such membranes is that the photocatalysis properties of the titanium dioxide can decompose organic compounds during filtration processes which possibly overcome the quick fouling and replacement of membranes. These were few

examples among numerous applications that NPs has been used directly as a novel separation technique and performance enhancement of current separation processes.

Second, many studies also used NPs in order to perform membrane integrity tests to gain more insights on the performance of the existed commercial and non-commercial membranes. Among different separation processes, the separation of particles in the size range of nano (1-100 nm) and micro (0.1-100 μm) from a liquid stream using membranes/filters has been exceptionally studied in many separation processes, particularly bioprocessing in pharmaceutical and environmental studies. NPs not only been used in establishing novel separation processes and enhancement of conventional separation techniques but also used as model solutes for performance evaluation of various separation processes such as, chromatography [42–44], sand filtration [45], and membrane-based separation technologies, including microfiltration (MF) [46–53], ultrafiltration (UF) [49,54–58], virus filtration (VF) [59–64], NF [65], and reverse osmosis (RO) [65,66]. Some studies have used NPs to estimate membrane's/size-exclusion chromatography column's pore-size distribution or performance evaluation of separation systems [42,43,46,55,61,64]. Many other studies have used NPs during filtration experiments to produce a mathematical model of solute transport through MF and UF membranes [67,68]. These applications will be discussed profoundly throughout this thesis.

However, among different motivations of using NPs in separation studies, the third common and interesting motivation is their potential to be used as surrogates for various types of biological substances especially pathogenic agents such as viruses and bacteria. The current thesis will focus on this motivation through the entire next three chapters. Surrogates are defined as organisms, particles, or substances that are used to study the fate of a pathogenic substance in a particular environment [69]. The interest in using NPs as surrogates of pathogenic biological

agents, viruses, in particular, is motivated by the significant challenges of working with actual pathogenic substances. One of the most critical challenges associated with working with biological solutions, especially pathogenic to human, is the hazard analysis and risk reduction which must be considered for each experiment. Generally, the risk assessment of pathogenic substances are significantly different from the chemical risk assessment, thus every stage of pathogenic substance-based (e.g. virus-based) experimental research should carry on with tremendous safety procedures in the designated level of biosafety laboratory (e.g. level two or higher). Biosafety facilities are needed in order to run the assays that are used to quantify the concentration of pathogenic biological substances; furthermore, these assays are more complicated and time-consuming than non-biological assays. For example, the 50% tissue culture infective dose (i.e. $TCID_{50}$) procedure—which is used to quantify the amount of an infectious virus in a preparation—requires replicate cultures of serial dilutions of each sample and typically takes 3 to 7 days to complete (with the actual time determined by the cell line and virus type). Moreover, the need for dedicated facilities and specially trained technicians make the entire process expensive and challenging to produce even the small amounts of feed material usually required for lab-scale studies. At last but not least many of the biological assays use expensive materials and in some cases materials are rarely available. Thus, due to the ease of working with nonpathogenic substances and also the simplicity of detecting assays, scientists have moved to use different surrogates such as bacteriophages (i.e. non-pathogenic to human) virus-like particles along NPs as human virus surrogates in their study for preliminary stage of research and evaluation of different applications. A brief description of two of the most used separation techniques in the field of separation science, chromatography and membrane filtration, which surrogates have been

employed enormously with the motivations mentioned above will be discussed in the next two sections.

1.2.1. Chromatography systems

Chromatography is a separation technique based on the interaction of a mobile phase (the fluid contain a mixture of dissolved materials) and a stationary phase (the solid structure which mobile phase passes through). Essentially the principle of separation can be categorized based on four different characteristics of substances, size, charge, hydrophobic and affinity. The majority of the current chromatography techniques such as ion-exchange, size exclusion, and reversed-phase are established based on these characteristics. Chromatography has been used as an analytical tool to a great extent for various applications for detecting the presence or measuring the relative proportion of analytes in a complex mixture. The chromatography-based separation process is widely used as a preparative technique for separation of biological solutions in pharmaceutical, diagnostic, and biotechnology industries and thus is a form of purification of different therapeutic products [70].

There is a great interest in the exploitation of NPs in chromatography systems in order to increase the efficiency of separation of specific substances by engineering the surface structure of NPs. NPs are also being used directly as a probe in order to evaluate the performance of different chromatography columns in many different fields. For example, gold nanoparticles (GNPs) were used in many studies to appraise the separation performance of chromatography systems. In a study conducted by Liu et al. [43] the effect of mobile-phase additives on separation of GNPs were examined by a nucleosil column size-exclusion chromatography. In the field of environmental science, Tiede et al. [71] investigate the fate, behavior, and occurrence of engineered NPs in the natural environment using chromatography systems. In their study, they successfully demonstrated

the applicability of using a hydrodynamic chromatography coupled to plasma mass spectrometry to size and elementally characterize silver NPs in highly complex liquid matrices natural resources.

Recent advances in drug delivery, nanomedicine and pharmaceutical applications is indebted to exceptional characteristics of NPs. As mentioned earlier currently numerous NP-based therapeutics are being manufactured by the pharmaceutical industry. In order for these products to be approved by regulatory agencies (e.g. FDA) they must conform to good manufacturing practice (GMP) guidelines enforced by these agencies. Therefore, reaching a pure final product where the products may cause health risks to the users is crucial in these types of applications [72–75]. Currently, existing downstream processes in pharmaceutical applications use a combination of chromatography and membrane base purification in order to remove process-related and product-related impurities [76,77] from different product manufacturing lines. Itoh et al. [78] developed a fast and simple method for evaluation of the number of drugs encapsulated in NPs by high-performance liquid chromatography in a monolithic silica column. There were also studies that have used NPs as a probe to study the transmission of virus-sized particles (i.e. virus surrogates) through chromatography columns. For instance, Iyer et al. [44] established a method for flow-through purification of viruses and NPs using a combination of binding and size-exclusion chromatography. In this study, bovine serum albumin (BSA) coated latex NPs were used as a model of influenza virus and herpes simplex virus.

1.2.2. Membrane filtration studies

Membrane filtration is another separation technique that has been incorporated into many bioprocessing and environmental applications. Generally, in the pharmaceutical industry (for production of therapeutics/biotherapeutics) and environmental applications (for water/wastewater treatment), filtration is a preferable separation technology in many of the downstream processes,

due to the simplicity of the equipment and operations. Filtration processes are more utilized in the pharmaceutical industry due to the limitations associated with processing biological agents and active pharmaceutical ingredients. Many of the therapeutic/biotherapeutic products are sensitive to other means of separation techniques and can be destructed during harsh separation processes (e.g. heating, distillation, chemical separation). Moreover, membrane separation processes also offer many advantages in bio-processing since they are highly selective operations. Another most important advantages of membrane-based separation technologies are their ability to be readily scaled up at any stage of process development [79].

Membrane filtration processes can be classified based on their pore size and driving force (Figure 1.3). Pressure-driven processes for liquid separation includes MF, UF, NF and RO. Moreover, two different modes of operation, dead-end, and cross-flow filtration (see Figure 1.4), can be used for membrane filtration processes. The dead-end filtration process is the most widely used filtration process, which the flow is forced through the membrane. However, in cross-flow filtration, the solution passes across the surface of the filter producing parallel streams, the filtrate, and the concentrated feed solution. It is noteworthy to mention that membrane filtration in the cross-flow operation provides a much longer membrane lifetime and higher permeation rate, however, it requires more complex equipment [80].

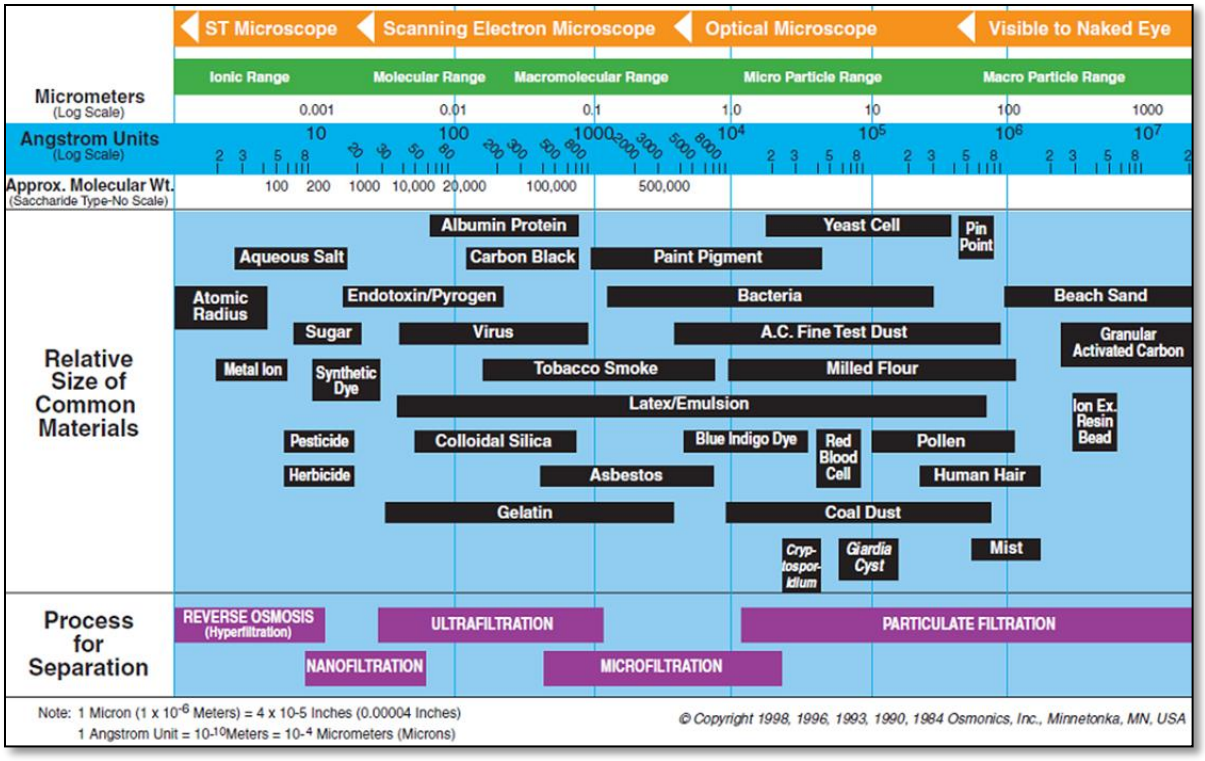

Figure 1.3 Filtration spectrum of different types of filtration processes relative to the pore size of the common material (reprinted from [81]).

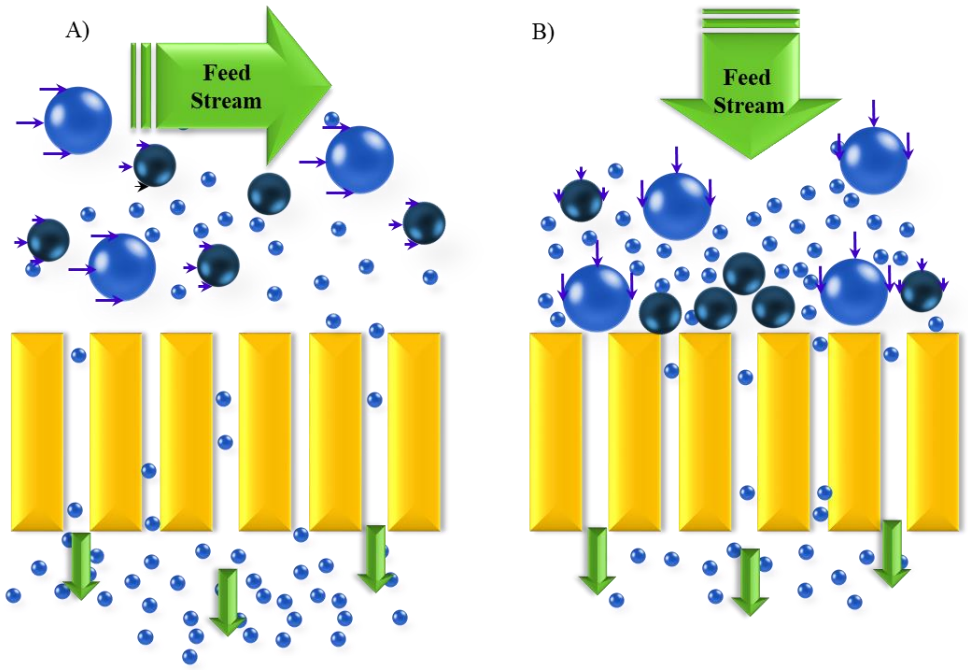

Figure 1.4 Modes of operation in membrane filtration processes. Panel (A): cross-flow filtration; Panel (B): dead-end filtration.

Like chromatography systems, NPs have been vastly been used in membrane filtration studies to directly enhance the performance or properties of membranes or as a tool to gain insights on the transmission of solute through membrane's internal structure. In the last decade, several studies introduced the use of NPs for membrane integrity monitoring. Some studies have used NPs as model solutes to estimate membrane's pore-size distribution. Many other studies have developed a mathematical model of solute transport through membranes. The broadness of the use of NPs in membrane filtration researches has also extended into many separation processes, where NPs has been employed as surrogates to mimic the filtration of actual virus contained solution for different applications. The next three subsections are dedicated to a brief description of MF, UF and VF processes and examples on how utilization of NPs has provided comprehensive insights on the transmission of solute during filtration processes.

1.2.2.1. Microfiltration

Microfiltration (MF) is a physical separation process in order to separate particles with diameter between 0.1 and 10 μm within their structure in various applications. The current status of MF membranes is indebted to the development of nitrocellulose membranes in the 1920s and 1930s and the successful usage of these membranes during World War II as a rapid method to control the water supply for any contamination [80,82]. After this period, many manufacturing companies (e.g. Millipore and Sartorius) started to produce different polymeric phase inversion membranes (e.g. polyvinylidene fluoride) with different pore size for a variety of applications, including wastewater treatment plants and bioprocessing applications. One of the main application of the MF membranes is in the pharmaceutical industry, where the injectable drug solutions need to be sterilized by sterilizing grade MF membranes (with 0.22 μm pore size) in the manufacturing processes which is the main focus of this thesis. In filtration processes, sterility can be achieved

by using MF membrane with a rated pore size of 0.2 μm (or smaller) that has been validated for the removal of a challenge microorganism, *Brevundimonas diminuta (B. diminuta)* [83].

As mentioned earlier, filtration of NPs has been widely used for the entire spectrum of membrane-based separation processes, including MF, for numerous reasons. In a study conducted by Bondy and Santeufemio [84], latex microsphere (a mixture of 0.24, 0.3, 0.35, 0.4 and 0.5 μm in size) were used in filtration of MF membranes with nominal ratings of 0.4 and 0.8 μm separately and in combination with sterilizing grade membranes (nominally 0.2 μm). The motivation of this study was to better understand, how biological fluids, especially those that have a high load of submicron particles (e.g. cell debris and agglomerated proteins) foul membrane filters in downstream processes. Grant and Liu [47], investigated the particle removal efficiency of 0.45μm Polyvinylidene fluoride (PVDF) microporous membrane filtration using twelve different sizes of microspheres ranging from 0.337to 0.741μm made from various materials (e.g. carboxylate modified latex, polystyrene latex, polyvinyl toluene). Later results from the filtration experiments were used in order to develop a mathematical model to predict particle capture as a function of particle diameter, filter thickness, and filter loading.

1.2.2.2. Ultrafiltration

Ultrafiltration (UF) is another type of membrane-based separation process which forces like pressure or concentration gradient will cause the particles to separate from the fluid stream. UF membrane pore size can vary from 10 to 100 nm depending on the type of application. Like MF membranes, UF membranes also has its modern origin from the development of nitrocellulose membranes but no industrial application existed until the 1960s, where Abcor (now a division of Koch Industries) used tubular membrane modules, to recover electrocoat paint from paint shop rinse water at an automobile assembly plant [80,82]. This separation process in industry and

research studies is mainly being used for purification of macromolecules with the size range of 10^3 to 10^6 Da. UF membranes are also being used extensively in a huge number of applications such as pulp and paper industry, waste water treatment and pharmaceutical industry.

Similar to MF processes, NPs have also been used in the UF studies in order to characterize and evaluate the performance of the UF membranes. For instance, Duek et al. [55] proposed a new, simple and effective method for UF pore size determination using aquasols of gold and silver NPs in the size range of 3 to 50 nm. Abdelrasoul et al. [85] investigated the influence of aggregation of particles on membrane fouling and UF performance of latex contaminated water/wastewater. In another earlier study by the same group, a mathematical model was developed by UF of latex paint solution in order to precisely predict the increase in transmembrane pressure (TMP) and the mass of fouling retained by the homogeneous and heterogeneous membrane. Interestingly, this mathematical model could accurately estimate the TMP of the experimental value within 5–8% error [86]. In a study conducted by Pontius et al. [49], the filtration performance of hydrophobic and hydrophilic properties of PVDF MF and UF membranes were challenged using 26 and 67 nm fluorescent latex microspheres as surrogates of bacteriophages. Later two different bacteriophages (i.e. MS2 and PRD1) were also used in filtration processes in order to compare the transmission results of biological and non-biological solutes.

1.2.2.3. Virus filtration

Although virus filtration (VF) is not included in the filtration spectrum as a separate type of membrane filtration process (i.e. MF, UF and NF), it is a well-known process in industry and research studies which is used as virus clearance operation in the purification processes of biopharmaceuticals [87,88] and water treatment [89,90]. Due to the importance of this separation process in these applications, it has been accepted as a common terminology to refer to membranes

used for virus capturing as VF membranes. VF membranes pore size range falls between the two common types of filtration membranes, UF, and NF (see Figure 1.3). Therefore, the categorization of the type of the membrane (UF or NF) used for virus filtration is basically dependent on the type and size of the virus that needs to be captured/retained by the membrane. The first commercial VFs were produced by membrane manufacturers to capture larger viruses with diameters larger than 50 nm using UF membranes, however, nowadays VFs have to ensure efficient and robust virus removal of small viruses like parvoviruses by using NF membranes.

NPs have also been employed in VF processes for the same reasons outlined in section 1.2. Kitis et al. [65] used fluorescent-dye polystyrene microspheres with the size of 24 nm in order to investigate the integrity of NF membranes. This study was conducted in order to study the performance of NF membranes in the removal of virus-sized particles to meet microbial and disinfection by-product regulation in certain applications. Kosiol et al. [61] used virus-size GNPs with nominal diameters ranging from 5 to 50 nm in order to determine pore size distributions (PSDs) for a wide range of different commercial and non-commercial parvovirus retentive membranes in terms of their internal structure, material and surface chemistry. Within their study, they have shown that the presence of certain chemicals (i.e. surfactants) can totally change the mechanisms of retention from adsorption to a size exclusion mechanism. In another study, Roberts et al. [59] used GNPs (18-25 nm) to ensure the effectiveness of removal of various sizes of enveloped and non-enveloped viruses by Kasei Planova 15N (pore size 15 ± 2 nm) filters that the manufacturer of factor IX (i.e. coagulating protein) concentrate REPLENINE®-VF (i.e. a medicine for treatment and prophylaxis of bleeding in patients with hemophilia B) has developed.

1.3. Research motivation – Sterile filtration of NPs as virus surrogates

There is considerable interest in the development of virus-based therapeutics for various diseases related to neurological, metabolic disorders and the development of oncolytic viruses (OVs), an advanced approach to cancer treatment based on targeted lysis of cancer cells and the stimulation of an anti-tumor immune system [76]. The first OV-based therapy for the local treatment of melanoma lesions was approved in 2015 by the FDA [91]. In 2016 approximately 40 clinical trials in different phases of developments existed and the number is increasing each year [92] for using engineered therapeutic viruses individually or in combination with other therapeutic viruses and cancer therapies [93–95]. Table 1.1 shows a summary of different types of OVs and their clinical phase for curing different types of cancers.

Table 1.1 Summary of clinical trials of OV therapy for cancer treatment.

Virus	Virus Type	Clinical Phase	Tumor type	Reference
MG1 (Maraba)	Rhabdovirus	I	Lung cancer	Zhang et al. [96]
Psostvac	Vaccinia Virus	I and II	Castration-resistant prostate cancer	Singh et al. [97]
Pelareorep (REOLYSIN)	Reovirus	II	T2 prostate cancer	Stoeckel and Hay [98]
Pexa-Vec (pexastimogene devacirepvec)	Vaccinia virus	II	Metastatic, refractory renal cell carcinoma	Kim et al.[99]
Sorafenib	Vaccinia Virus	III	Hepatocellular carcinoma	Lawler et al. [92]
Talimogene laherparepvec	Herpesvirus	III	Advanced melanoma	Andtbacka et al. [100]

The growing interest in virus-based therapeutics, OVs in particular, has developed a concomitant need for research on the development of large-scale virus manufacturing and

purification strategies. Any step in production and purification of therapeutic viruses for a variety of phase I/II/III clinical trials and manufacturing must be done under GMP guidelines enforced by FDA [101]. GMP is a system for ensuring that products are consistently produced and controlled according to quality standards. The GMP guidelines are precisely designed in order to reduce the risks involved in any pharmaceutical production since the quality of the product is a crucial factor that may cause health-risk to the users. Figure 1.5 shows the current GMP guideline enforced by different health regulatory agencies (e.g. FDA, EMA, and BGTD) for manufacturing therapeutic viruses. Final sterile filtration, as a mandatory step prior to vialing and storage of any pharmaceutical product, is one of the most important challenges and concerns in the purification of therapeutic viruses, including OVs.

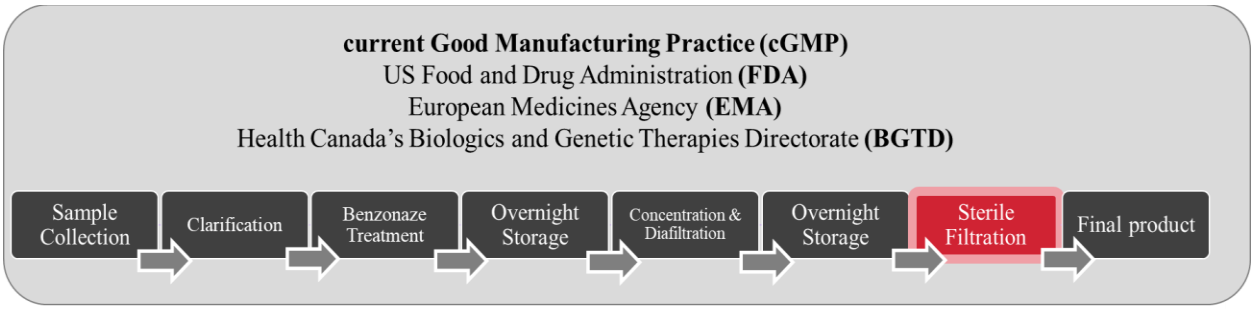

Figure 1.5 Current GMP for manufacturing of therapeutic viruses which shows the different steps in the manufacturing process, including the mandatory sterile filtration.

In the field of separation sciences, viruses are typically regarded as an impurity that needs to be captured and removed during production of other therapeutics such as monoclonal antibodies [102–105]. Currently, viruses engineered for cancer treatment are among novel therapeutics that are growing in the market due to their profound implications on human health. To date, there have been only a few studies focusing on transmission of viruses through the membranes as a final product (not impurities), especially sterile filtration of therapeutic viruses which is challenging given their large size compared to other bio-therapeutic molecules. In one of the most recent

studies on sterile filtration of OVs, Shabnam et al. [106] investigated the performance of 0.2 or 0.22 µm commercial sterile filters in constant flux filtration tests with a promising OV candidate (Rhabdovirus Maraba). These studies were performed in order to solve the significant operational and technical challenges associated with 'large-scale' OV purification processes since the commercial success of OVs is critically dependent on solving the current issues and increasing the efficiency of downstream processes. Hence, although the area of therapeutic virus purification has been studied a lot still there are gaps that need to be filled by conducting further researches to fulfill the pressing need on developing new separation technologies, novel membrane materials and methods for purifying newly discovered bio-therapeutics (i.e. viruses).

Due to the importance of the current topic and its profound implication on human health, it has been determined that a comprehensive understanding of the performance of sterilizing-grade MF membranes (e.g. fouling behavior, virus transmission) is critically needed. However, as mentioned in section 1.2, virus-based experimental researches are associated with many difficulties in terms of complication of assays, time-consuming processes, health risks and expenses involved for such experiments. Thus, using NPs as virus surrogates is considered to be a potential approach to better understand the basic fundamentals of sterile filtration of OVs in order to reduce the difficulties in the early stages of research.

Along with many advantages of employing NPs in filtration studies as pathogenic surrogates, unfortunately, there also exist some important drawbacks that needs be considered in each experimental work. Basically, NPs need to be suspended in specific buffer solutions in terms of pH, salt concentration and chemical composition based on their material, size or surface functional groups in order to minimize the aggregation of particles in the media, and these solutions are very different than biological media that viruses are suspended. The differences in the nature

of therapeutic virus solutions and synthetic solutions (for suspending NPs) is one of the hurdles that affect the outcome of experimental studies which avoids us to draw a strong correlation between VF studies and ones used surrogates as mimicry of virus particles. Unfortunately, there is also a large variation in the solution composition, especially the type and concentration of surfactant that currently is being used for suspending or diluting NPs in various filtration studies. The little inconsistency between these studies makes a big confusion in terms of the proper chemical composition that needs to be used in order to truly study the transmission behavior of virus-sized NPs through membranes. Hence, there is a great need to have a comprehensive study on the role of different buffer compositions and additives in filtration studies to have a better understanding of the rate of their effect on filtration results. It was determined that a detailed study on the role of different surfactants and surfactant concentration would benefit this field which will be discussed profoundly in the second chapter.

Moreover, the general mechanism of solute transport is greatly affected by physio-chemical properties of the solute, and the solution environment, thus the resemblance of NPs to pathogens can be questioned. Another drawback of such surrogates is that the surface properties (e.g. surface charge and composition) of NPs are quite different to actual viruses. Hence, although NPs can mimic multitude characteristic of virus particles such as shapes, sizes, and buoyant densities, their surface charge, but surface properties can be quite different. Many studies have questioned the potential of using NPs as viruses or bacteria surrogates due to differences in their physicochemical properties. Other studies have also raised this concern but with the attitude to solve the problem by modifying the NPs surface to be a better resemblance of a virus particle. These studies have suggested that coating NPs with a proper protein molecule can solve the problem effectively. This solution is suggested based on the fact that the surface structure of

viruses is basically made of proteins molecules. Therefore, there is also a great need to study the effect of surface properties of virus-sized particles in filtration studies where the particles are considered as the final products that need to pass through filtration membranes and not retained by the membrane.

1.4. Objective

According to Canadian Cancer Society 2018 Special report, nearly 1 in 2 Canadians is expected to be diagnosed with cancer at some point during their lifetime and about 1 in 4 Canadians expected to die from cancer which continues to be the leading cause of death in Canada [107]. Unfortunately, the medications and anticancer drugs for curing fatal tumors that currently exist are very expensive and according to statistics, the average price for a month of oral cancer medications is about $6,000. The exorbitant fees associated with the treatment of such fatal disease is a reasonable justification for more research and study in different branches of science in order to develop novel treatment techniques and establish cost-effective manufacturing processes. OVs are a new generation of biotherapeutics that has been found to have an extraordinary potential to cure different types of cancer cells of patients even during their late stage. Currently, there are many different types of OVs going through clinical trials on their way to full approval from regulatory health agencies for cancer treatment.

However, one of the hurdles to be overcome in developing these biotherapeutics, especially OVs, is the necessity to overcome current operational and technical challenges that exist in manufacturing processes to reduce the cost of production of such therapeutics after getting approval from regulatory health agencies. In this path, basically, purification of therapeutics involves a sequence of filtration and in this step, virus purification and filtration have been poorly studied. Some recent studies have reported that just 5% of the yield in the manufacturing process

is achieved due to different phenomena occurring in the process. Hence the challenge is to conduct more research and study different aspects of therapeutic virus purification and filtration to comprehensively understand the fundamentals and develop new strategies in order to increase the efficiency of filtration processes in downstream processing sections.

It is believed that further research and study on fundamental aspects that affect the transmission of therapeutic virus-sized particles through sterilizing grade membrane filters will help us to better understand the fundamental aspects of transmission of native viruses (i.e. OVs) through sterile filtration membranes. The outcome of such researches will be beneficial for solving the current deficiencies that exist in operational manufacturing processes especially increasing the efficiency of the sterile filtration processes. Thus, the objective of the present study is to produce detailed analyses of the transmission of fluorescently labeled polystyrene nanoparticles (PNPs), as therapeutic viruses (i.e. OVs) through commercial MF sterilizing grade membranes. These studies will mainly focus on the chemical composition of the media that NPs are suspended (in the second chapter) and the effect of NP surface composition and charge (in the third chapter).

With this regard, the importance of using NPs in separation science and the concept of using NPs as virus surrogates were profoundly discussed in **Chapter 1**. It is widely established that physicochemical properties of the membrane (e.g. membrane material, pore morphology), the solute (e.g. material, shape, particle charge, and composition), and the solution environment (e.g. pH, surfactant concentration, salt concentration) that particles are suspended has a significant effect on the outcome of results. Also, the importance of further research and studies to enhance the current technical and operational challenges of production and purification of OVs, especially the mandatory sterile filtration step, in the manufacturing process were explained.

The effect of adding surfactants to the NP suspension on transmission behavior of NPs through MF membranes is described in **Chapter 2**. Although the effect of adding surfactants to the NP suspension have been explored for a number of different applications, there is significant variation in the amounts and types of surfactants used in filtration studies. Hence, it was determined that a detailed study of surfactant concentration's influence on membrane behavior could help optimize the final sterile filtration step during the manufacturing of numerous therapeutic viruses currently being developed for the treatment of infectious diseases and cancer. Three different sizes (59, 188, and 490 nm) of fluorescent PNPs to mimic the length, width, and aggregates of Rhabdovirus Maraba, a bullet-shape envelope virus. This study aims to evaluate the transmission of these virus-sized particles as virus surrogates in a MF process. For this purpose, the performance of two commercial sterile filtration membranes Durapore PVDF and MiniSart polyethersulfone (PES) with 0.22 μm pore size ratings were investigated. The NPs were suspended in solutions with varying concentrations of Tween 20 (a nonionic surfactant)—0.0005% to 0.1% (v/v) in the feed buffer solution (0.1 M carbonate with 0.1% (w/v) sodium azide)—and were filtered via constant-flux dead-end filtration.

The effect of protein concentration (in the suspending buffer) as an additive and coating agent of PNPs on filtration behavior of commercially available sterilizing membrane is described in **Chapter 3**. It has been proved that BSA coated latex particles can make a good model for viruses since they have size and charge similar to common viruses such as herpes simplex virus [44,108,109], thus BSA has been used in this study in order to coat fluorescently labeled PNPs. NPs with the size of 188 nm was used to mimic the dimension of various OVs and also to challenge the performance of a Durapore PVDF membrane which is close the pore size of the membranes (i.e. 0.22 μm). The NPs were suspended in solutions with varying concentrations of BSA—0 to

0.5 mg/mL) in the feed buffer solution (0.1 M carbonate with 0.1% (w/v) sodium azide)—and were filtered via constant-flux dead-end filtration.

At the end of this document, the general conclusion, recommendation for future works and other applications that the current strategy in studying the transmission of particles through filtration membranes can be applied is described in **Chapter 4**.

Declaration of academic achievement: The majority of this chapter has been submitted to the Separation and Purification Technology journal on October 9th 2018.

Chapter 2: Sterile filtration of fluorescently labeled NPs – the importance of surfactant concentration

2.1. Introduction

The use of NPs has garnered widespread interest in the field of separation sciences. Most experimental studies use spherical NPs, as they are widely available in different materials (e.g. silica, gold, polystyrene), possess different functionalities (e.g. fluorescently-labeled) and various surface functional groups (e.g. carboxyl and amines), and can be obtained from different suppliers in very monodisperse forms across a broad range of sizes. Conversely, other studies have used nanorod-shaped particles [68,110–112]. Given recent advances in the synthesis of variously shaped NPs/colloids [113], the study of shape-based separations would appear to be a promising direction for further research. NPs have been used in various separation processes, such as chromatography [42–44], sand filtration [45], and the entire 'spectrum' of membrane-based separation technologies, including MF [46–53], UF [49,54–58], VF [59–64], NF [29], and RO [65,66]. Not surprisingly, these studies have utilized a variety of membrane materials. For instance, most studies focusing on MF and UF processes have used conventional phase-inversion membranes with significant variations in both the lateral and axial pore dimensions. However, other studies have used membranes fabricated using advanced manufacturing techniques. Examples of such membranes include track-etch polycarbonate membranes with well-defined cylindrical pores [58,67,68] and ultrathin silicon-based nanoporous membranes [114].

As mentioned in the previous chapter (see section 1.2) the use of NPs has been incorporated into separation studies, membrane filtration processes in particular (see section 1.2.2), for a variety of reasons. Some studies have used NPs as model solutes to estimate a membrane's pore-size distribution [46,55,61,64], while others have used the results from NP filtration tests to guide the development of mathematical models of solute transport through MF and UF membranes [67,68]. In a recent study, Helling et al. (2017) examined the role of particle deformation on retention of biological and non-biological particles by porous MF membranes. This study was conducted to compare the pressure-dependent filtration behavior of PNPs, bacteria, and a PP7 bacteriophage in PES membranes based on their deformability [53]. The most common motivation for studying NP filtration is their potential to be used as surrogates for various types of viruses encountered in water treatment and bioprocessing applications. In an early study, Tsurumi et al. [54] investigated the filtration behavior of GNPs (18 to 60 nm in diameter) in hollow fiber UF membranes in order to gain a better understanding of the results of their previous research using the hepatitis B virus [115]. Over the past 10 years, numerous studies have used NPs as virus surrogates for various applications, including membrane integrity tests [49,57,59,60] and filtration challenge tests [61,64], and there has been a recent trend towards using advanced microscopy techniques to image the spatial distribution of NPs within the internal structure of membranes [62,63]. The interest in using NPs as virus surrogates is motivated by the significant challenges of working with actual viruses. As explained in the previous chapter, first, biosafety facilities are needed in order to run the assays that are used to quantify virus concentration; furthermore, these assays are more complicated and time-consuming than non-biological assays. Second, the need for dedicated facilities and specially trained technicians make it expensive and challenging to produce even the small amounts of feed material usually required for lab-scale studies of membrane filtration

processes. For example, in a recent study wherein the sterile filtration of a therapeutic virus solution were investigated, the filtration experiment required three different batches of feed material in order to adequately evaluate how membrane morphology affects filtration performance [106].

Due to the numerous challenges associated with working with actual virus solutions, using NPs as virus surrogates considered a potential opportunity to better understand the sterile filtration of viruses. Unfortunately, there is a large variation in the solution composition that is used for suspending or diluting NPs in filtration studies. This inconsistency covers a wide range of solution composition from deionized water to traditional buffers such as phosphate buffered saline (PBS) with a wide variety of concentrations of different additives like salt (e.g. NaCl) or surfactants (e.g. sodium dodecyl sulfate (SDS), Tween 20 and Tween 80) which brings a lot of confusion. Choosing the proper solution composition for suspending NPs is very critical since it is known that NPs, depending on their aqueous solutions composition undergo different physical stages regarding their interfacial energies which can lead to aggregation of particles or adsorption onto different surfaces [50]. It is also well known that the general mechanism of solute removal is determined by a multitude of factors including the physicochemical properties of the membrane, the solute, and the solution environment. Tale 2.1 shows a summary of variations in terms of chemical compositions of suspending buffer, especially the amount and type of surfactant used in these studies.

Table 2.1 Variations in terms of the chemical composition of the suspending solution, especially the amount and type of surfactant used in recent filtration studies.

NP material	NP size	Suspending solution	Application	Reference
Polystyrene	26 and 67 nm	Water with the pH value of 6.5 or 8.5	Study the transportation of PNPs as virion surrogates in UF and MF membranes	Pontius et al. [49]
Polystyrene	20 and 100 nm	1xPBS with 0.1% Tween 20	Investigating membrane capacity and fouling mechanisms for ultrathin nano-membranes (nanofilters)	Winans et al. [114]
Silica	11, 25 and 92 nm	1mM ammonium bicarbonate	Investigating the role of NP size and polydispersity on fouling and rejection development during MF	Trzaskus et al. [52]
Gold	5 to 50 nm	Deionized water with 0, 0.1 and 0.26 wt% SDS	Determination of PSDs of VF membranes	Kosiol et al.[61]
Gold	20, 40 and 100 nm	Deionized water	Probing pore structure of virus filters	Nazem-bokaee et al. [63]

In an early study, Pall et al. (1980) detailed how surfactant concentration critically affects the transmission of NPs through MF membranes. Constant pressure filtration tests with a nylon MF membrane revealed a significant reduction in the retention of 0.22 μm NPs when the concentration of Triton X-100 was increased to 0.05%, with retention rates staying fairly constant up to 0.1% [116]. However, Lee et al. (1993) subsequently reported that they had been able to achieve very significant retention (i.e. greater than 99%) of 0.2 μm NPs using 0.2/0.22 μm membranes at the same surfactant concentration (i.e. 0.1% Triton X-100) [48]. Unfortunately, no explanation was provided for this large difference in filtration behavior. In the same study, Lee et

al. also utilized a sophisticated system capable of monitoring of NP concentrations in real time in order to examine how surfactant (Triton X-100) concentration affects the transmission of large 0.74 μm PNPs through a PVDF MF membrane (0.45 μm pore size). Interestingly, surfactants have been used very infrequently in subsequent NP filtration studies. In fact, the majority of filtration studies have been conducted using NPs that are suspended in a surfactant-free solution [49–52,56,58,62,63,67]. A few studies have used a fixed concentration of the nonionic surfactant, Tween20 [59,114], or the anionic surfactant, SDS [53,64]. Kosiol et al. (2017) studied the retention behavior of 20 nm GNPs in parvovirus retentive virus filters and documented the effect of SDS concentration on two different membranes (identified as VF3 and VF4) [61]. They observed major differences in the performances of the two membranes, both in terms of the change in flux for the NP-free SDS solution and the distribution of GNPs within the membrane after the filtration test. However, the authors did not specify what each membrane was made of (PES, PVDF, or regenerated cellulose) or who had supplied it (Asahi Kasei Medical, Millipore, Pall, or Sartorius), thus making it possible to only draw very limited conclusions about the exact separation mechanisms.

Although Lee et al. (1993) and Kosiol et al. (2017) highlighted the effect of surfactant concentration on the filtration behavior of NPs, these results were part of a larger study, thus limiting the scope of the relevant reported information. Additionally, neither study focused on the use of MF sterilizing-grade membranes with a 0.2 μm pore size rating. The author of the thesis is interested in this specific MF membrane because it is widely used in the final sterile filtration step during the manufacturing of numerous therapeutic viruses that are currently being developed for the treatment of infectious diseases and cancer [117]. Although the author acknowledges that Pall et al. (1980) demonstrated how surfactant concentration affected the filtration behavior of a 0.2

μm MF membrane, their study only reported results for one size of NP and one nylon membrane that had specifically been synthesized for their study. Furthermore, the authors did not include a study that documented how the surfactant concentration influenced NP suspension stability. Thus, the objective of the present study is to produce detailed analyses of the transmission of fluorescently labeled PNPs through two commercial MF membranes over a range of surfactant concentrations.

Currently, surfactants are also being used as an excipient in pharmaceutical applications including vaccine manufacturing to stabilize emulsions and suspensions. For example, Flublok® and Flublok® Quad are two vaccines for preventing infection by influenza virus which both contains ≤27.5 mcg Tween 20 in their final formulation solution [118]. Therefore the outcome of this study is helpful in order to better understand the effect of surfactant concentration in downstream processes and the mandatory sterile filtration step in particular. It should be noted that the Durapore PVDF MF membrane used in this study is the same as the one used in the recent Rhabdovirus Maraba filtration study [106]. The sizes of the three types of PNPs used in this study were chosen based on the dimensions of Rhabdovirus Maraba's unique bullet-shaped (59 nm width and 188 nm length) and aggregates of this virus (490 nm) [96]. In order to develop a fundamental understanding of the surfactant effect, a set of constant-flux dead-end filtration tests were run. TMP was continuously monitored and multiple post-filtration analyses were conducted, including measuring changes in the membrane's hydraulic permeability, capturing images of the membrane's surface using scanning electron microscopy (SEM), and characterizing NP distribution via confocal laser scanning microscopy (CLSM). Furthermore, each experimental condition was tested in triplicate using a new MF membrane for each filtration test in order to

account for any potential variations in membrane properties. Thus, in total, the results from 78 filtration tests are reported in this study.

2.2. Experimental

2.2.1. Membranes

Sterile syringe filter units containing MiniSart PES from Sartorius and Durapore PVDF from Millipore were obtained for this study. Both sets of syringe filters were single-layer and had a pore-size rating of 0.22 µm. The Durapore PVDF syringe filters featured an active membrane area of 4.5 cm^2, while the Minisart PES filters had an active membrane area of 6.2 cm^2. In order to examine each membrane's pore structure and morphology, samples were extracted from the syringe filter and imaged via SEM. For SEM imaging, the extracted membranes were individually mounted on specimen carriers and gold sputtered for 1.5 minutes under vacuum conditions with a current of 20 mA. Figure 2.1 shows the SEM images of each membrane's top surface.

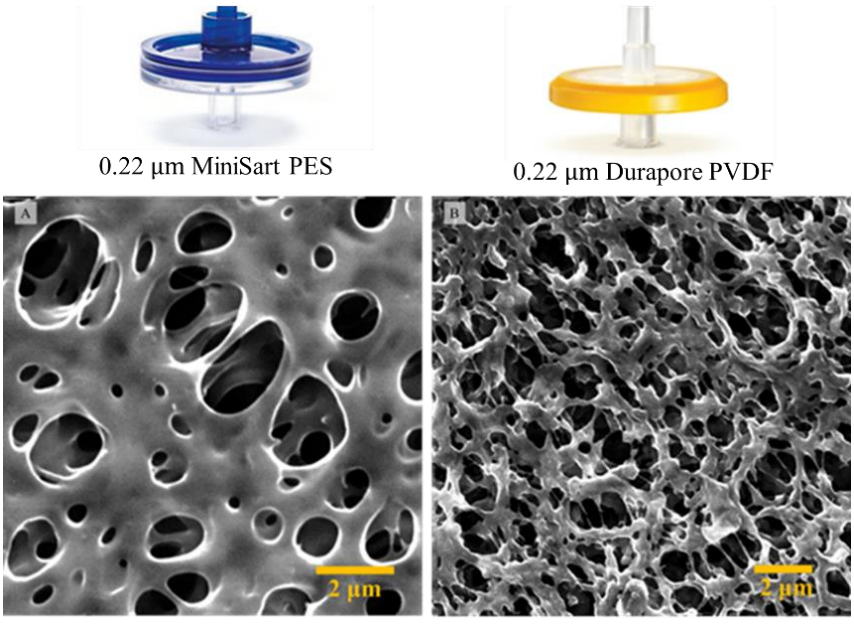

Figure 2.1 SEM images of the top surface of the commercial sterile filters; Panel (A): MiniSart 0.22 µm PES membrane (20,000 × magnification); Panel (B): Durapore 0.22 µm PVDF membrane (15,000 × magnification).

Although both membranes had a pore-size rating of 0.22 μm, their pore structures and morphologies were considerably different. Indeed, as can be seen in Figure 2.1 the SEM images of each membrane's top surface clearly show a wide distribution of pore sizes. Interestingly, pores with dimensions significantly greater than 0.22 μm have been observed, which increases the likelihood of particles larger than 0.22 μm passing through the membrane. Pore-size rating is likely determined based on the smaller pores in the membrane's internal space, but the manufacturers do not disclose how the membrane pore size rating is determined.

2.2.2. Polystyrene nanoparticle (PNP) solutions

A 0.5 M solution of pH 9.5 carbonate buffer (Alfa Aesar) was diluted to 0.1 M with ultrapure water (resistivity greater than 18.2 MΩ.cm) from a Milli-Q system. In order to prevent any bacterial growth, sodium azide (99%, extra pure, ACROS Organics™) was added to achieve a final concentration of 0.1% w/v. Finally, Tween 20 (VWR) was added to achieve a final concentration of 0.1% v/v. This stock solution was then serially-diluted with a surfactant-free carbonate-azide solution to create five additional buffer solutions with Tween 20 concentrations (v/v) of 0.01, 0.004, 0.002, 0.001, and 0.0005%. The room temperature viscosity of each buffer solution was measured using an SV-10 Vibro-viscometer (A&D Instruments). Three types of fluorescently labeled PNPs were purchased from Spherotech. The colors and reported size ranges of these PNPs are provided in Table 2.2. The PNP solutions used in the filtration experiments were prepared by diluting 65 μL of the as-purchased solutions 100-times by volume with the corresponding buffer solution in order to obtain a final PNP concentration of 0.01% w/v. As per the recommendation of the manufacturer, each PNP solution was vortexed and ultrasonicated (BRANSON 2800) for fifteen minutes in order to separate any possible aggregates.

In order to verify the monodispersity of the PNPs, the as-purchased stock solution was diluted to 0.01% w/v with the carbonate buffer containing the highest concentration (0.1% v/v) of Tween20 and then analyzed using dynamic light scattering (DLS) via a Zetasizer NanoZS (Malvern). During DLS measurement, the position of the laser attenuator was set at 173° relative to the laser source in order to ensure backscattering detection. The reported sizes (see Table 2.2) are the average particle size of 5 measurement runs of 100 seconds for each PNP solution. As shown in Figure 2.2A, the prepared sample showed only a single peak for each case, with mean sizes of 59 ± 12 nm, 188 ± 24 nm, and 490 ± 244 nm. No considerable overlap in size distribution between samples was observed.

Table 2.2 Properties of fluorescent PNPs used in this study.

NP Color	Reported NP Size[1](nm)	Measured NP Size[2] (nm)	Excitation Wavelength (nm)[3]	Emission Wavelength (nm)[3]	Number Concentration of Particles in 1.0% w/v Solution ($\times 10^{12}$)[4]
Purple	40-90	59 ± 12	580	635	88.6
Yellow	100-300	188 ± 24	485	535	2.7
Sky-blue	400-600	490 ± 250	620	680	0.1

[1] As per manufacturer

[2] In buffer with 0.1% (v/v) concentration of Tween 20 - according to DLS results shown in Figure 2.2A.

[3] Excitation and emission wavelengths used for detection with the Spark 10M microplate reader (TECAN).

[4] Calculated, as per the manufacturer's suggestion, according to $N = (\frac{6W}{3.14PD^3}) \times 10^{12}$ where N is the number of particles, W is the weight of the polymers (g), P is the density of polystyrene (1.05 gcm^{-3}), and D is the measured diameter of the particles (μm) using DLS.

In order to evaluate PNP stability as a function of surfactant concentration, the DLS analysis was repeated on samples prepared in five other buffers (i.e. 0.01, 0.004, 0.002, 0.001, and 0.0005% v/v). As shown in Figure 2.2B (for purple PNPs; 59 nm) and Figure 2.2C (for yellow PNPs; 188 nm), the DLS results indicated some degree of aggregation of PNPs as the Tween 20 concentration in suspending buffer decreased to 0.001% v/v. The size distribution of the smaller PNPs (i.e. 59 nm) showed a small peak around 500 nm (bigger than the pore size of the membranes), which was obtained by decreasing the suspending buffer's Tween 20 concentration to 0.004% v/v. This behavior is due to the termination of steric stabilization, which occurs as a result of reducing the number of surfactant molecules in the solution. Used in many applications, the steric stabilization mechanism involves coating the surface of the particles with a long hydrophobic tail of surfactants, which extends out into the solution to prevent the coagulation of colloidal suspensions [119]. By further decreasing the surfactant concentration, the size distribution of the 59 nm PNPs covered a wider range of particle sizes due to more aggregate growth. The DLS results indicated that the 59 nm PNPs had a higher aggregation rate than the 188 nm PNPs. This result can be explained by the fact that the number of 59 nm PNPs—and, thus, the total surface area at the same concentration (0.01% w/v) of particles—is considerably higher that of the 188 nm PNPs. Therefore, while the amount of surfactant added to the suspending buffer solution was sufficient to prevent aggregation among the 188 nm PNPs, it was not sufficient to cover the whole surface of the 59 nm PNPs. Detectable aggregates did not form for the 188 nm PNPs until the Tween 20 concentration in the suspending buffer reached 0.001% v/v.

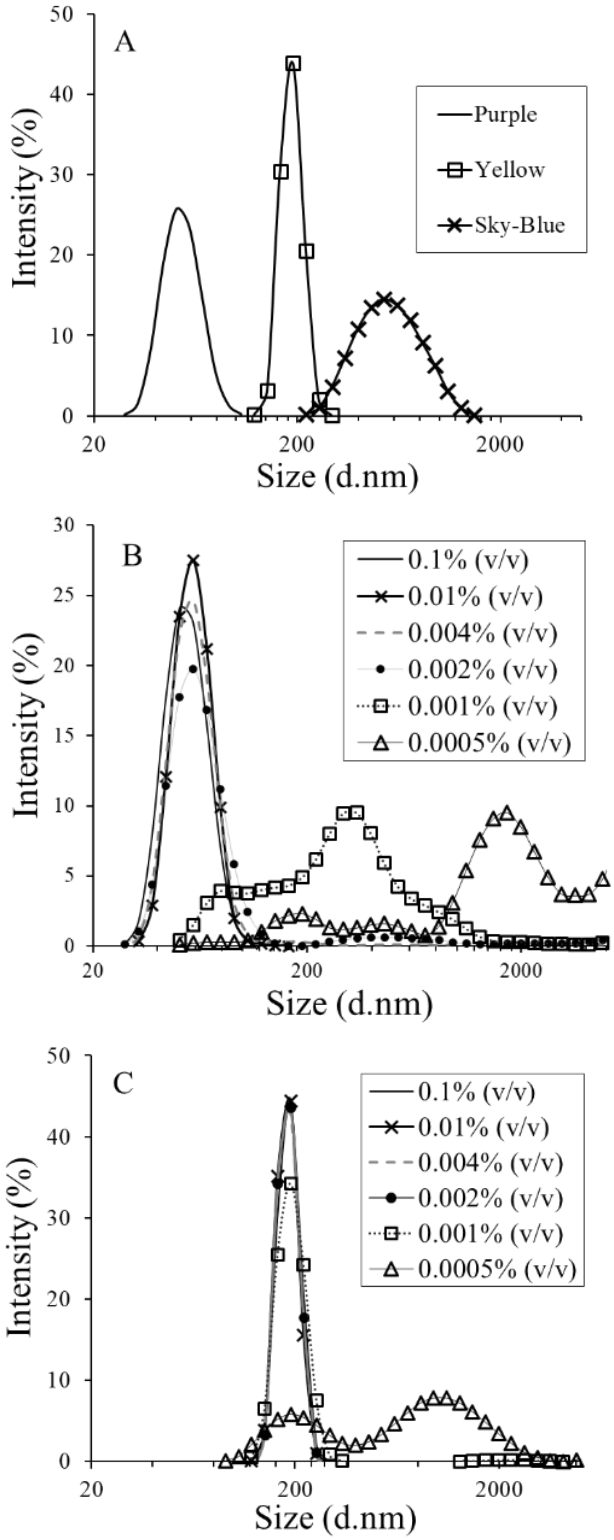

Figure 2.2 Panel (A): DLS results of three different fluorescent PNPs (purple, yellow and sky-blue) in suspending buffer containing 0.1% v/v Tween 20. Panel (B): Size distribution of 'purple' PNPs in six buffers with different Tween 20 concentrations. Panel (C): Size distribution of 'yellow' PNPs in six buffers with different Tween 20 concentrations.

2.2.3. Filtration Experiments

Constant-flux filtration experiments were performed using the experimental setup shown in Figure 2.3. Teflon tubing (1.58 mm outside diameter) and appropriate fluidic connectors were used to connect the PHD programmable syringe pump (Harvard Apparatus) to a custom cylindrical filtration module made of polyetheretherketone (PEEK). The filtration module's outlet was outfitted with a luer-lock adapter in order to connect syringe filter, and the TMP signal was continuously monitored and logged on a laptop via a PX409 pressure transducer (Omega Engineering). Note that each condition (i.e. combination of membrane type, PNP, and buffer solution) was tested in triplicate and a brand new syringe filter was used for each individual test. The membrane in each syringe filter was wetted by passing 60 mL of buffer solution through it in 10 mL increments, alternating from front-to-back to back-to-front for each 10 mL injection. The membrane's pre-filtration hydraulic permeability, L_P ($mL.s^{-1}.m^{-2}.Pa^{-1}$), was determined using Equation (2.1):

Eq. 2.1
$$L_p = \frac{J}{TMP}$$

where J denotes the flux of the buffer solution ($mL.s^{-1}.m^{-2}$), which is calculated as the flow rate divided by the effective membrane area. Permeability measurements were made for five randomized flux values (between 1.9 and 19 $mL.s^{-1}.m^{-2}$ for the MiniSart PES membrane and between 3.7 and 37 $mL.s^{-1}.m^{-2}$ for the Durapore PVDF membrane) and repeated twice. The flux-TMPs were plotted for all permeability measurements, and a highly linear relationship ($R^2 > 0.95$) was observed.

After the permeability test was complete, the syringe containing the buffer solution was replaced with a standard 10 mL syringe that had been pre-filled with 6.5 mL of the PNP solution.

The PNP solution was then passed through the membrane at a constant flux of 9.7 $mL.s^{-1}.m^{-2}$ for the MiniSart PES membrane and at 18.5 $mL.s^{-1}.m^{-2}$ for the Durapore PVDF membrane. The filtrate was continuously collected as 300 µL samples in a flat-bottom 96-well microplate (Greiner Bio-One). After the filtration experiment was complete, the syringe filter was disconnected from the module and the 'dead volume' above the membrane was manually washed multiple times using a pipette and the same PNP-free solution. The Teflon tubing and the internal channels of the PEEK filtration module were also extensively washed to remove any residual PNPs. Finally, the syringe filter was reconnected to the module and the membrane's post-filtration hydraulic permeability was measured using the same procedure described above.

The concentration of PNPs in the filtrate was determined by transferring 135 µL aliquots of all the collected filtrate samples into a flat-bottom, black, 96-well half-area microplate (Corning) and measuring their fluorescent intensity (see Table 2.2 for excitation and emission wavelengths) with a Spark 10M microplate reader (TECAN). Multiple measurements were performed on spatially separated spots arrayed across each well (circle filled 2×2) in order to increase the accuracy of the measurements for each collected sample. The fluorescent intensity results for the filtrate samples were normalized by including samples of the starting PNP feed solution and the PNP-free buffer solution in each 96-well half-area microplate.

After PNP filtration, the used membranes were carefully extracted from the syringe filter and SEM imaged, while the suspending buffer was analyzed for two extreme concentrations of Tween 20 (i.e. 0.1 and 0.0005% v/v) using the same method explained earlier (see c 2.2.1). A confocal laser scanning microscope (Leica SP5) was used to determine the spatial distribution of the fluorescently labeled PNPs within the internal structure of the MF membranes in different depths. The post-filtration CLSM images were obtained by cutting the extracted membranes into

pieces measuring approximately 0.5 cm × 0.5 cm and then placing them on glass slides, covering the samples with thin glass coverslips, and imaging them with the Leica SP5 confocal microscope. Yellow PNPs were excited with a 465 nm laser (10-15% laser power), and the emitted fluorescent light was collected using a 63× oil objective lens. Confocal images were obtained at x-y cross-sections through different filter depths at 10.2 μm intervals from top to bottom.

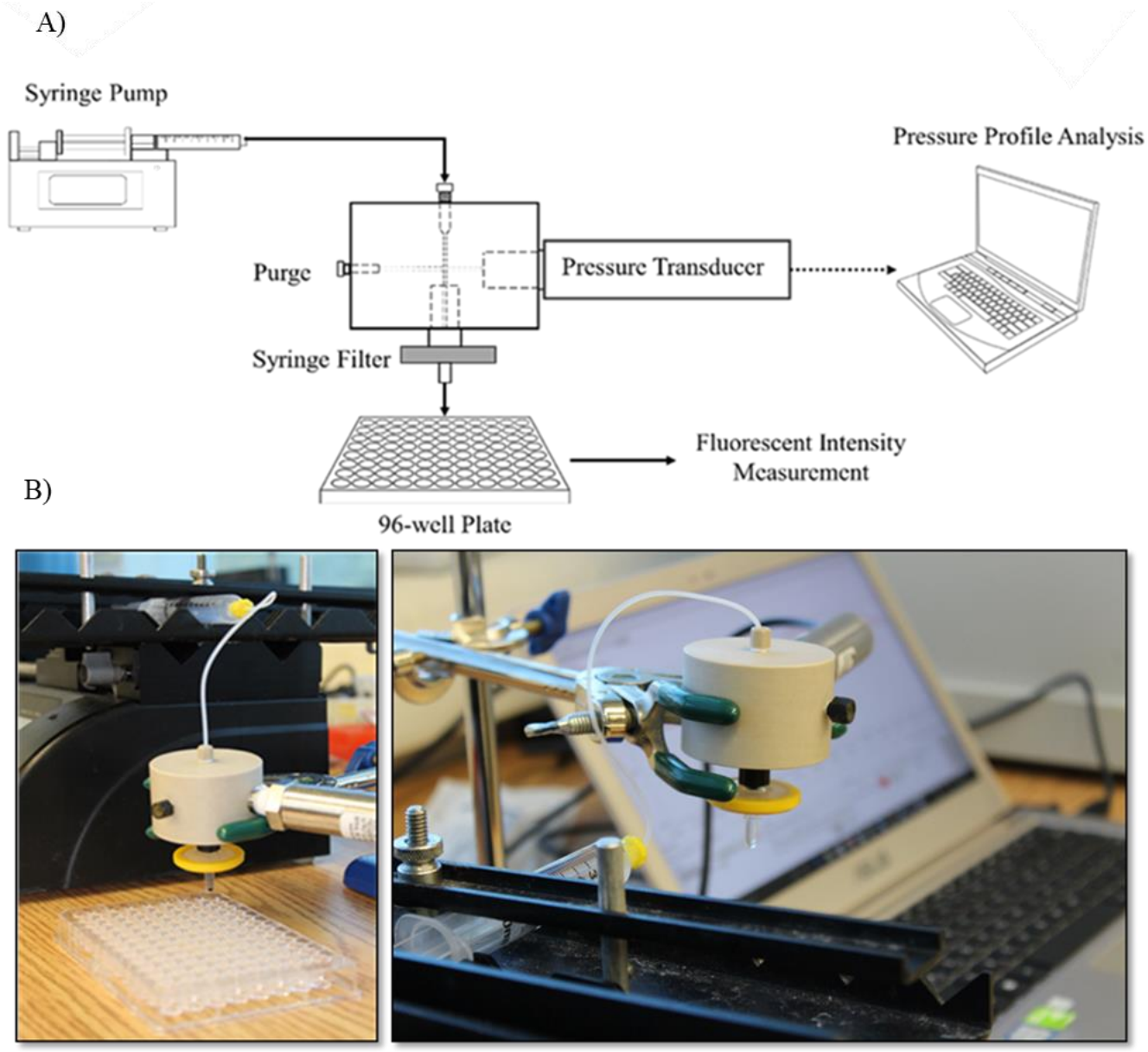

Figure 2.3 Panel (A): Schematic of constant-flux filtration setup – see text for details on the components. Panel (B): Picture view of the experimental setup.

2.3. Results and Discussion

In order to provide a quantitative comparison of the effect of surfactant on PNP transmission through MF membranes, Figure 2.4 illustrates the relative fluorescent intensities of the filtrates collected during 24 different tests. Each test is a different combination of the two membranes, the two PNPs (59 nm and 188 nm), and the six solutions that were used. Since the 490 nm, PNPs were unlikely to be transmitted due to being larger than the sterile filter's pore size (i.e. 0.22 μm), the effect of surfactant concentration on their transmission was limited to high concentrations of Tween 20 in the suspending buffer (see Figure A3).

The three data series in each panel correspond to the separate filtration tests—which were each run with a new membrane—for each condition. As a cursory glance reveals, there is excellent reproducibility within each of the 24 conditions. In order to account for the differences in fluorescent intensity among the different combinations of PNPs and solution conditions, the results in Figure 2.4 are reported in terms of the relative fluorescent intensity between the filtrate sample and the initial feed sample. Thus, a filtrate sample with a normalized fluorescent intensity of exactly 1 has the same number of PNPs as the feed sample. Furthermore, any considerable decrease in a sample's fluorescent intensity is correlated to the retention or capture of the PNPs by the membrane. It should be noted that the low fluorescence signals at the beginning of each filtration test are simply due to the solution being diluted by the PNP-free buffer that was injected into the filtration module during the pre-filtration permeability measurements.

The results in Figure 2.4 clearly show that, at the highest Tween 20 concentration (panels A through D), the 59 and 188 nm PNPs are completely transmitted during the filtration of 6.5 mL of solution, which is approximately 50 times greater than the 'hold up' volume for each syringe

filter. The complete transmission of the 188 ± 24 nm PNPs was somewhat surprising for two reasons: first, the diameter of these PNPs was very close to the pore-size ratings for both membranes (0.22 μm); and second, the SEM images of the membranes showed a considerable number of pores that were smaller than these PNPs, which means that many should have been caught by the membrane. It is noteworthy that these results differ significantly in terms of particle retention from previous studies that have used Triton X100, which is also a nonionic surfactant. For example, Simonetti and Schroeder (1986) reported retention values of 16, 44, and 96% for 0.2 μm particles suspended in 0.1% Triton X100 with Nylon, PVDF, and polysulfone membranes (all rated as 0.2 μm) [46]. In another study, Lee et al. (1993) reported retention values of 99% for a 0.22 μm -rated PVDF membrane and 99.99% for a 0.2 μm rated PTFE membrane. Filtration results for the 490 nm PNPs at high Tween 20 concentrations show that all of the PNPs were retained by the membrane (Figure A3); thus, the critical size cutoff for these two membranes is between 188 and 490 nm, which may be a helpful contribution to future studies in this area. For smaller PNPs, full transmission in high concentrations of surfactants was expected to be observed due to their adsorption to the surfaces of PNPs and membranes, which serves as a buffer between the two substances and prevents any particle-particle or particle-membrane adsorptive interaction [120]. However, the differences between reported results in this study and those of previous works of high surfactant concentrations are surprising because all of the membranes used in this work were rated as 0.22/0.2 μm filters. Although various techniques have been employed to measure pore sizes (e.g. mercury intrusion measurement and direct methods using NPs), there is no way to ascertain the number of pores in a filter with certainty, as these measurement techniques are predicated on a number of assumptions (e.g. pores are cylindrical passageways) [46,121]. Unfortunately, the manufacturers remain unwilling to disclose their methods for determining the

pore size of their membranes, so, for the time being, approximations are the best the author has to work with.

Conversely, full PNP retention (panels U through X) occurred at the lowest Tween 20 concentration (i.e. 0.0005% v/v). This result was predictable based on the DLS results shown in Figure 2.2. As discussed in section 2.2.2, the PNP solution's steric stabilization is terminated by decreasing the surfactant concentration in the suspending buffer, which in turn causes the PNPs to form aggregates approximately 10-15 times bigger than the membrane's pore size, thus resulting in the retention of PNPs.

The analysis of the performance of sterile filters in solution conditions featuring a range of Tween 20 concentrations in the suspending buffer yielded results that showed that the performance of membranes varies from complete transmission to complete retention, depending on the concentration of Tween 20 and the membrane-PNP combination. The results also indicated good agreement between the DLS results and the fluorescent profiles of the 188 nm PNPs and the Durapore membranes. In contrast, there was a poor agreement between the DLS results and the fluorescent profile of the 188 nm PNPs and the MiniSart PES membrane, with the switch from full transmission to retentive behavior occurring somewhere between 0.01% (panel H) and 0.004% (panel L). The dramatic difference in filtration behavior between the Durapore PVDF and MiniSart PES membranes is likely a product of their different surface chemistries. It is also possible that their pore morphologies contributed to this effect as well. For all conditions shown in Figure 2.4, the relative fluorescent profile is very flat after the low signals at the beginning of filtration due to the PNP solution being diluted by the preexisting buffer in the module. This means that the concentration of filtrate remained unchanged during filtration. Figure 2.4 also contains one notable exception to these transmission behaviors: the filtration of 59 nm PNPs suspended in buffer with

0.002% Tween 20 using a Durapore PVDF membrane. In the early stages of filtrations using this combination, the TECAN plate reader detected some initial transmission of PNPs in the filtrate samples, but the transmission rate dropped off with remarkable consistency over the three different runs. This behavior is likely due to the pores becoming blocked by aggregated PNPs during the initial stages of filtration (Figure 2.4M). However, since there are fewer of these aggregates than there are non-aggregated PNPs, the non-aggregated PNPs are able to pass through until all the pores on the top surface of the membrane become blocked.

The results illustrated in Figure 2.4L provide further insight into the retentive behavior of the PES filters. As this figure shows, there is a conspicuous and sudden change from full transmission to full retention of 188 nm PNPs when the concentration of Tween 20 in suspending buffer solution is lowered from 0.01 to 0.004% v/v. According to the DLS results, there is no aggregate formation at this surfactant concentration; this introduces the possibility that the observed particle retention may be due to PNP-membranes interaction (adsorption). Therefore, PNPs may be retained as a result of a size-exclusion mechanism or by adsorption to the membrane surface. As stated above, the differences in the results obtained for the two different membranes are likely related to four key characteristics: differences in surface chemistry, the degree of hydrophobicity/hydrophilicity, surface charge, and pore morphology. Indeed, differences in these areas may very well explain the filters' respective retentive behaviors, as MF removals are based more on surface interactions and particle adsorption than simple size exclusion [49,122]. A comparison of the results for filtering PNPs using PES and PVDF membranes shows a clear dissimilarity in their respective particle transmission patterns. In addition, PES membranes seemed to foul quicker than PVDF membranes.

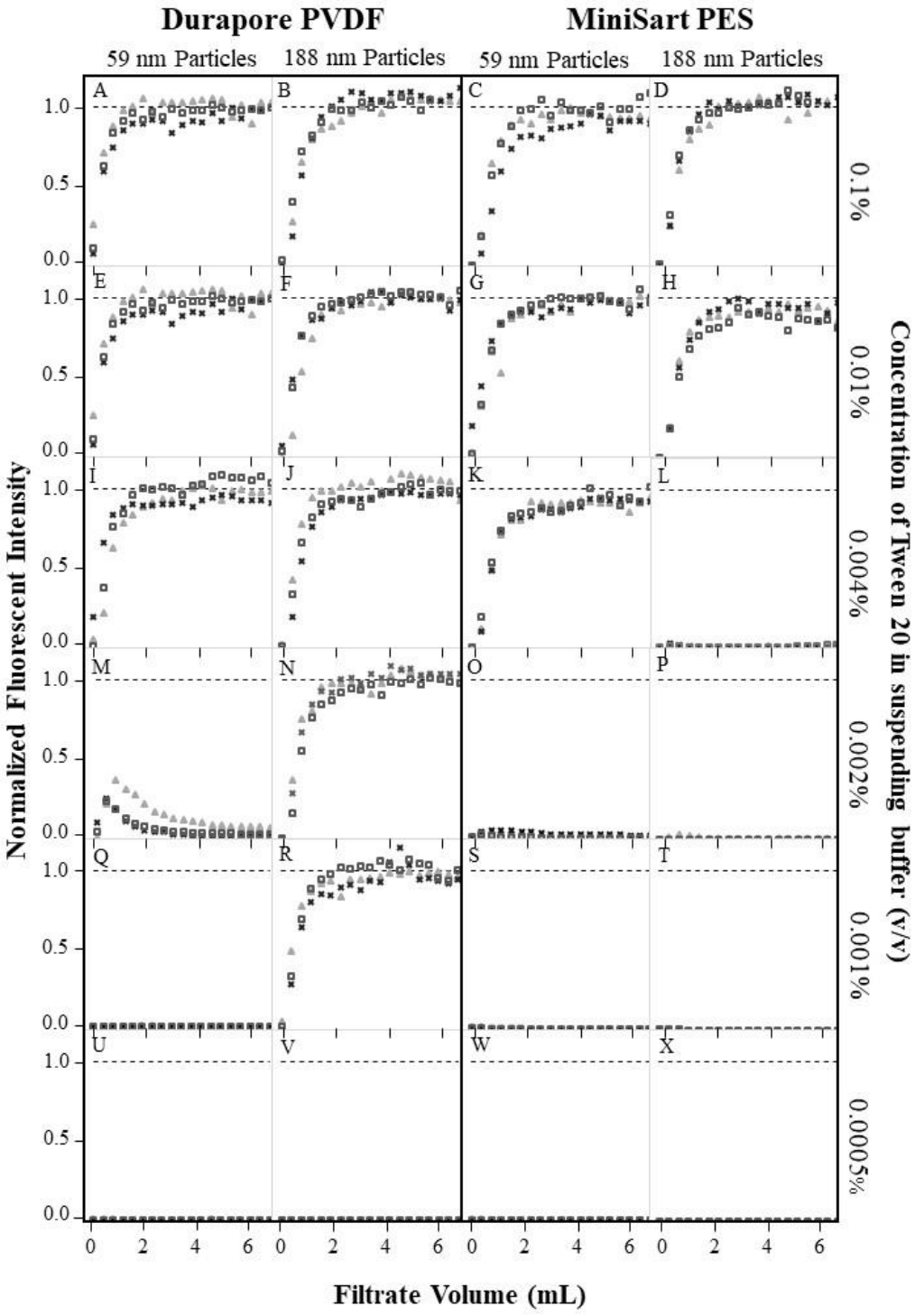

Figure 2.4 Normalized fluorescent intensity profiles for filtrate samples collected during constant-flux filtration tests at different combinations of PNPs (59 and 188 nm), MF membranes (Durapore PVDF and MiniSart PES), and Tween 20 concentrations (0.1% to 0.0005%). The profiles from the three separate trials that were conducted at each experimental condition are displayed by △, □, and × in each panel.

In order to investigate the effect of surfactant concentration on the performance of the membrane itself, the sterile filtration of PNPs suspended in a low Tween 20 concentration were performed on a membrane which has been wetted by a higher surfactant concentration. For this purpose 188 nm, PNPs were diluted in the buffer with 0.0005% (v/v) surfactant and filtered through the PES membranes wetted with buffer containing 0.1% (v/v) of surfactant. The result shown in Figure 2.5 indicates that the wetting procedure has a little effect on transmission behavior of the PNPs and the transmission is solely related to the chemical composition of the media that PNPs are suspended in. By comparing the current transmission results with the same combination of PNP solution and membrane material (Figure 2.4X), no significant differences can be found. Even a little increase in the transmission of the PNPs at the beginning of the filtration (around 1 mL) can be contributed to the blending effect of the high Tween 20 concentration in the dead volume of the syringe filter with the coming PNP solution.

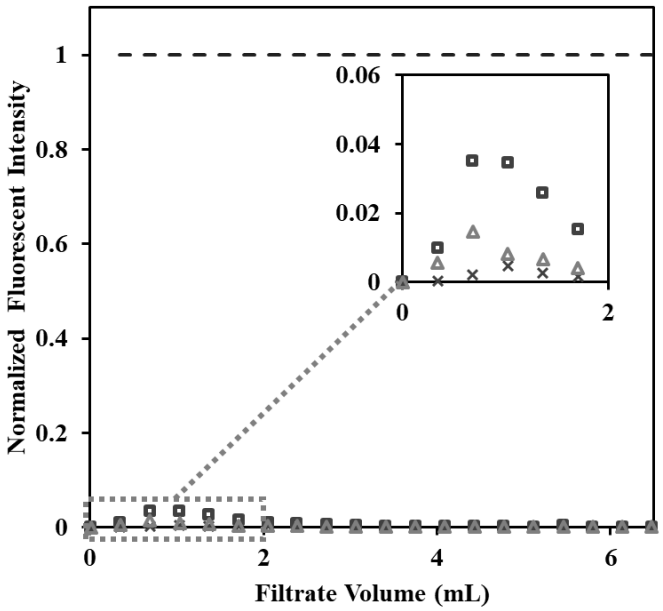

Figure 2.5 Normalized fluorescent intensity profiles for filtrate samples collected during constant-flux filtration of 0.01% (w/v) 188 nm PNPs suspended in buffer containing 0.0005% (v/v) Tween 20 using MiniSart PES membrane wetted with buffer containing 0.1% (v/v) Tween 20. The profiles are from the three separate trials are displayed by △, ◘, and ✕.

During each constant-flux filtration test, the TMP was simultaneously displayed and logged (via the USB pressure transducer) in order to monitor any changes in the total resistance. Sample data for the filtration tests with 188 nm PNPs and the Durapore PVDF membrane is shown in Figure 2.6. Each profile is the average of the triplicate experiments that were conducted at each Tween 20 concentration. There was no significant change in TMP during the filtration tests conducted for the five highest Tween 20 concentrations: the TMP at the 6 mL mark was between 0.34 and 4.36% higher than that at the 1 mL mark. At the lowest Tween 20 concentration of 0.0005%, however, there was a noticeable increase in TMP from 0.98 to 1.68 kPa (~70% increase). The good agreement between TMP and the fluorescent intensity profile results in Figure 2.4 is likely attributable to increased resistance due to the buildup of PNPs on the membrane surfaces. The same trend of increasing TMP at lower Tween 20 concentrations were observed for the other three PNP-membrane combinations (results not shown).

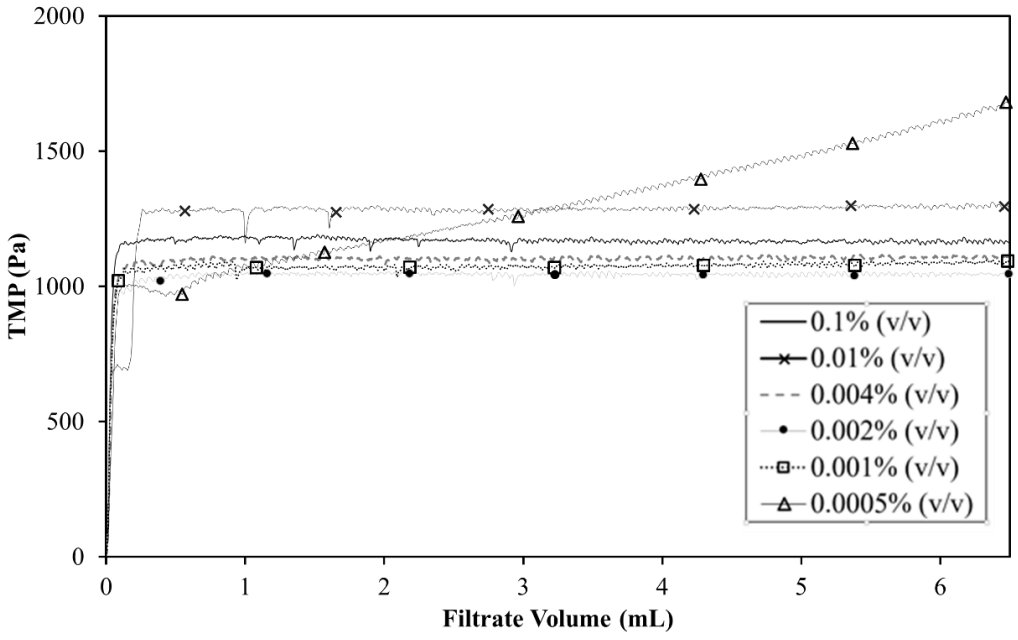

Figure 2.6 Comparison of average TMP profiles as a function of filtrate volume for the Durapore PVDF membrane and 188 nm PNPs in six buffers with different Tween 20 concentrations.

The final quantitative measurement of how surfactant concentration affects the MF filtration of PNP solutions is based on membrane hydraulic permeability. The two panels in Figure 2.7 display the results for 144 individual measurements, wherein hydraulic permeability was measured both pre- and post-filtration for each triplicate evaluation of the 24 different experimental conditions (two MF membranes, two PNPs (59 and 188 nm), and six solutions). The permeability measurement results for the 490 nm PNPs are also shown in Figure A4. The pre-filtration hydraulic permeability values for the MiniSart PES membrane were approximately 3 times higher than the corresponding values for the Durapore PVDF membranes across the different buffer solutions. As can be seen, the pre-filtration hydraulic permeability values noticeably decreased for both filters as the Tween 20 concentration increased, though this effect was more pronounced for the MiniSart PES membrane. This change in membrane performance is most likely due to the increase in solution viscosity that occurs when the Tween 20 concentration is increased (see Figure A1 in the Appendices). Overall, however, no strong conclusions can be made for the MiniSart PES membrane based on the permeability results. In contrast, the Durapore PVDF membrane exhibited a significant drop in post-filtration permeability at the lowest Tween 20 concentration (0.0005%) for both PNPs (59 & 188 nm PNPs). For example, the PVDF membrane's hydraulic permeability decreased from 0.0187 ± 0.0003 to 0.0133 ± 0.0026 $mL.s^{-1}.m^{-2}.Pa^{-1}$ after the filtration of 188 nm PNPs. Likewise, the PVDF membrane's permeability decreased from 0.019 ± 0.0001 to 0.0146 ± 0.0001 $mL.s^{-1}.m^{-2}.Pa^{-1}$ for the 59 nm PNPs at a Tween 20 concentration of 0.002% after filtration. However, no significant change in permeability was observed for this membrane at three highest Tween 20 concentrations (0.004% to 0.1%).

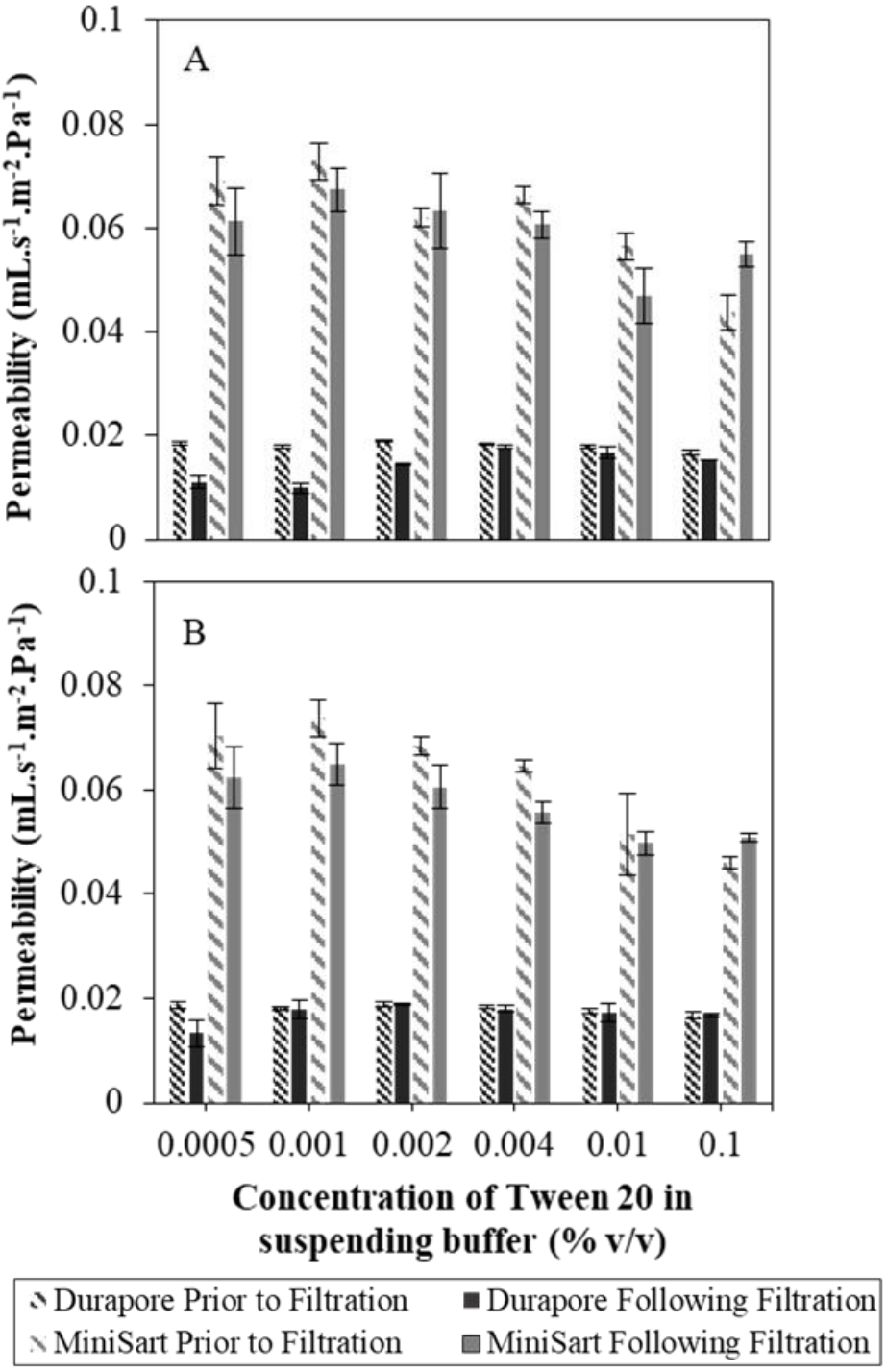

Figure 2.7 Comparison of hydraulic permeability measurements of the Durapore PVDF and MiniSart PES membranes pre- and post-filtration of 0.01% w/v of 59 nm PNPs (panel A) and 188 nm PNPs (panel B) in six buffers with different Tween 20 concentrations. The value for each vertical bar is the average of the measurements from the triplicate tests for each condition, while the error bars are the standard deviation calculated for the triplicate tests.

The hydraulic permeability results in Figure 2.7 generally show good agreement with the filtrate fluorescent profiles in Figure 2.4 and the TMP profiles in Figure 2.6. All three figures illustrate a critical change in MF membrane performance when there are low surfactant concentrations in the suspending buffer. It should be noted that the strategy of repeatedly washing the membrane with a micropipette to remove any unbound PNPs from the surface and within the pore structure makes it difficult to characterize the exact nature (i.e. reversible vs irreversible) of the membrane fouling.

In order to gain a better understanding of fouling among the smaller PNPs (i.e. 59 and 188 nm), SEM imaging were used first to visualize the top surface of the MF membranes. As mentioned in section 2.2.1, this was done by carefully disassembling the syringe filter device and extracting the MF membrane. As shown in Figure 2.8 (panels A and B), there is negligible particle accumulation/adsorption at the highest Tween 20 concentration (0.1%) when compared to the SEM images of the un-used membrane in Figure 2.1. In contrast, significant accumulation/adsorption occurs at the lowest Tween 20 concentration (0.0005%), which is consistent with the results shown in Figures 2.4, 2.5, and 2.6. It is interesting that PNPs remained attached to the membrane surface and continued to block a great number of pores (as is evident from the SEM images) despite the strategy of repeatedly washing the membrane surface before conducting the permeability measurements.

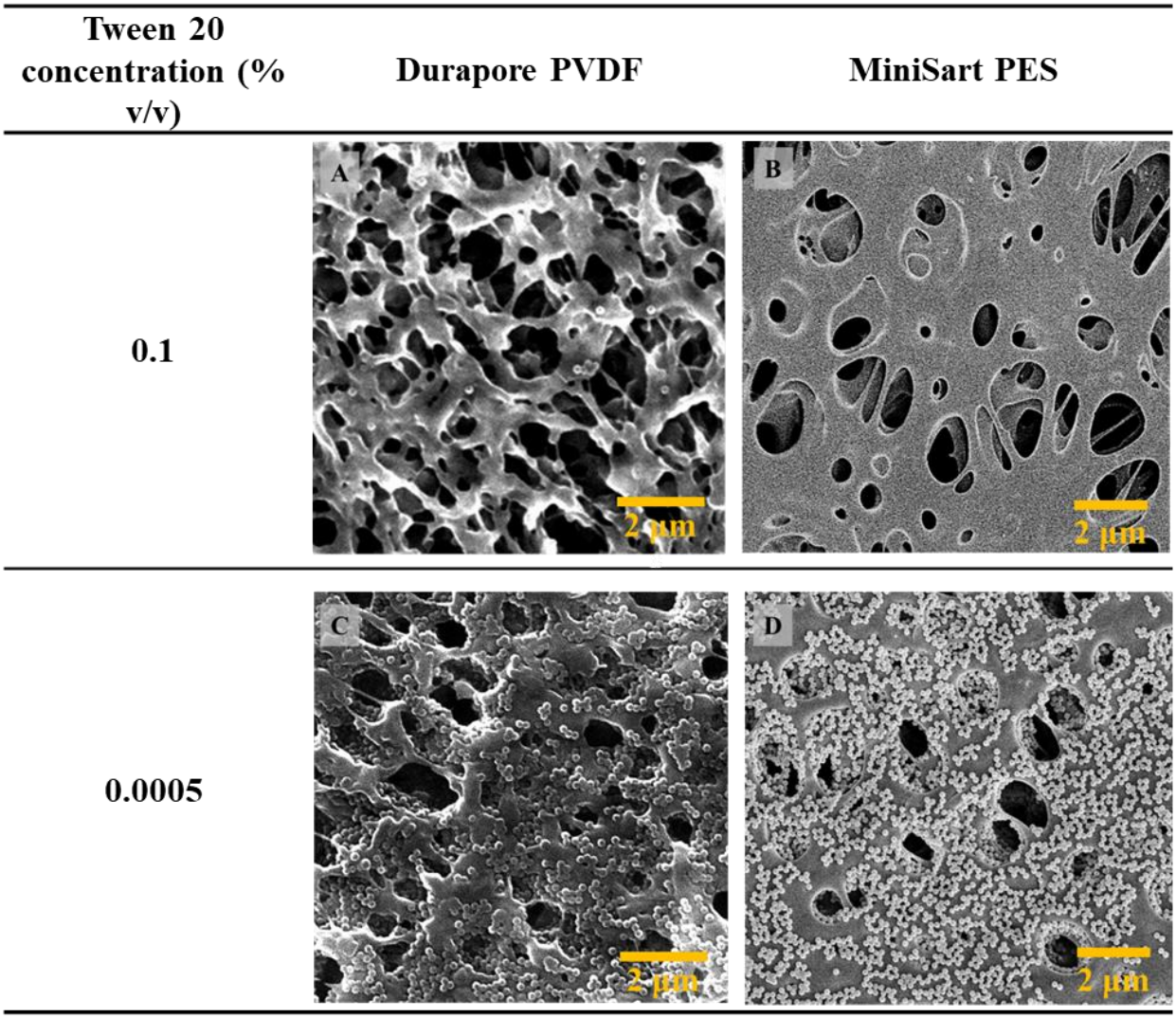

Figure 2.8 SEM images of the Durapore PVDF and MiniSart PES membranes after the filtration of 188 nm PNPs; Panels (A) and (C) are the SEM images (15,000× magnification) of the Durapore PVDF membrane after filtering 188 nm PNPs suspended in buffer with 0.1% and 0.0005% (v/v) concentrations of Tween 20, respectively; Panels (B) and (D) are the SEM images (10,000× magnification) of the MiniSart PES membrane after filtering 188 nm PNPs suspended in buffer with 0.1% and 0.0005% (v/v) concentrations of Tween 20, respectively.

The SEM images in Figure 2.8 show extensive PNP adsorption to the top surface of the MF membrane at the lowest Tween 20 concentration. In order to better understand how and why PNPs adsorb within the internal structure of the MF membranes, CLSM were used. This approach was inspired by the recent series of studies by Zydney and colleagues that examined the performance of virus-retentive membranes [63,105,123,124]. Figure 2.9 shows confocal images

of the x-y planes at the top, middle (depth of approximately 50 μm), and bottom (depth of approximately 120 μm) of the MiniSart PES membrane for the highest and lowest Tween 20 concentrations (0.1% and 0.005% respectively) used in this study. The individual red dots correspond to a single or aggregate of fluorescently labeled 188 nm PNPs. The objective of this analysis was two-fold: first, to confirm the absence of PNPs within the membrane's structure after filtration using a buffer with a high Tween 20 concentration (shown in Figures 2.9A, B, and C); and second, visualizing the location of retained PNPs within the filters when the filtered PNPs were suspended in a buffer with a low Tween 20 concentration (shown in Figures. 2.9D, E, and F). The confocal images show that the fluorescence intensity is considerably higher closer to the membrane's upper surface than it is in the middle and that there is no trace of PNPs at the bottom. These results confirm that PNPs were unable to completely pass through the membranes. The mid-membrane confocal image also reveals the presence of some non-aggregated PNPs that may have been able to pass through the membrane but were unable to due to some adsorption mechanism. Overall, the confocal images confirm previous findings that MF removals are based more on surface interactions and particle adsorption than simple size exclusion. Similar results were observed from CLSM of membranes after filtration of 188 nm PNPs and Durapore PVDF membranes and 59 nm PNPs and MiniSart PES membranes in two extreme conditions (See Figure A5 and A6).

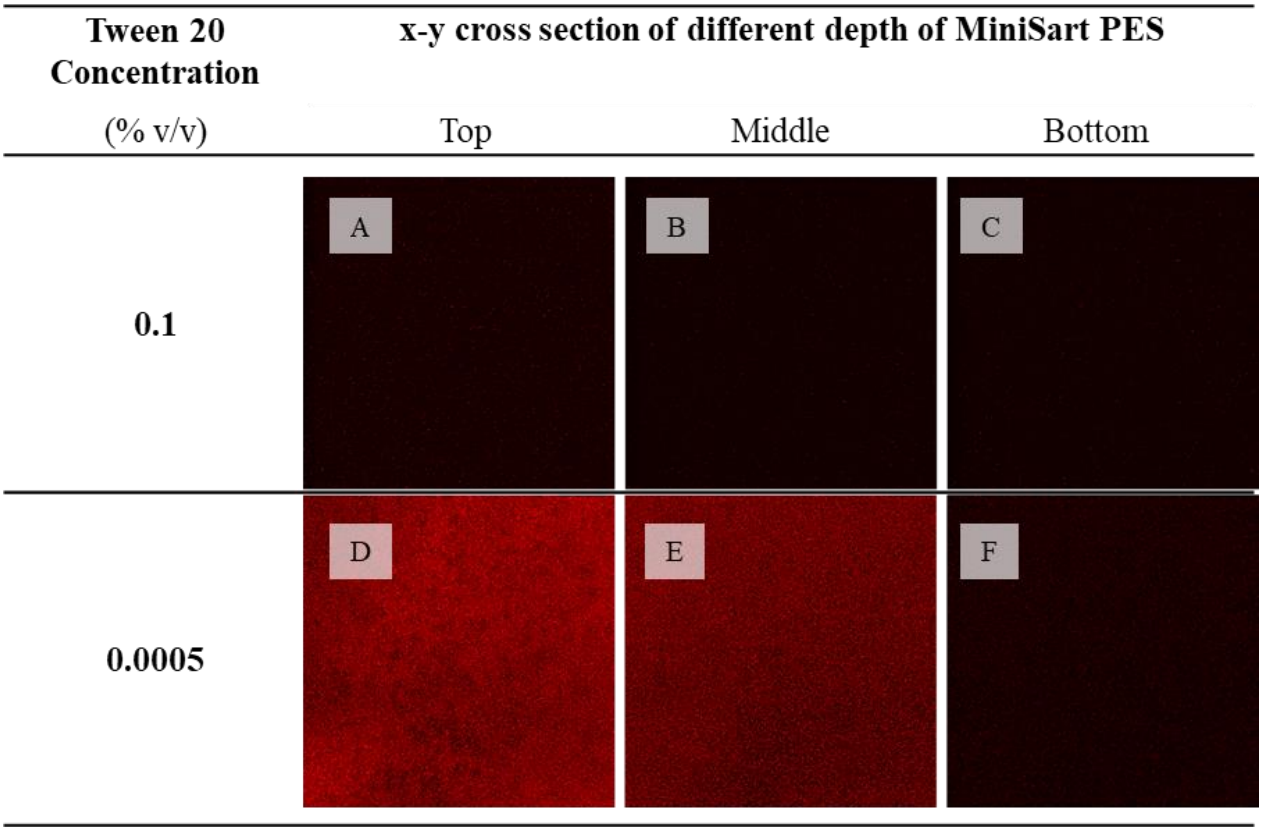

Figure 2.9 CLSM images of the MiniSart PES membrane after filtering 0.01% w/v of 188nm PNPs suspended in buffers containing two different Tween 20 concentrations (i.e. 0.1 and 0.0005% v/v). Panels (A) and (D) are the images obtained at the membrane surface (i.e. 'top'). Panels (B) and (E) are the images obtained at a depth of approximately 50 μm from the top of the membrane (i.e. 'middle'). Panels (C) and (F) are the images obtained at a depth of approximately 120 μm from the top of the membrane (i.e. 'bottom').

2.4. Conclusions

The results presented in this study clearly demonstrate that adding a nonionic surfactant to a PNP solution will cause a shift from full retention to complete transmission during the dead-end MF of PNPs that are smaller than the pore size of an MF membrane. Similar findings have been reported in a study that used an anionic surfactant (i.e. SDS) and GNPs to determine the pore-size distribution of virus filters [61]. Hence, rejection and fouling development can be easily controlled, as the fouling behavior of the PNPs is demonstrably related to both particle-particle and particle-membrane interactions. It has also been shown that membrane chemistry and morphology can

significantly influence the transmission behavior of any particle, regardless of its nature (e.g. biological or non-biological).

Pore-size measurement and characterization seem to be a big challenge in membrane-based separation and purification studies and scientific works since manufacturers determine these specifications using different techniques, which they do not disclose to the public. Considering that, this poses a controversy, as these specifications will directly affect the performance of membranes with the same rating and material because different manufacturers used different techniques to rate their membranes. For example, the differences between results shown in this study and previous works conducted by Simonetti and Schroeder (1986) and Lee et al (1993) on transmission of particles using high concentration of surfactant (i.e. both nonionic) indicates the importance of further research in order to develop a universal method for determining membrane pore size measurements. Moreover, it has been proved that PNPs smaller than the pore size of a membrane not necessarily can pass through the membrane due to adsorptive mechanisms that are involved in the filtration processes of PNPs in specific conditions. However, the possibility of transmission of PNPs that are slightly smaller than cut-off size of the membrane but bigger than the pore size rating exist and this can be concluded by looking into the SEM images of the membranes with pores that are bigger than specified rating by the manufacturer (i.e. 0.22 μm) and the fact that in this study, PNPs close to the pore size rating (i.e. 188 nm) could fully transmit through the membrane.

While numerous studies have used virus-filtration membranes to selectively retain virus surrogates as model impurities in the production of bio-therapeutics or other applications, such as water treatment, this study is the first to use virus-sized particles as therapeutic virus surrogates (not an impurity) in order to obtain quantitative data for the fouling propensity of membranes (pore

sizes ~ 0.2–0.22 μm). However, the solution conditions (e.g. salt concentration, pH) in which the PNPs in this study were suspended were completely different than the solution conditions of biological media in which virus particles are suspended; as such, this study's findings do not allow theoretical conclusions to be drawn regarding the reliability of using PNPs as virus surrogates for the Rhabdovirus Maraba. Moreover, the size, shape, and surface chemistry of the PNPs are different than virus particles. These limitations notwithstanding, the findings presented in this paper demonstrate the importance of particle-membrane interaction with regards to membrane fouling during the sterile filtration of biological solutions. Specifically, the results show that a slight change in surfactant concentration (i.e. Tween 20) can dramatically affect the performance of a membrane. Thus, studying the effects of adding surfactant to an actual virus solution offers a potentially fruitful line of inquiry for future physicochemical research. Another point worth noting is that all of the experiments were performed using uniformly sized PNPs (i.e. not mixture of different sizes). However, since the targeted virus (i.e. Rhabdovirus Maraba) is bullet-shaped with possible aggregates in the actual solution, it would be useful to run experiments using a mixture of PNPs in order to simulate the effect of aggregates in the early stages before moving on to gold nanorod particles, which more closely resemble the virus' shape. Nonetheless, the current study offers a very simple model for the sterile filtration of spherical viruses with dimensions that are close to those of PNPs used in this work.

Finally, all of the filtration experiments in this study were performed using the same filtrate flux (but different for each membrane), pH, PNP concentration, and surfactant type. As such, future research can build upon this research by manipulating these variables further, which could potentially lead to a more robust understanding of the fundamentals underlying the sterile filtration of viruses. Moreover, future work should give careful consideration surface chemistry and shape

when selecting NPs, as these factors are key in determining the most optimal mimic of the virus particle to be studied.

Chapter 3: Sterile filtration of protein covered fluorescently labeled NPs as virus surrogates via a high throughput automated filtration (HTAF) setup

3.1. Introduction

It has been comprehensively explained in previous chapters that there is a substantial interest in the development of virus-based therapeutics for the treatment of various diseases related to neurological, metabolic disorders and the development of OVs. OV are types of viruses that can preferentially infect and kills cancer cells. These viruses possess this ability within their nature or have been engineered to obtain this desired ability. As the infected cancer cells are destroyed by oncolysis, they release new infectious virus particles or virions to help destroy the remaining tumor and stimulate host anti-tumor immune response [76,125–127].

As stated in chapter one (see section 1.3), any step in production and purification of these therapeutic viruses must be done under GMP guidelines, especially true for sterile filtration step prior to vialing and storage of final pharmaceutical product that is highly desirable from safety and regulatory perspective [101]. However, sterile filtration of therapeutic viruses especially OVs is challenging given their larger size compared to other bio-therapeutic molecules (e.g. monoclonal antibodies, proteins, and small viruses) which results in product loss and frequent membrane replacement [106]. Many of the OVs, especially vesicular stomatitis viruses are in the size range close to the sterilizing grade filter's pore size (0.2 μm) which makes the final mandatory sterile filtration of the OVs quite challenging. Although the area of virus purification of OVs has been studied a lot, there are still areas that need to be filled by conducting further researches to fulfill the pressing need on developing new separation technologies, novel membrane materials and methods for purifying newly discovered bio-therapeutics.

In the field of separation sciences, viruses are typically regarded as an impurity that needs to be captured and removed during production of other therapeutics such as monoclonal antibodies, [102–105] and VF has been studied extensively in this field. To date, there have been only a few studies focusing on the transmission of viruses through the membranes as a final product, especially sterile filtration of viruses. One of the earliest sets of studies on transmission of viruses through MF membranes was conducted by Cliver and colleagues with a variety of membrane types in terms of their materials (e.g. cellulose nitrate and polycarbonate) and pore sizes, ranging from 0.05 to 8.0 μm from different manufacturers and their interaction with different enteroviruses and polioviruses [128–130]. Recently, Shoaebargh et al. [106] evaluated the performance of four commercial sterile filters in terms of fouling propensity and recovery of Rhabdovirus Maraba, a bullet-shaped virus (80 nm width, 150 nm length) that has been recently shown to be a promising OV candidate for cancer treatment [127]. These experiments were performed with tremendous safety procedures, complicated and time-consuming assays which all adds to the complexity of such experiments.

In spite of the fact that sterile filtration of OVs, especially new engineered therapeutic viruses (some of them has been mention in Table 1.1) should be studied profoundly, there exist many challenges associated with these experiments which makes the entire process difficult, laborious and expensive to run in the early stages. One of the most critical challenges associated with working with biological solutions, especially pathogenic to human (e.g. bacteria and viruses), is the necessity to work in biosafety laboratories and the use of special instruments that are required to run various biological assays. Moreover, there is a great need for dedicated facilities and trained technicians to run experiments in the proper designated level of biosafety laboratory along with the expenses related to produce a small amount of biological feed material for such experiments.

Therefore many studies have moved toward using virus surrogates to model the transmission behavior of actual human viruses with fewer difficulties.

Currently, bacteriophages and NPs are the most common surrogates used in separation studies. Bacteriophage also known as phage is a virus that infects and replicates within Bacteria and Archaea and cannot infect mammalian cells, and due to this fact, studies associated with working with bacteriophages have less health risks to the researchers. Bacteriophages are composed of proteins that surround the DNA or RNA genome and their structure, size, shape and surface properties are very close to viral pathogen and human viruses. Therefore bacteriophages are considered to be the most relevant surrogates to mimic and investigate the transportation and survival of human viruses in separation processes [131–133]. For example in a VF study, Bakhshayeshi et al. [105] used fluorescently labeled MS2 and pp7 bacteriophages to develop a method to directly visualize virus capture within different virus filters (i.e. Ultipor® DV20 and Viresolve® Pro) using CLSM. Similar studies have been performed by Dishari et al. [123] and Woods and Zydney [134] using bacteriophage ΦX174 to study the effect of pressure release on virus capturing during VF. Some studies have also looked into the effect of suspending solutions properties (e.g. pH or ionic strength) on filtration of these biological surrogates. In a recent study conducted by Iskra et al. [135] Phi X174 and PP7 bacteriophages were used as surrogate of neutral and acidic isoelectric point retrovirus and parvovirus in an anion exchange chromatography system that has proven to be powerful polishing step and viral clearance step in Pfizer's monoclonal antibody (mAb) platform purification process .

Although the use of bacteriophages as pathogenic human virus surrogates provided lots of discretion in terms of health risk in experimental works, unfortunately, these experiments still need to deal with the tremendous amount of expensive and time-consuming biological assays arising

from their biological nature. Moreover, since bacteriophages and pathogenic viruses are not structurally completely the same, the survival (e.g. losing infectivity due to destruction) of these biological substances in filtration processes might affect the quantitative measurements of infective particle in the filtrate. Therefore, biological or physical inactivation of the surrogate should be carefully considered in order to generate a true correlation between the transmission of surrogates and the actual pathogenic virus.

NPs are another common group of surrogates that are currently being used in filtration studies. The most important advantage of NPs as virus surrogates in compare to bacteriophages is that the quantitative assays are much easier and cost-effective. Furthermore, they can be fabricated easily to meet physical properties of pathogenic substances in terms of their sizes, buoyant densities, and shapes. Kosiol et al. [61] used virus-size GNPs with nominal diameters ranging from 5 to 50 nm in order to determine PSDs for a wide range of different commercial and non-commercial parvovirus retentive membranes in terms of their internal structure, material and surface chemistry. Within their study, they have shown that the presence of certain chemicals (i.e. surfactants) can totally change the mechanisms of retention from an adsorption to a size exclusion mechanism. This finding is also consistent with results shown in chapter two. In another study, Roberts et al. [59] used GNPs (18-25 nm) to ensure the effectiveness of removal of various sizes of enveloped and non-enveloped viruses by Kasei Planova 15N (pore size 15 ± 2 nm) filters that the manufacturer of factor IX (i.e. coagulating protein) concentrate REPLENINE®-VF (i.e. a medicine for treatment and prophylaxis of bleeding in patients with hemophilia B) has developed.

Therefore it has been determined that NPs are the most suitable surrogates that can be used in filtration studies by solving the technical and operational challenges of working with actual viruses at a reasonable cost. Moreover, given the advances in the field of nanotechnology and

colloid science, the use of NPs has also gained widespread interest in separation studies. In this field, NPs has also been used enormously for many years in various applications including studies related to membrane-based separation technologies [47,50,52,55,56,59,60] or performance evaluation of chromatography [42,43] systems and other separation processes for variety of reasons which has been explained by detail in the previous chapters (see section 1.2 and 2.1). However, the motivation of using NPs as virus surrogates is more interesting for us since it provides a great opportunity to reduce the expenses and difficulties associated with working with actual biological pathogenic solutions and also helps us to better understand different aspects that affect the filtration of actual virus particles [49,57,59,60,136,137]. For example, Antony et al. [57] used citrate stabilized silver NPs as MS2 bacteriophage surrogate in order to assess a challenge test for 0.04 μm PVDF hollow fiber UF membrane due to limitations of incorporating membrane challenge tests with actual viruses in a full-scale plant. They have proved the suitability of citrate-stabilized silver NPs as virus surrogates in terms of shape, size, rigidity, charge, and ease of detection and also it's potential to be an alternative indicator for challenging UF membranes for validation purposes. Advances in the production of NPs with unique properties (e.g. fluorescently labeled), shapes and materials have also given the opportunity to study the performance of different membranes in very unique and comprehensive ways. For instance, Zydney and colleagues have established a new approach using advanced microscopy techniques to image the spatial distribution of NPs within the internal structure of the membranes [105,123,138]. In one of their studies, fluorescently-labeled NPs of different sizes (20, 40 and 100 nm) as virus surrogates were used to study the internal pore structure and virus capture behavior within different virus filters by using CLSM [124].

However, the use of NPs in filtration experiments as biological surrogates should be performed with careful considerations to be able to confirm the validity of any correlation between the acquired results and the results obtained from filtration of actual native viruses. This is due to the fact that general mechanisms of retention or transmission of particles through the membrane filters are determined by a large number of factors (e.g. surface charge, pH value of the solution, salt concentration) and unfortunately surrogates and virus particles have some important and critical dissimilarities. Many studies have questioned the potential of using NPs as virus surrogates due to differences in their physicochemical properties, mostly stemming from differences in their surface properties (see Figure 3.1).

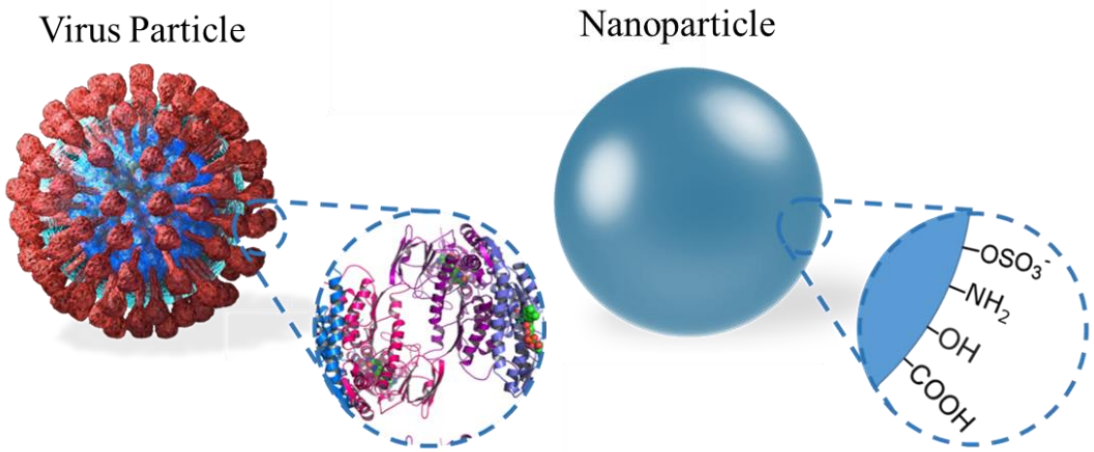

Figure 3.1 Differences in the surface properties of virus particles and synthetic NPs.

There are studies that clearly stated that NPs are poor surrogates for studying the transportation of virus particles due to the dissimilarities of their surface structure. For instance, Pontius et al. [49] used 26 and 67 nm fluorescently labeled microspheres for challenge studies of a variety of hydrophilic and hydrophobic MF (pore size of 0.22 μm) and UF membranes (100 kDa cutoff) and compared their results with filtration of MS2 and PRD1 bacteriophages. They have concluded that inconsistent results may yield if surface charge and other characteristics are not

considered properly. Similar to results obtained by Pontius et al. (2009), Harvey, et al. [139] investigated the transportation of indigenous bacteria through sandy aquifer sediment and compared the results with bacteria-sized (0.2-1.3 μm) microspheres having different surface groups (i.e. carboxylated, carbonyl and neutral). They have discovered that surface characteristics had the greatest effect on transportation of microspheres and were substantially different from the transport behavior of indigenous bacteria. In another study which has also been mentioned in the previous chapter, Helling et al. [53] used both biological (bacteria and PP7 bacteriophage) and non-biological particles (polystyrene) in a filtration study in order to compare the pressure dependent behavior of different particles in porous PES membranes based on their deformability. Their results indicate that some biological substances are easily deformable due to the nature of their structure and can squeeze through the membrane as the TMP increases over the filtration process.

Thus, the resemblance of NPs as pathogens (e.g. viruses) can be questioned in different ways. Yet, it is important to remember that although the use of NPs as virus surrogates may not fully represent the nature of actual virus solution and virus particle, it is useful to obtain important preliminary insights over different factors affecting the performance of a filtration process. With this being said, many studies have moved toward modifying the surface of NPs in order to make a better resemblance of a pathogenic surrogate in separation studies [44,45,140,141]. Generally, viruses consist of a protein capsid which covers the RNA and DNA within their structure, hence the surface charge and chemistry of a virus can be mimicked easily by coating NPs with the same protein or proteins that have similar properties (e.g. similar pH_{PZC}[1]) to the virus of interest [140].

[1] The point of zero charge

In order to properly modify the surface of surrogates (i.e. NPs) to match the surface properties of an actual pathogen of interest, a detailed study on the surface chemistry of the native pathogen is needed. It is noteworthy to mention that after modifying the surface of the NPs by coating protein, the transmission is no longer affected by the properties of the NP material and is a function of the protein properties. Pang et al. [45] have investigated the transportation of rotavirus and adenovirus in sand media using DNA-labeled, protein-coated silica NPs. They covalently coated 70 nm size silica NP with specific proteins and DNA markers for sensitive detection. Their results indicate that protein-coated NPs are promising potential new surrogates for studying virus retention in porous media. In another study conducted by Iyer et al. [44], 100 nm latex influenza virus surrogate coated with BSA protein were used to develop a method for flow-through purification of viruses using a combination of binding and size-exclusion chromatography. Their results show that BSA coated latex NPs make a good model for viruses since they have size and charge similar to common viruses such as influenza virus and herpes simplex virus.

Although Pang et al (in a series of studies) [45,140,141] and Iyer et al.[44] emphasized the effect of surface modification of NPs on their transmission behavior, these experiments were performed by coating the microspheres by the desired protein and re-suspending the coated NPs in a protein-free solution in the process. Additionally, none of these studies focused on the use of MF sterilizing-grade membranes with a 0.2 μm pore size rating. It is noteworthy to mention again that the interest in filtration experiments using MF membrane is due to its enormous use in the final sterile filtration step during the manufacturing of numerous therapeutic viruses that are currently being developed for the treatment of infectious diseases and cancer. While the author acknowledges all these studies, the objective of the present study is to produce detailed analyses of the transmission of fluorescently labeled PNPs suspended over a range of BSA concentrations

(as an additive to the NP suspension solution) through a commercial MF membrane. It should be noted that the 0.22 μm Durapore PVDF MF membrane used in this study is the same as the one used in the recent Rhabdovirus Maraba sterile filtration study [34] and the previous work explained in the second chapter. The sizes of the PNP used in this study (i.e. 189 nm) is chosen based on the challenging dimension (i.e. length) of the Rhabdovirus Maraba's unique bullet-shaped (80 nm width, 150 nm length) which is close to the pore size of sterilizing-grade membranes with a 0.2 μm pore size rating [37] and also the size of different spherical OVs that are currently on their way passing the clinical trials. In order to develop a fundamental understanding of the BSA effect as an additive and also a coating agent, a set of constant-flux dead-end filtration tests were run within this study. Also, new MF membrane was used in each experimental condition for each filtration test in order to account for any potential variations in membrane properties. TMP was continuously monitored and multiple post-filtration analyses were conducted, including measuring changes in the membrane's hydraulic permeability, capturing images of the membrane's surface using SEM. Furthermore, each experimental condition was tested in triplicate using a new high throughput automated filtration (HTAF) system which will be explained later in section 3.2.3.

3.2. Experimental

3.2.1. Membranes

Durapore PVDF sterile membrane filter discs with 13 mm diameter and pore-size rating of 0.22 μm Millipore were obtained for this study. Membranes were single-layer and placed in reusable polycarbonate filter holders (Sartorius) specifically designed for disk filters with 13 mm diameter to make a complete filtration unit. A silicon gasket was used in order to seal the unit from any leakage during filtration and thus the effective filtration area of 0.5 cm^2 is determined by the gasket. In order to examine pore structure and morphology of the membranes, fresh membrane

filters were imaged via SEM. For SEM imaging, the membranes were mounted on specimen carriers and gold sputtered for 1.5 minutes under vacuum conditions with a current of 20 mA. Pore structure, morphology, and distribution of membrane filters were identical to the Durapore PVDF syringe filters from the previous study in the second chapter. Figure 3.2 shows the complete membrane filtration unit and the SEM image of the top surface of the 0.22 μm PVDF membrane. By looking into SEM images of the top surface of the membranes, once more, pores with dimensions significantly greater than 0.22 μm were observed, which theoretically is a concern due to the possibility of transmission of PNPs larger than 0.22 μm through the membrane.

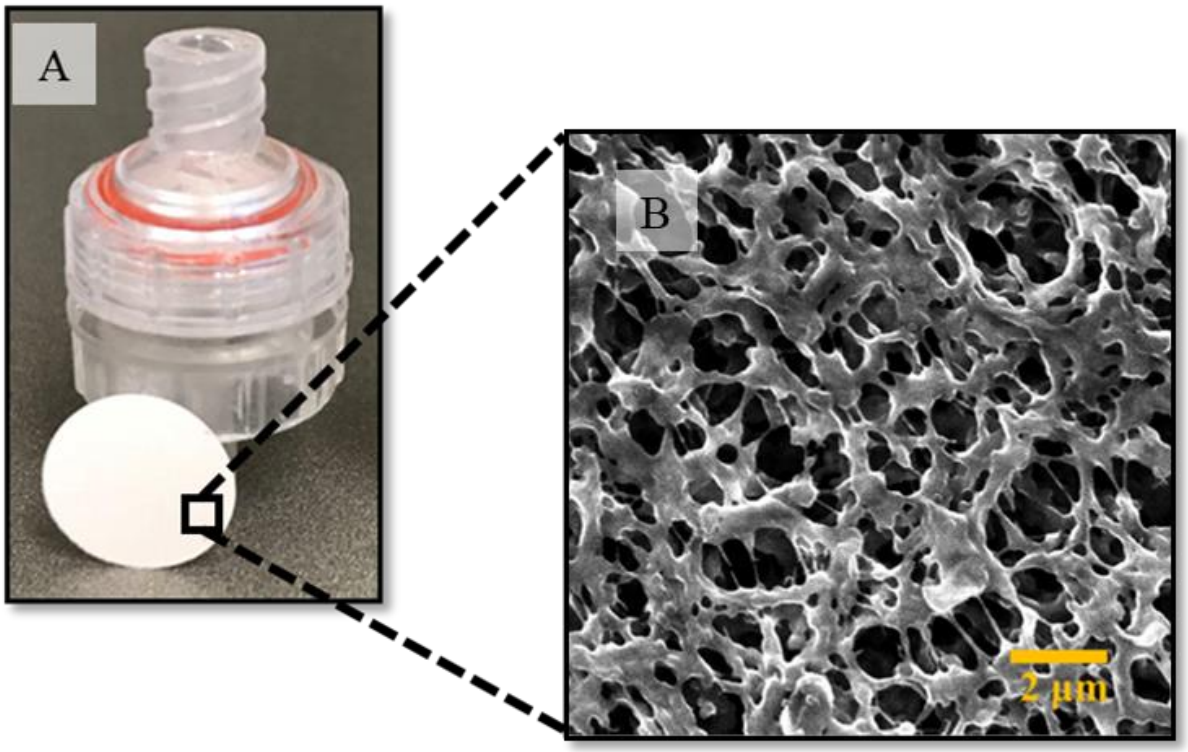

Figure 3.2 Panel (A): the membrane filter and the filter holder; Panel (B): SEM images of the top surface of the commercial Durapore PVDF sterile membrane filter (9,000 × magnification).

3.2.2. Polystyrene nanoparticle (PNP) solutions

A 0.5 M solution of pH 9.5 carbonate buffer (Alfa Aesar) was diluted to 0.1 M with ultrapure water (resistivity greater than 18.2 MΩ.cm) from a Milli-Q system. Sodium azide (purity higher than 99.5%, ReagentPlus®, Sigma-Aldrich) was added to achieve a final concentration of 0.1% w/v. Finally, BSA (purity higher than 98%, BioShop) was added to achieve a final concentration of 0.5 mg/mL. This stock solution was then serially-diluted with a BSA free carbonate-azide solution to three additional buffer solutions with BSA concentrations (mg/mL) of 0.05, 0.015 and 0.005 and filtered through 0.22 μm PVDF syringe filters to make a homogenous buffer solution and stored in the fridge. Suspending buffer solution containing two other protein were also prepared by adding Lysozyme (purity higher than 90%, Sigma-Aldrich) and α-Lactalbumin (purity higher than 85%, Sigma-Aldrich) to a final concentration of 0.5, 0.05 mg/mL using the same method.

Fluorescently labeled PNPs were purchased from Spherotech. The reported size ranges of these PNPs are provided in Table 3.1. The PNP solutions used in the filtration experiments were prepared by diluting 140 μL of the as-purchased solutions 100-times by volume to a final volume of 14 mL with the corresponding buffer solutions in order to obtain a final PNP concentration of 0.01% w/v. 13.5 mL of the solution was used for three separate simultaneous filtration experiment (4.5 mL PNP solution for each filtration run) and the remaining (0.5 mL) was used as a reference to compare the quality of the filtrate with the feed as a function of fluorescent intensity. After suspending the PNPs in the suspending buffer solutions all the PNP solutions vortexed several times and placed on a rocking tray for 10-15 minutes following one hour ultrasonication (using BRANSON 2800) in order to disaggregate PNPs that are possibly attached together in the process of solution making.

In order to verify the monodispersity of the PNPs, the as-purchased stock solution was diluted to 0.01% w/v with the free protein carbonate-azide buffer and ultrasonicated for one hour and then analyzed using DLS via a Zetasizer NanoZS (Malvern). The position of the laser attenuator was set at 173° relative to the laser source in order to ensure backscattering detection during DLS analysis. The reported sizes (including Table 3.1) are the average of three separate DLS measurements and the value of each measurement is the mean of particle size of 5 sub-measurement runs for the duration of 100 seconds. Later, the particle size distribution of PNPs in different buffer solutions as a function of protein (i.e. BSA) concentration were also performed using the same method to investigate any size change due to adsorption of BSA to the surface of PNPs.

Table 3.1 Properties of the fluorescent PNP used in this study.

Reported NP Size[1](nm)	**Measured NP Size[2] (nm)**	**Excitation Wavelength (nm)[3]**	**Emission Wavelength (nm)[3]**	**Number Concentration of Particles in 1.0% w/v Solution ($\times 10^{12}$)[4]**	**Total Surface Area of 1ml of 1.0% w/v Solution (cm^2)[5]**
100-300	189 ± 43	485	535	2.7	3023.4

[1] As per manufacturer

[2] In buffer with no protein

[3] Excitation and emission wavelengths used for detection with the Spark 10M microplate reader (TECAN).

[4] Calculated, as per the manufacturer's suggestion, according to $N = (\frac{6W}{3.14PD^3}) \times 10^{12}$ where N is the number of particles, W is the weight of the polymers (g), P is the density of polystyrene (1.05 gcm^{-3}), and D is the measured diameter of the particles (μm) using DLS.

[5] Calculated, as per the manufacturer's suggestion, according to $S = (\frac{6W}{PD}) \times 10^4$ where N is the number of particles, W is the weight of the polymers (g), P is the density of polystyrene (1.05 gcm^{-3}), and D is the measured diameter of the particles (μm) using DLS.

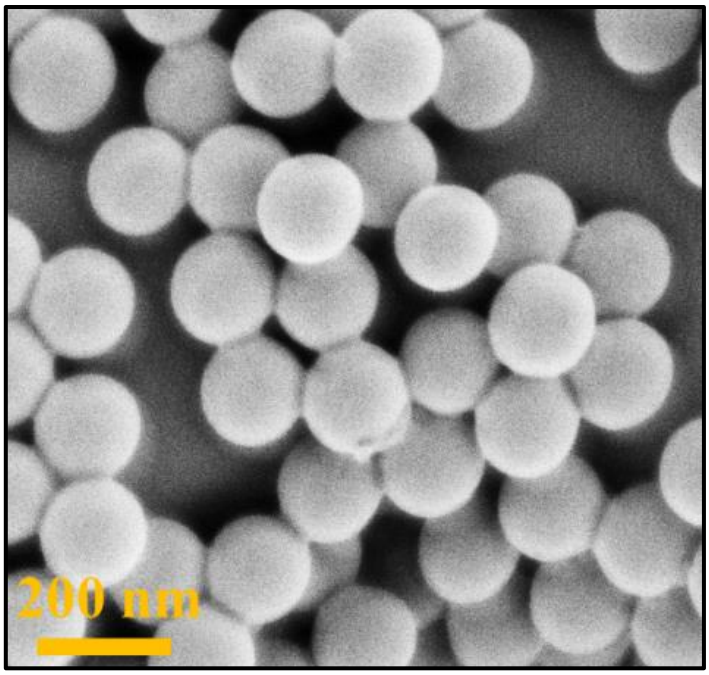

Figure 3.3 SEM images of the bare (not covered with protein) spherical PNPs (200,000 × magnification)

The zeta-potential measurement was also performed in order to investigate the changes of the surface charges of the PNPs suspended in different buffer solutions as a sign for protein adsorption on the surface of PNPs. After preparation of the PNP solutions following the method described above, 1 mL of the PNP solution transferred into a standard-sized cuvette and the zeta-potential of the aqueous solution was measured via Zetasizer NanoZS (Malvern) equipped with universal 'dip' cell kit. SEM images of the PNPs shown in Figure 3.3 were obtained by inoculating the PNP solution (suspended in the protein-free carbonate-azide buffer) on a flat clean substrate and gold sputtered using the method described in section 3.2.1 for the SEM images of the membranes. As shown in the SEM image, PNPs are monodispersed and spherical.

3.2.3. Filtration Experiments

Constant-flux filtration experiments were performed using the experimental setup shown in Figure 3.4 and B1. The experimental setup consisted of three main parts, 1) the flow generator, 2) the high throughput filtration module and 3) the automated sampling section. A PHD programmable syringe pump (Harvard Apparatus) was used to generate a constant flux which pushes the PNP solution filled inside three separate 5 mL syringes through separate Teflon tubing (1.58 mm outside diameter) toward the filtration module. The high throughput filtration module consists of three internal channels similar to the previous study (see section 2.2.3) but individually separated (not connected) from each other, machined on an Acetal (polyoxymethylene copolymer) block (70 × 70 × 25 mm) with proper fluidic connectors on top to receive the constant flow of PNP solution. During filtration, the PNP solution passed through the internal channels, filter holders and the membranes inside—which both together served as a unit— that is connected to the module via a Luer-lock adapter outfitted on the bottom of the block. Meanwhile, during filtration, there separate PX409 pressure transducers (Omega Engineering) on the sides of the module and perpendicularly connected to the channels, constantly monitored and logged the TMP signal on a laptop. In order to investigate the quality of the filtrate in terms of the number of PNPs that could pass through the membrane at different conditions, the filtrate was directed via Teflon tubing to sampling section and samples were tested for their fluorescent intensity using TECAN microplate reader.

The automated sampling section is designed based on the exploitation of unique abilities of 3D printers in precise and accurate movements in three dimensions. As explained in the previous chapter, filtrate samples were collected manually by moving the 96-well microplate under the

syringe filters during the long period of filtration process and collecting filtrate droplets. This process was a labor-intensive approach, hence the design and strategy have been improved to a more efficient system in terms of productivity (high throughput module) and time-saving (automated sampling device). This system is carefully and accurately designed in order to ease the sampling process of three simultaneous filtration experiment and dispense the filtrate samples in a 96 well microplate during the filtration automatically. Basically, the automated sampling section use a 3D printer (Monoprice Maker Select Plus 3D Printer) in its core structure which has been modified at the nozzle (i.e. the moving part in x and z-direction) of the 3D printer to be able to attach the three filtrate tubing branched out from the bottom of the filter holder. On the nozzle of the 3D printer, the three filtrate tubing were also connected to dispensing needles from Becton Dickinson and carefully placed on the modified section to accurately dispense the filtrate droplets onto the 96-well microplate located on the moving stage of the 3D printer (i.e. the moving part in the y-direction). The 3D printer was programmed by G-code [2] in order to move the modified nozzle and the moving stage—with the 96-well microplate mounted on it—in different directions according to the coding. For the purpose of the work, at the beginning of the filtration, the nozzle was placed on top of the 96-well microplate such that needles positioned exactly on top of the first three wells in different rows of the microplate. After filtration starts, the 3D printer follows the pattern of movement which has been programmed (using G-code) and described before to the 3D printer so that the needles will fill up the wells of the microplate in each row and will move to the next three wells until the end of the filtration. The G-coding consists of coding loops to move the modified nozzle slightly (1mm) upward and downward (in the z-direction) at a fixed x and y location (on top of the well) in order to fill the wells. Since the filtration experiment is running in

[2] Numerical control programming language

a constant flux mode, the loops were repeated several times in order to fix the location of the nozzle on top of the well, until the well is fully filled (about 300 µL). More details on the pattern of movement and the coding has been added to the appendices at the end of this chapter (see Figure B3 and the following page for the pattern and the G-code). To best of the author's knowledge this approach has never been used in any published literature, hence it is a very novel, unique and inexpensive (in order of hundreds of dollars) but very accurate technique for online sample collection. Although there exists commercial linear actuator in the market that can move a microplate reader under the filtration module to collect samples in the 96-well microplate, these linear positioning slides and actuators are very expensive (in order of thousands of dollars) and can just move in one or two directions. Note that each condition (i.e. different buffer solution) was tested simultaneously in triplicate by the aid of the HTAF setup described above and in each test, a brand new PVDF membrane filter was used for every individual filter holders. The membrane in each filter holder was wetted by passing approximately 20 mL of the same buffer solution used for filtration through the membrane in 5 mL increments, alternating from front-to-back to back-to-front for each 5 mL injection. The membrane's pre-filtration hydraulic permeability, L_P (mL.s^{-1}.m^{-2}.Pa^{-1}), was determined using Equation (3.1):

Eq. 3.1
$$L_p = \frac{J}{TMP}$$

where J represents the flux of the buffer solution (mL.s^{-1}.m^{-2}). The flux can be calculated as the flow rate divided by the effective membrane area. Permeability measurements were made for six randomized flux values (between 16.66 and 150 mL.s^{-1}.m^{-2}) and repeated twice in order to check the reproducibility of the TMP within each flux. The flux-TMPs were plotted for all permeability measurements, and a highly linear relationship ($R^2 > 0.95$) was observed.

After the permeability test was complete, the syringes containing the buffer solution was replaced with a standard 5 mL syringes that had been pre-filled with 4.5 mL of the PNP solution. The PNP solution was then passed through the membrane at a constant flux of 50 $mL.s^{-1}.m^{-2}$. The filtrate was continuously collected as 300 µL samples in each three wells of a flat-bottom 96-well microplate (Greiner Bio-One) from the needles attached to the modified nozzle. As explained earlier, in order to fill each well with exactly 300 µL filtrate, the 3D printer was programmed to stay still on top of each well for 2 minutes which was determined by the flow rate (150 $\mu L.min^{-1}$). After the completion of the filtration experiment, the filter holders were disconnected from the module and the 'dead volume' above the membrane was manually discarded using a pipette. Later, the membranes were washed several times by passing the same buffer used for suspending the PNPs (free PNP buffer) in order to remove any loosely bounded PNPs in case if there exist any. The Teflon tubing and the internal channels of the material filtration module were also extensively washed to remove any residual PNPs. Finally, the filter holders were reconnected to the module and the membrane's post-filtration hydraulic permeability was measured using the same procedure described above. After the filtration is finished, the concentration of PNPs in the filtrates as a function of fluorescent intensity was determined by transferring 135 µL of the filtrate collected in the 96 well microplates to a flat-bottom, black, 96-well half-area microplate (Corning) and measured using Spark 10M microplate reader (TECAN). Details have been described in the previous chapter (see section 2.2.3). After the post permeability data acquisition, the filter holder was carefully opened in order to take out the membrane for SEM imaging. The SEM images of the top surface of the membranes were taken using the same method described earlier in this chapter (see section 3.2.1) and second chapter (see section 2.2.1).

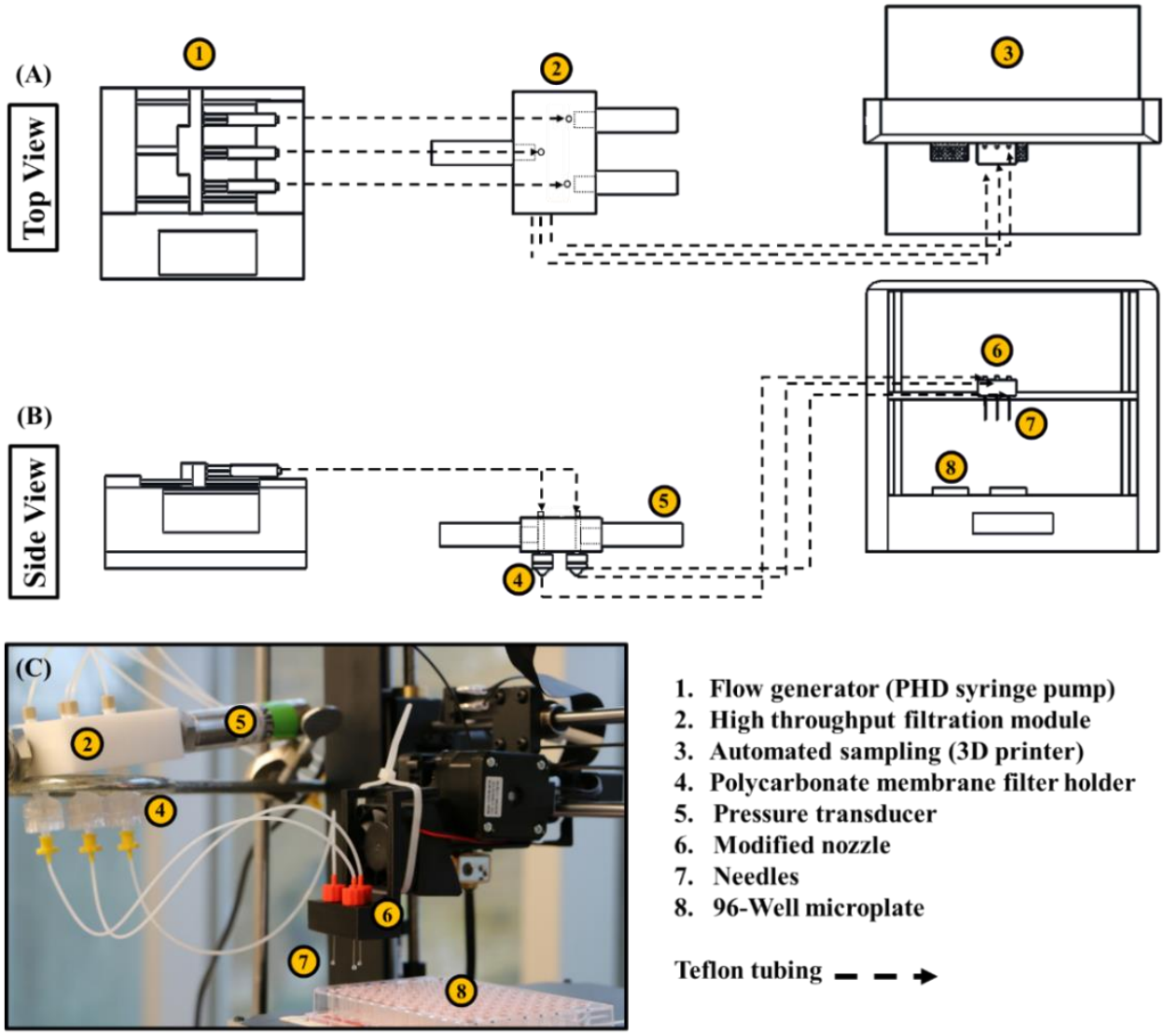

Figure 3.4 Schematic of constant-flux filtration setup, (A) top view, (B) side view and (C) Actual HTAF setup.

3.3. Results and Discussion

3.3.1. DLS and Zeta-Potential

In order to evaluate particle size distribution, the DLS analysis was performed on PNP solutions suspended in BSA free carbonate-azide buffer. As shown in Figure 3.5A, the DLS results for the prepared PNP solution showed only a single peak, with size distribution of 189 ± 43 nm.

The results from particle size distribution matches with the results from the previous study for the selected size of the fluorescently labeled PNP. The DLS results show that the PNP solutions were stable (due to steric stabilization) with no secondary peak due to particle aggregation. The stability of the PNP solution also did not change during the filtration process. This can be realized by the fact that the DLS analysis were also not performed right after solution preparation and took approximately 20-30 minutes from preparation until DLS measurements were performed. Particle size alteration of PNPs in different buffer solutions as a function of protein (i.e. BSA) concentration were also performed. Interestingly, the results are shown in Figure 3.5B clearly demonstrates the sizes of PNPs increased by adding more protein (i.e. BSA) in the suspending buffer. This increase is undoubtedly due to the adsorption of proteins molecules onto the PNP's surface. The adsorption mechanism is believed to be mainly through hydrophobic interaction between BSA and PNPs [142,143]. However, the effect of electrostatic interaction, among other types of interactions (e.g. van der Waals interactions and hydrogen bonds) on adsorption of the protein molecules should not be completely neglected. For example, although the PNPs and BSA molecules are both negatively charged at the working pH 9.5, and it is expected to not observe any attraction/adsorption from two negatively charged particles due to repulsive forces, but BSA molecules are strongly bounded onto the PNP's surface. Along hydrophobic interaction, this can also be due to the fact that the BSA molecule has different positively charged fragments that can possibly be oriented toward the adsorption surface and passively attach to the negatively charged surfaces. In a study conducted by Jachimska et al. for investigating the structure of BSA adsorbed on silica and mica surfaces, their results showed a significant amount of adsorption of BSA on

silica and mica surfaces over a wide pH range whether the protein is charged positively, negatively or when it is neutral [144,145].

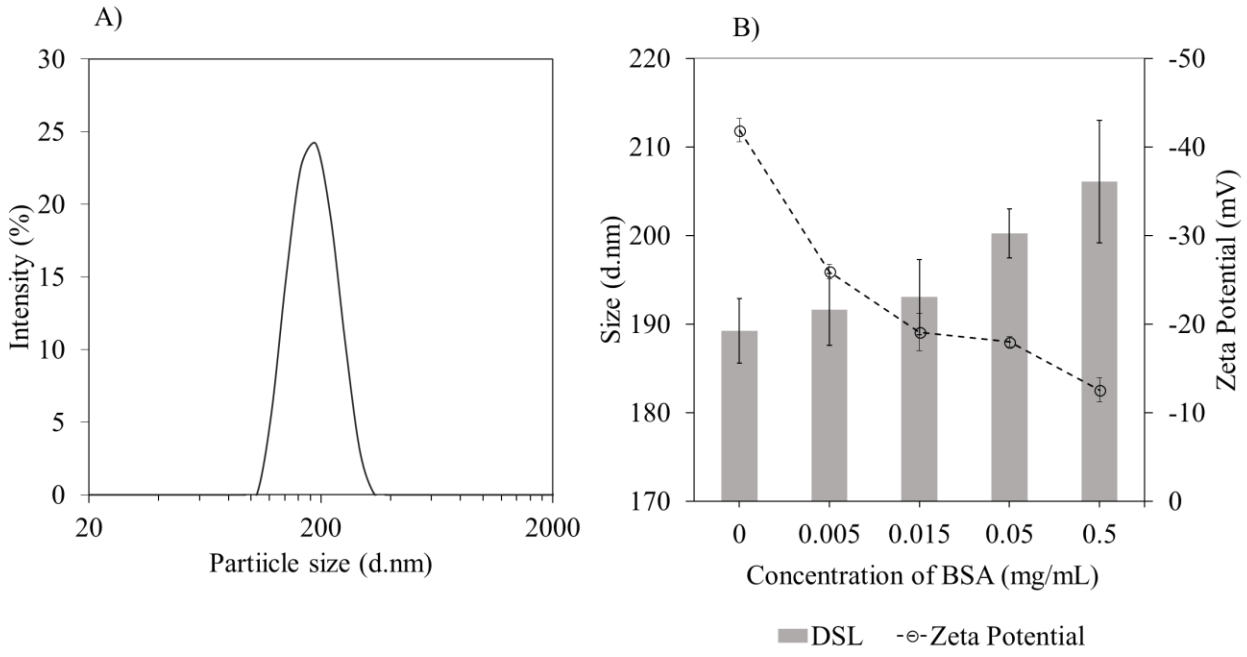

Figure 3.5 Panel (A): Size distribution of PNPs suspended in BSA free carbonate-azide buffer; Panel (B): Particle size and zeta potential of the PNP solution as a function of BSA concentration in the suspending buffer. Results are reported as the average of three separate measurements and error bars are the standard deviation calculated for the triplicate tests.

Based on the information provided by the manufacturer of the PNPs, sulfate groups are dominant functional groups on the surface since the manufacturer has used sodium persulfate as the initiator during the polymerization process. The zeta-potential measurement of no protein solution shown in Figure 3.5B also confirms the existence of negatively charged surface with zeta-potential of -42 ± 1mV for bare PNPs, which is probably due to the existence of SO_4^{2-} groups. The zeta-potential measurement was also performed for PNPs suspended in different buffer solutions and the results (shown in the same figure) indicates a reduction of zeta-potential by increasing the concentration of BSA in the suspending buffer. This attributes to adsorption of BSA on the surface

of PNPs which covers the SO_4^{2-} groups under the protein layers and creating another layer on the surface of the PNPs with a different value of negative charge determined by negatively charged protein. Figure 3.6 is a schematic demonstration of the process of the adsorption of BSA onto the surface of PNPs resulting in an increase of particle size and reduction of the zeta-potential of the PNP solution.

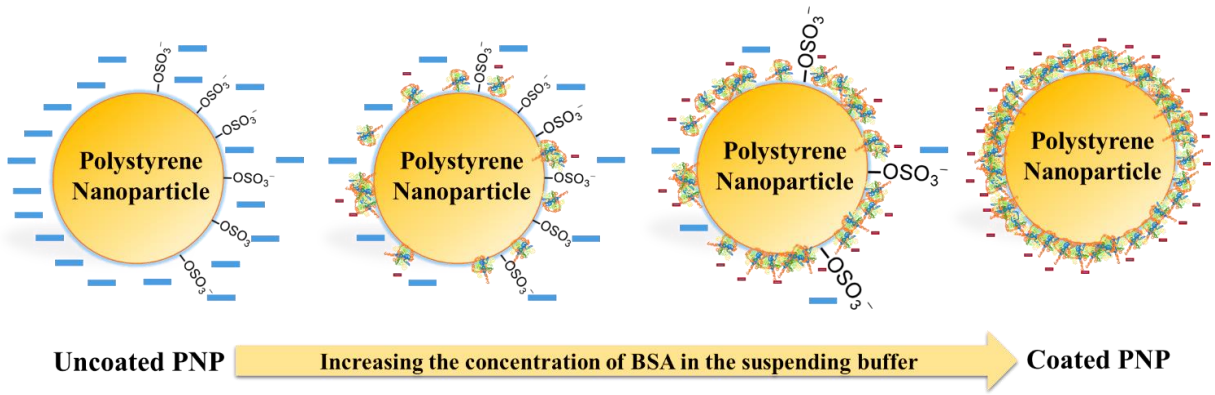

Figure 3.6 Schematic of the BSA protein adsorption onto the PNP's surface.

The adsorption of the BSA onto the PNP's surface is believed to be irreversible and the protein molecules are immobilized covalently onto the surface. This can be interpreted from the fact that even the harsh environment of one hour ultrasonication in the process of solution making didn't affect the adsorption and BSA molecules stayed attached to the surface. The DLS results show an increase in particle size from 189 ± 3 nm to 206 ± 7 nm by increasing the BSA concentration in the sodium azide-carbonate buffer from 0 to 0.5 mg/mL. Considering the fact that protein colloids can rearrange their structure and make different molecular shapes, for BSA isomers, a compact molecular form of the BSA (i.e. N form) with an approximate size of 6 nm in diameter is expected in the working pH [146,147]. An increase of approximately 18 nm of the PNP size which is three times higher than the approximate size of the BSA molecule (in the N form), suggests that there might be some secondary protein layer formed on top of a primary layer,

probably due to an excessive amount of protein molecules in the solution. However, the relatively big error bars in the highest concentration of BSA in compare to other DLS results also can be due to the low stability of the second layer which is in an attaching-detaching state.

The same trend of increase in the particle size and decrease in zeta potential of the PNP solutions were observed for the solutions containing 0.5 and 0.05 mg/mL α-Lactalbumin in the suspending buffer (shown in Figure 3.7). α-Lactalbumin in the working pH (9.5) is negatively charged (pH_{PZC} of 4.2) therefore, as explained earlier, hydrophobic interaction between the protein molecule and the PNP's surface leads to attachment of protein molecules on the surface of the PNPs. Since α-Lactalbumin, with 14 kDa molecular weight, is smaller than the BSA molecule (66 kDa), no significant increase in the particle size was observed, however, the decrease in the zeta-potential value indicates that protein molecules are attached to the surface of the PNPs.

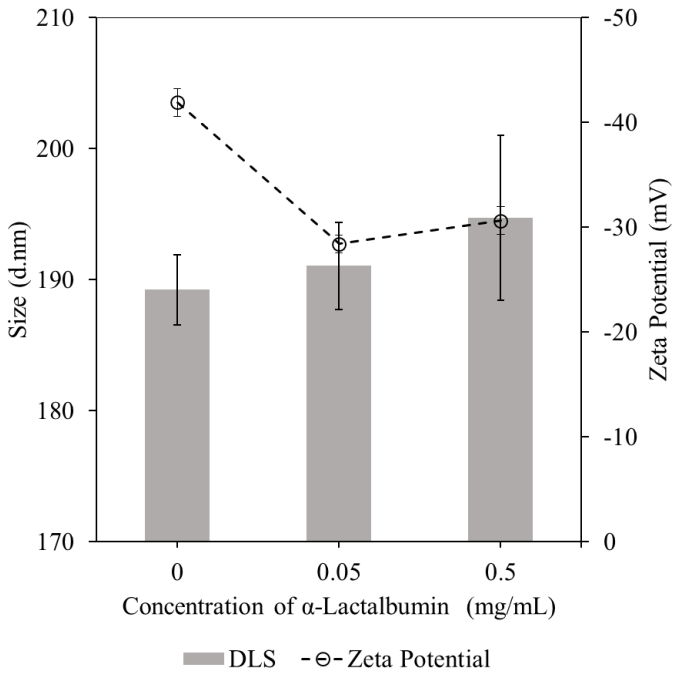

Figure 3.7 Particle size and zeta potential of the PNP solution as a function of α-Lactalbumin concentration in the suspending buffer. Results are reported as the average of three separate measurements and error bars are the standard deviation calculated for the triplicate tests.

Unlike BSA and α-Lactalbumin, the addition of PNP to the suspending buffer containing Lysozyme protein resulted in flocculation (see Figure 3.8). Lysozyme has an isoelectric point of 11.35 meaning that at the working pH 9.5, Lysozyme molecules are positively charged. At the first sight and based on electrostatic interactions rules, that negative and positive particles attract each other, and there should not be any problem in coating the PNPs with the protein molecules but, presence of positively charged proteins in a colloidal solution can result in 'patch' or 'bridging flocculation' in certain conditions. Similar results were observed with suspending buffer with 0.05 mg/mL Lysozyme. Hence, DLS analysis, zeta potential measurement and filtration experiment for this PNP solution were not performed.

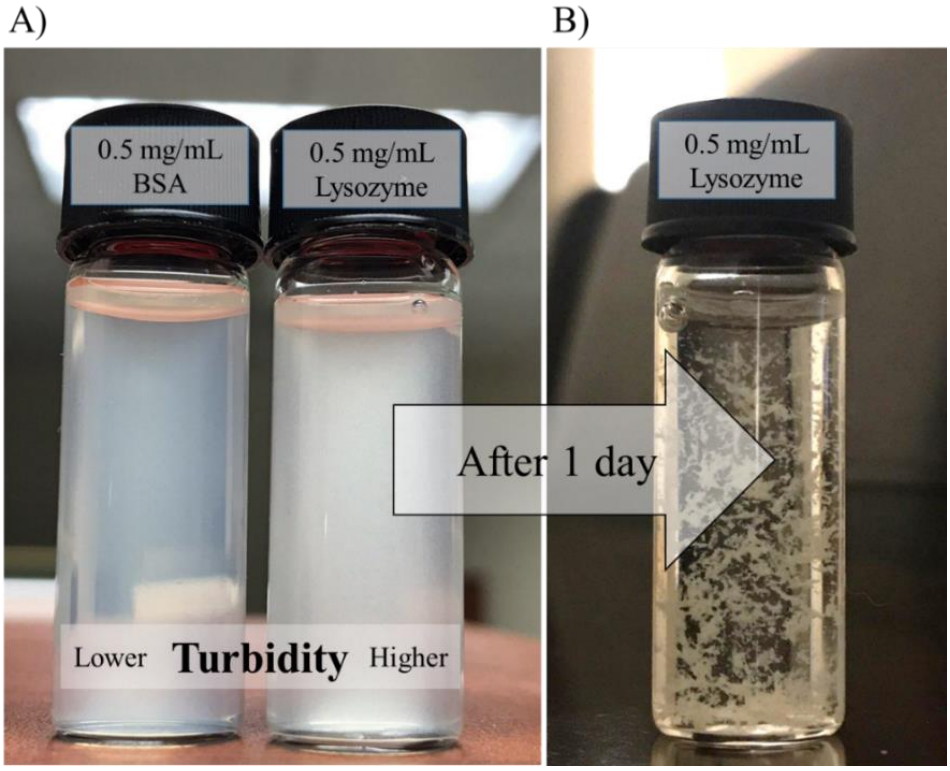

Figure 3.8 Panel (A) Picture demonstration of the difference between the PNP solution containing 0.5 mg/mL of BSA and Lysozyme in terms of turbidity (Lysozyme has a higher level of turbidity); Panel (B) Picture demonstration of flocs after one day of suspending PNPs in the buffer with 0.5 mg/mL Lysozyme.

3.3.2. Sterile filtration of fluorescently labeled PNPs

Transmission of PNPs through 0.22 μm sterile PVDF filters were quantitatively compared as a function of BSA concentration (no BSA, 0.005, 0.015, 0.05 and 0.5 mg/mL) in the suspending buffer. Figure 3.9 shows the fluorescent intensities of the filtrate samples—which were automatically collected in the 96-well plate using the modified 3D printer and high throughput module—relative to the fluorescent intensity of the feed (using the 0.5 mL extra solution prepared in the beginning) used for filtration of the PNPs. The results for each condition were shown in terms of relative fluorescent intensity (relative to its own feed) in order to make a fair comparison between different solution conditions. To put it in a nutshell, a filtrate sample with a normalized fluorescent intensity of exactly 1 has fairly the same number of PNPs as the feed solution used during filtration of the three separate trials. Note that, any decrease in a sample's normalized fluorescent intensity in the proposed dead-end filtration process is due to the retention or capture of the PNPs by the membrane. It should also be mentioned that at the beginning of the filtration process, PNPs are being diluted by the preexisted buffer (from pre-permeability measurement) inside the channels, tubing and dead volume of the filter holders, hence low fluorescent signals were detected/measured by the TECAN plate reader. Moreover, each experiment was performed in triplicates using the HTAF system and different data sets in each panel correspond to the three separate simultaneous filtration experiments. Excellent reproducibility of results in each condition is clearly observed from the results. The results in the Figure 3.9E evidently shows that PNPs suspended by carbonate-azide buffer containing 0.5 mg/mL BSA in the suspending buffer, transmitted completely through filtration of 4.5 mL of the PNP solution. In the second chapter, it has been mentioned that complete transmission of 188 nm PNP through 0.22 μm pore size membranes is surprising due to the fact that the diameter of the PNPs was close to the pore size

rating of the membrane. However, in the current work, the complete transmission of the PNPs through the membrane turns to be a bigger concern since, at the highest concentration of the BSA inside the suspending buffer, the diameter of the PNPs have been increased to 206 ± 7 nm and yet full transmission is still being observed. By another look into the SEM images of the top surface of the PVDF membrane (Figure 3.2B), there exists a considerable number of pores that are smaller than the BSA covered PNPs which are expected to capture/retain a fair number of PNPs within its structure. However, it is clearly evident that the complete transmission of PNPs is due to the existence of many other pore sizes greater than 0.22 μm.

The collected results support previous thoughts and concerns regarding the necessity of establishing a universal standard method for pore size measurement of membranes, especially for the phase-inversion membranes with a porous structure. Currently, different techniques and methods (e.g. mercury intrusion porosimetry) are being used to measure the PSD of the membranes. Since the manufacturers are unwilling to disclose their method for determining the exact pore size of their membranes, it has been hypothesized that pore size of these membranes is most likely determined by smaller pores within the internal structure of the membrane. However, It should be noted that there is no way to give a quantitative result of the number of pores with a specific diameter in a porous membrane with certainty since many of the current techniques are based on assumptions which give us an approximate result [46,121].

Contrarily to the results for filtration of the PNPs suspended in the highest concentration of BSA in the carbonate-azide buffer, PNPs got retained/captured by the membrane during filtration when free BSA carbonate-azide were used in the PNP suspension (shown in Figure 3.9A). Interestingly, the DLS results shown in Figure 3.5A and 3.7B at this BSA concentration not only indicates that a monodispersed solution without any trace of aggregation existed (PNPs bigger

than the pore size) but also the particle size were smaller than the time when they were suspended in the carbonate-azide buffer containing 0.5 mg/mL BSA (shown in Figure 3.5B). Therefore, size exclusion has been determined to not have any effect on retention of PNPs by the membrane and has been hypothesized that the retention behavior of the membrane at this condition is most likely due to particle-membrane adsorptive interaction. By looking into the zeta-potential results, a cursory glance reveals a considerable difference between the surface charges of the PNPs from -42 ± 1 to -13 ± 1 mV (shown in Figure 3.5) in these two solution conditions.

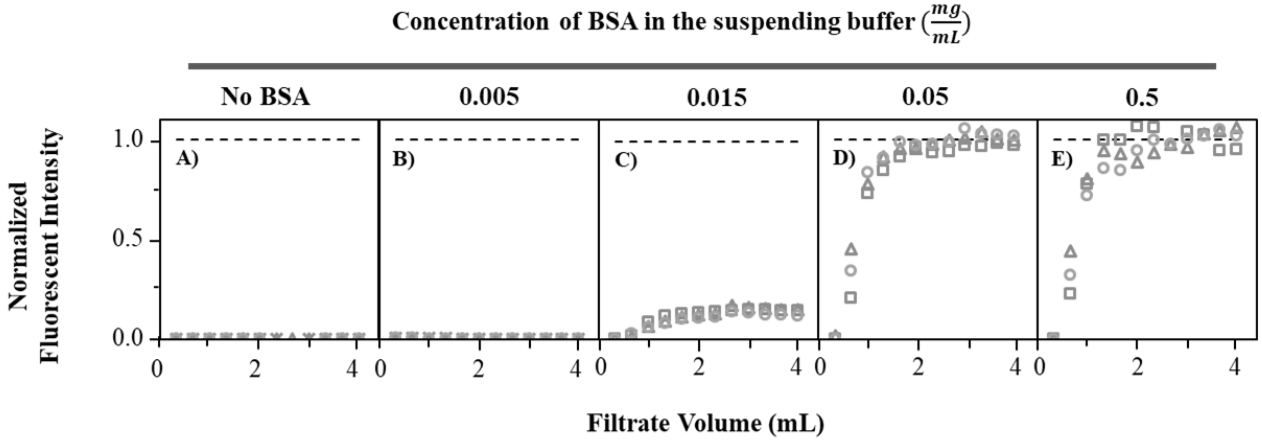

Figure 3.9 Normalized fluorescent intensity profiles for filtrate samples collected during constant-flux filtration tests of 189 nm PNPs suspended in different buffer composition by changing the concentration of BSA from 0 to 0.5 mg/mL using Durapore PVDF. The profiles in each panel are from the three separate trials that were conducted at each experimental condition are displayed by △,□ , and ○ in each panel.

By comparing the filtration results in Figure 3.9 for solution conditions between the two extreme conditions explained above, a trend of PNP transmission from full retention to complete transmission can be clearly observed by increasing the concentration of BSA. Interestingly, the particle size measurement (shown in Figure 3.5) has an opposite trend to the transmission profile since it is expected that smaller PNPs (not coated) potentially would less be retained by the membrane's pores. On the other hand, by considering the electrostatic interaction as the main

source of effect on the performance of the membranes, the results indicated a good agreement between the zeta-potential results and the fluorescent profiles. The results clearly show that by diluting the BSA concentration in the suspending buffer down to 0.015mg/mL, PNP transmission dropped off remarkably for more than 86%. Further decrease of the BSA concentration down to 0.005 mg/mL results in a complete retention by the membrane.

From the filtration results shown in Figure 3.9, transmission of PNPs through the sterile filters are clearly related to the concentration of the BSA dissolved in the carbonate-azide buffer. However, this can also be correlated to the percentage of coverage of the PNP's surface by available BSA molecules within each condition. The amount of BSA molecules needed to completely cover all of the PNP's surface can be easily calculated by the amount of BSA needed to cover the surface of one PNP, times the total number of PNPs in the solution (Table 3.1). The maximum protein adsorbed, Γmax ($g.m^{-2}$) on a surface can be calculated using the equation (3.2):

Eq. 3.2

$$\Gamma max = \frac{\frac{MW}{N_{av}}}{\pi {r_g}^2}$$

where the numerator of the fraction is the mass of one protein molecule and can be calculated by molecular weight of the protein divided by Avogadro's constant (N_{av}). The denominator of the fraction is the area covered (or occupied) per protein molecule that can be calculated by the projection area of a protein molecule (assuming spherical) using molecular weight-gyration radius[3] (r_g). Note that, since the BSA is believed to be in its compact form (i.e. N form) in the working pH 9.5, and at this arrangement the BSA fragments collapse on each other to create the desired compact form, therefore, assuming that the BSA molecule is spherical is not far

[3] Radial distance of a point from the axis of rotation at which, if whole mass of the body is assumed to be concentrated, its moment of inertia about the given axis would be the same as with its actual distribution of mass.

from reality and molecular weight-gyration radius is approximately accurate. Different studies have measured and calculated the radius of the BSA using different experimental and theoretical methods [148,149]. Based on the literature review, 3 nm has been chosen as the gyration radius for the following calculations. Using the equation (3.2) the maximum protein (here BSA) adsorbed on a surface is 152.6 g/cm^2. Note that this is the maximum protein adsorbed on a surface which covers the surface completely without any empty site left on a surface. However, in reality, this is not the case and protein molecules might not be able to fully cover the surface. Basically, the density (or compactness) of the protein layer adsorbed on a surface is a function of the protein characteristics (e.g. size, shape, and orientation) and solution conditions (e.g. pH, salt concentration and protein concentration). Many studies have shown that how different variables can affect the compactness of the protein adsorbed layer on a surface for various applications. Even if all the variables mentioned above are favorable for full coverage of the surface with the highest compactness, there still exist some physical limitations which leave some vacant sites (uncovered with proteins) on the surface. Figure 3.10 shows two different circle packing models with different arrangements on a surface such that no two overlaps and all of them are tangent. The densest packing of circles on the surface is the hexagonal lattice with a packing density of approximately 0.907 which has been mathematically calculated by the fraction of an area filled by a given collection of shapes (here circles). Table 3.2 shows the amount of BSA protein needed to cover the available surface (i.e. total PNP's surface area) in the solution based on two different packing arrangements and assuming all the other variables (e.g. pH and salt concentration) are favorable for maximum coverage.

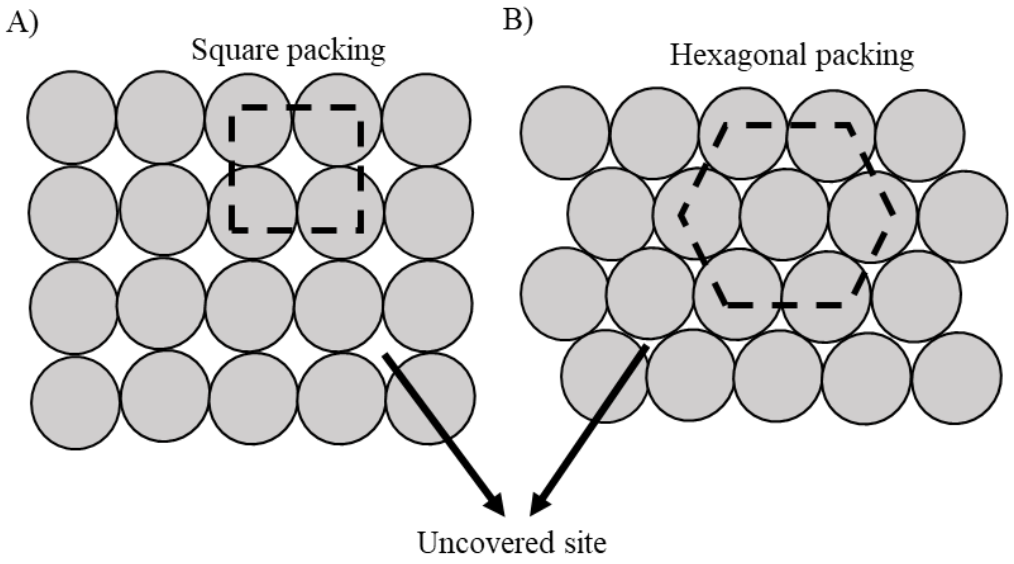

Figure 3.10 Different surface packing arrangements; (A) Square packing and (B) Hexagonal packing (adapted from [150]).

Table 3.2 Minimum amount of BSA needed in the solution to have maximum surface coverage on the surface of the PNPs based on two different packing arrangements

Packing	Packing density	Maximum Surface Coverage (g/cm^2)	Minimum BSA Concentration Needed for the Coverage (mg/mL)
Hexagonal	0.907	138.3	0.0418
Square	0.785	119.8	0.0360

Table 3.2 clearly emphasize the importance of the BSA concentration in the suspending buffer on the transmission of PNPs through the membrane filters (shown in Figure 3.9). According to the mathematical calculation, the two highest concentrations of BSA in the carbonate-azide buffer (i.e. 0.05 and 0.5 mg/mL)—where PNPs could fully pass through the membranes—had more BSA molecules than needed to fully cover the surface of the PNPs. The DLS results at these

two conditions also confirm that the PNPs are fully covered by the BSA molecules. Therefore, it has been hypothesized that there should be extra BSA molecules in the solutions that are creating the unstable secondary layer is somewhat true.

Conversely, any PNP retention by the membrane can be correlated to insufficient coverage of the surface by the BSA molecules. Based on the calculations, the two lowest protein concentrations (0 and 0.005 mg/mL) in the PNP solution had not enough number of molecules in their solution to cover the PNP's surface. Thus, this opens the bare surface of the PNPs to the membrane filter which increases the adsorption mechanism resulting in PNP retention described before. There is one interesting result shown in Figure 3.9 which indicates a partial transmission of PNPs at 0.015 mg/mL BSA dissolved in the suspending buffer. Interestingly, the 14% transmission (or 86% retention) of the PNPs have a direct correlation with the maximum percentage of surface coverage that can be reached within the solution. By assuming that the square packing is the dominant packing arrangement for the BSA molecules and 0.036 mg/mL is the amount needed for the full coverage, with 0.015 mg/mL BSA in the carbonate buffer, 18% (close to 14% transmission of PNPs) of the surface gets covered by the BSA molecules (assuming all the BSA molecules are evenly distributed and attached to the PNP's surface). However a stronger possibility is that, while diluting the PNPs by the suspending buffer solution, the very first drops of the concentrated PNP suspended in the solution gets covered (approximately 18% of all PNPs) by the majority of the BSA molecules and the other PNPs (approximately 82%) that are added later stayed uncovered due to lack of any BSA molecule in the solution. Therefore, around 18% of the PNPs could pass through the membrane structure.

Another set of data that has been monitored and acquired during the constant-flux filtration experiment is the TMP profile. During each set of filtration, three separate USB pressure

transducers displayed and logged the TMP of each membrane at the same time in order to monitor the changes in the total resistance. The data presented in Figure 3.11 is the average TMP of the triplicate experiments that were conducted at each BSA concentration. The TMP profile results show a good agreement with the filtrate profile (shown in Figure 3.9). There was no notable change in TMP during the filtration tests conducted for the two highest BSA concentrations. The TMP at the end of the 4.5 ml mark for the 0.5 and 0.05 mg/mL increased 23.2% and 13.8% respectively in comparison to the TMP at the beginning of the filtration. This increase most likely attributes to pore blocking that are taking place within the structure of the membrane by BSA covered PNPs with a mean size of 200 ± 3 nm (for 0.05 mg/mL BSA) and 206 ± 7 nm (for 0.5 mg/mL BSA) shown in Figure 3.2B. For the rest of the conditions, a significant increase of 199.0, 386.3 and 457.1% in the TMP were observed for 0.015, 0.005 and 0 mg/mL BSA solutions respectively.

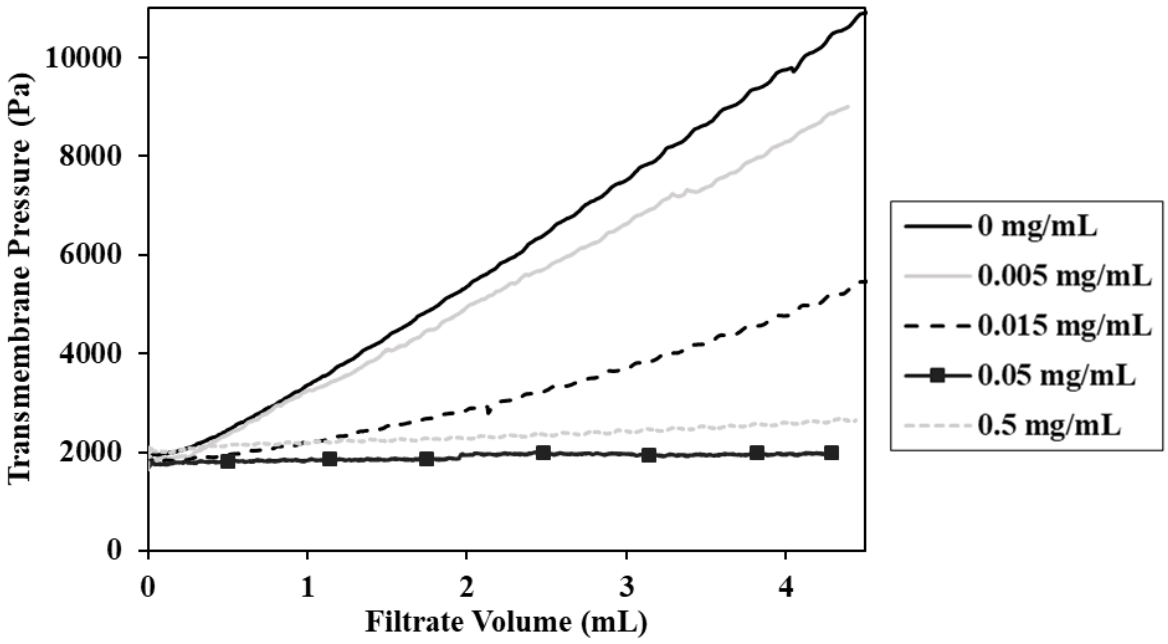

Figure 3.11 Comparison of average TMP profiles as a function of filtrate volume for the filtration of PNPs suspended in carbonate-azide buffer containing different concentrations of BSA.

The efficiency of filtration processes has been shown to be directly connected to the severity of membrane fouling, which can be measured by hydraulic membrane permeability [151,152]. Hence, hydraulic permeability measurements as the final quantitative measurement have been performed in order to comprehensively study how the BSA concentration is affecting the MF of the PNPs solution. The permeability results shown in Figure 3.12 indicates that at two high concentration of BSA in the suspending buffer (i.e. 0.5 and 0.05 mg/mL)—which the PNPs were fully covered by the BSA molecules—there was no significant decrease in the permeability of the membranes after filtration in compare to the permeability of the fresh membrane. In contrast, the filtration of the PNPs suspended in the carbonate-azide buffer with lower BSA concentrations (0.015, 0.005 and 0 mg/mL), resulted in a remarkable reduction in the permeability. Note that, a slight decrease in the permeability of the membranes for filtration of PNPs suspended in the buffer containing 0.5 and 0.05 mg/mL BSA, is due to retention of the BSA-covered PNPs that have sizes close to the pore size of the membrane. It can also be mentioned that the negligible difference of (~9.6%) in the permeability of the membrane from 0.033 ± 0.005 to 0.030 ± 0.003 $mL.s^{-1}.m^{-2}.Pa^{-1}$ by increasing the BSA concentration from 0.05 to 0.5 mg/mL is due to the differences in the particle sizes at these two conditions. At the highest concentration of BSA (i.e. 0.5 mg/mL) in the suspending buffer, PNPs are slightly bigger than the suspending buffer which has been one fold diluted in the BSA concentration, hence, it is expected to foul more due to the increased size of PNPs. The significant decrease in the permeability of the membranes at lower concentrations of BSA in the suspending buffer, most likely attributable to increased resistance due to the buildup of PNPs on the surface of the membrane and within the structure. At these three retentive conditions, there is one notable result that differs from the other two: the filtration of the PNPs suspended in buffer with 0.015 mg/mL BSA. The post-filtration membrane permeability of this

set of experiment is quite lower than the permeability of the membranes at the other two buffers with the lowest concentration of BSA (0 and 0.005 mg/mL). This can be explained by the fact that the fouling of the membrane for filtration of PNPs suspended in buffer with 0.015 mg/mL is mostly occurring in the internal structure and PNPs are retained within the membrane. Hence, the strategy in repeatedly washing the membrane and removing any unbounded or loosely bounded PNPs on the surface of the membrane didn't affect the permeability. However, for the filtration of the PNPs using the buffer containing 0 and 0.005 mg/mL BSA, fouling mostly occurred at the surface of the membrane due to the increase of membrane-PNP (uncovered) attractive interactions. Thus, a cake layer is formed faster at the beginning of the filtration not allowing the rest of the PNPs to pass through the surface into the structure of the membrane for the rest of the filtration process. This results in a very thick layer of cake which completely covers the surface of the membrane. One possibility is that during the repeated washing of the surface of the membrane after the filtration, the cake layer has been destructed and PNPs detached from the surface of the membrane thus, reviving the permeability of the membrane by unblocking some of the membrane pores on the surface of the membrane. It should be noted that the strategy of repeatedly washing the membrane with a micropipette to remove any unbound PNPs from the surface and within the pore structure makes it difficult to characterize the exact nature (i.e. reversible vs irreversible) of the membrane fouling and thus needs to be changed in future studies.

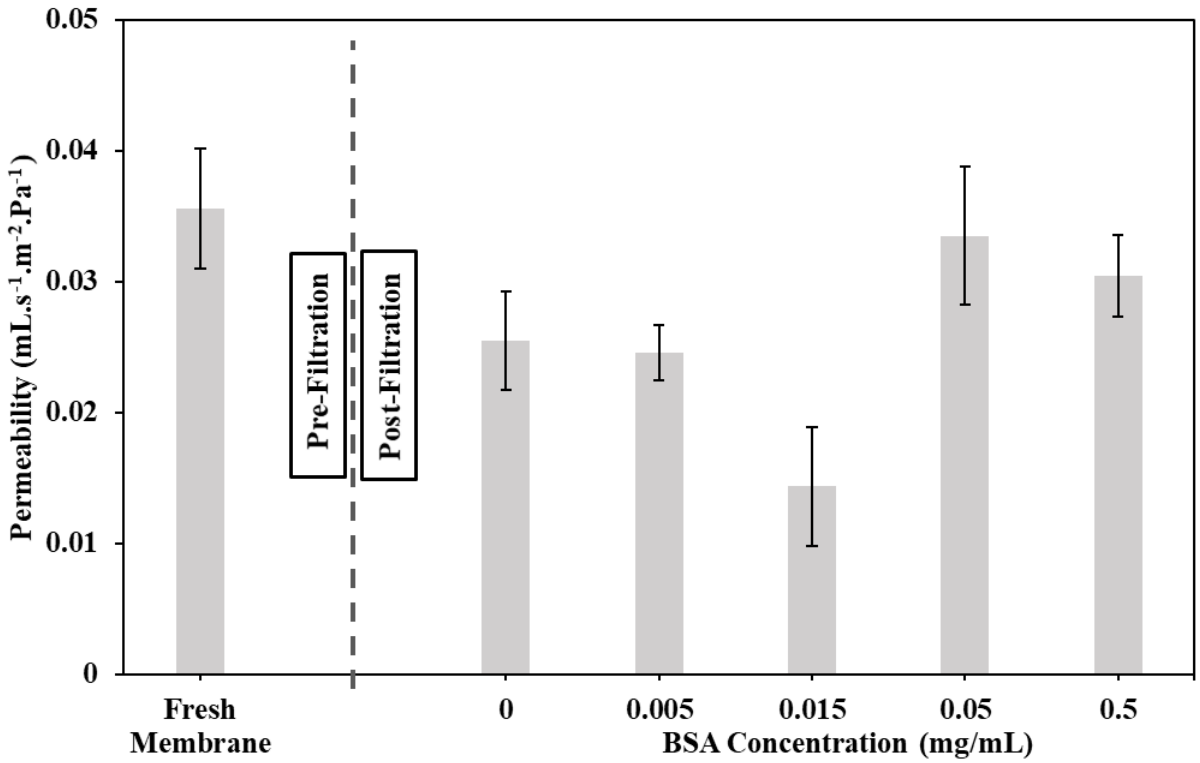

Figure 3.12 Comparison of hydraulic permeability measurements of the PVDF membranes pre- and post-filtration of 0.01% w/v of PNPs in five buffers with different BSA concentrations. The value for each post-filtration vertical bar is the average of the measurements from the triplicate tests for each condition, while the one vertical bar for pre-filtration permeability is the average of fifteen permeability measurements of fresh membranes before the filtration experiments at different BSA concentration. The error bars are the standard deviation calculated for these experiments.

SEM images of the top surface of the membranes were also obtained in order to gain a better understanding of fouling among the five different conditions. After filtration experiment, the membrane filter holders were opened and membranes were extracted from the holder. SEM images of the top surface of the membrane shown in Figure 3.13 are obtained after sample preparation mentioned in section 3.2.1. As shown in Figure 3.13 (panels E and D) there are negligible PNPs adsorbed or retained by the membrane at two high concentrations of BSA (0.5 and 0.05 mg/mL) in the suspending buffer. However, there were some scattered areas that few PNPs were retained by small pores all over the surface of the membrane. These few blocked pores

on the surface of the membrane are most likely due to the increased size of the PNPs at these two conditions (mostly for 0.5 mg/mL). As the BSA concentration decreased down to 0.015 mg/mL, more PNPs were adsorbed on the membrane which has been shown in Figure 3.13C. Severe fouling occurred when a little amount (0.005 mg/mL) or no BSA existed in the suspending buffer. Figure 3.13B and A clearly shows that a cake layer has been formed during the filtration of PNPs at these two conditions. The cake layer on the surface of the membrane was thicker when carbonate-azide free BSA solution were used for suspending the PNPs (Shown in Figure 3.13A).

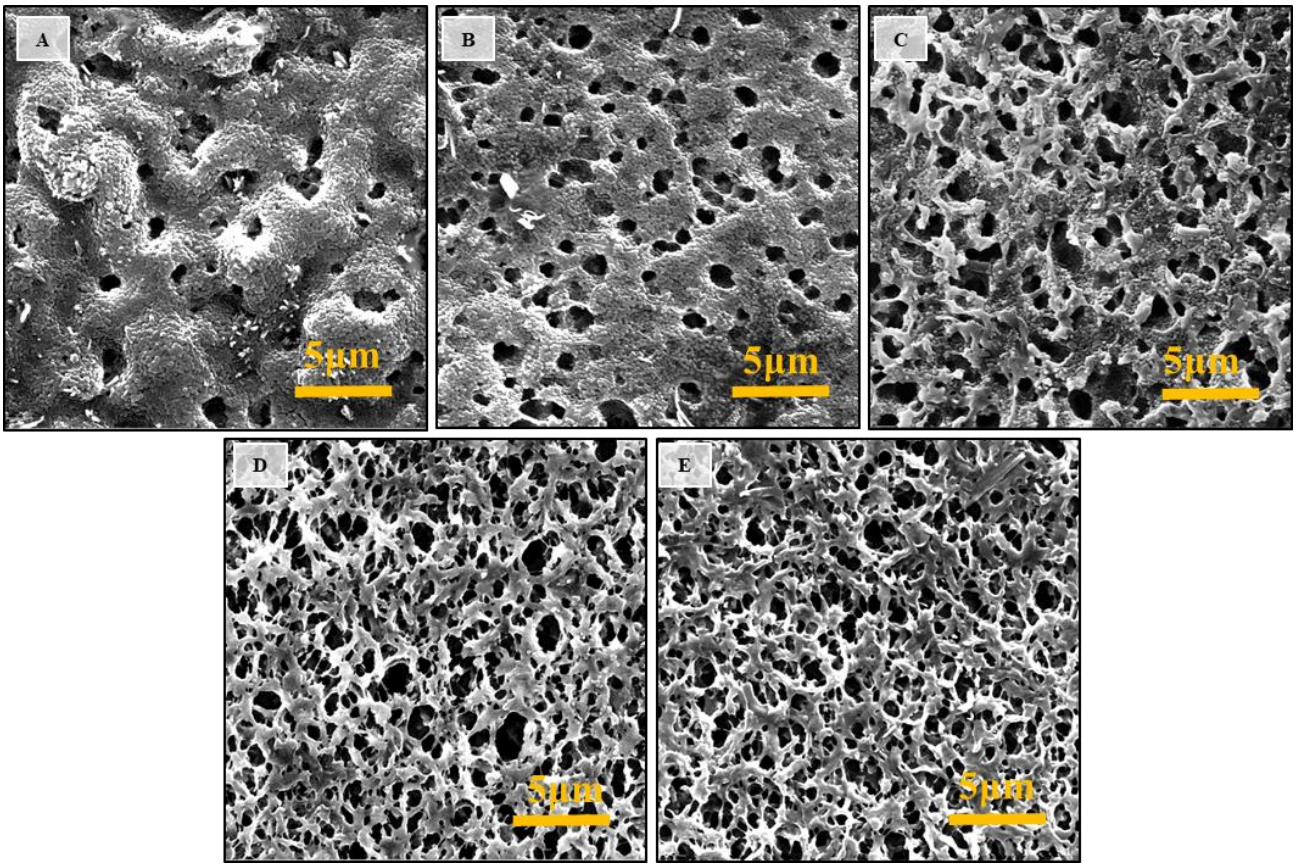

Figure 3.13 SEM images of the Durapore PVDF after the filtration of fluorescent PNPs; Panels A to E are the SEM images (10,000× magnification) after filtering PNPs suspended in buffers containing 0, 0.005, 0.015, 0.05 and 0.5 mg/mL BSA respectively.

Similar results were also observed during filtration of PNPs suspended in solutions containing α-Lactalbumin that are summarized in Figure 3.14. The analysis of the performance of sterile filters in solution conditions featuring α-Lactalbumin concentrations in the suspending buffer yielded results that were similar to results obtained from BSA experiments. Basically, results shown in Figure 3.14 indicates that the performance of membranes varies from complete transmission to complete retention, depending on the concentration of α-Lactalbumin used in the suspending buffer. The result in Figure 3.14I clearly shows that, at the highest α-Lactalbumin concentration, the PNPs are completely transmitted during the filtration of ~4.3 mL of the solution. The transmission of the PNPs at 0.05 mg/mL of α-Lactalbumin also followed the same mechanism of transmission, and the majority of PNPs transmitted through the sterile filtration membrane. The TMP of the membrane also did not show a significant increase in solutions containing α-Lactalbumin. However, the TMP for the highest concentration of α-Lactalbumin started to slightly increase during the filtration which is most likely due to the blockage of internal and surface pores of the membrane by protein-coated PNPs that now has bigger diameter in comparison to their original size. However, this is still surprising that a heavy larger size of PNPs (coated with protein) close to the pore size rating of the membrane could pass the membrane structure. The good agreement between TMP and the fluorescent intensity profile results in Figure 3.14E and 3.16F is likely attributable to increased resistance due to the buildup of PNPs on the membrane surfaces. These results, clearly show that surface properties of PNPs have a greater impact on their transmission through membranes in comparison to their size. The SEM image of the membranes gave us a better understanding of fouling. As shown in Figure 3.14C there is a negligible PNP accumulation/adsorption at the highest α-Lactalbumin concentration when compared to the SEM image of the fresh membrane (see Figure 3.2B). In contrast, significant accumulation/adsorption

occurs at the no α-Lactalbumin, which is consistent with the previous results shown in Figure 3.13D. As mentioned in the previous chapter (see section 2.3) it is interesting that PNPs remained attached to the membrane surface and continued to block a great number of pores (as is evident from the SEM images) despite the strategy of repeatedly washing the membrane surface before conducting permeability measurements.

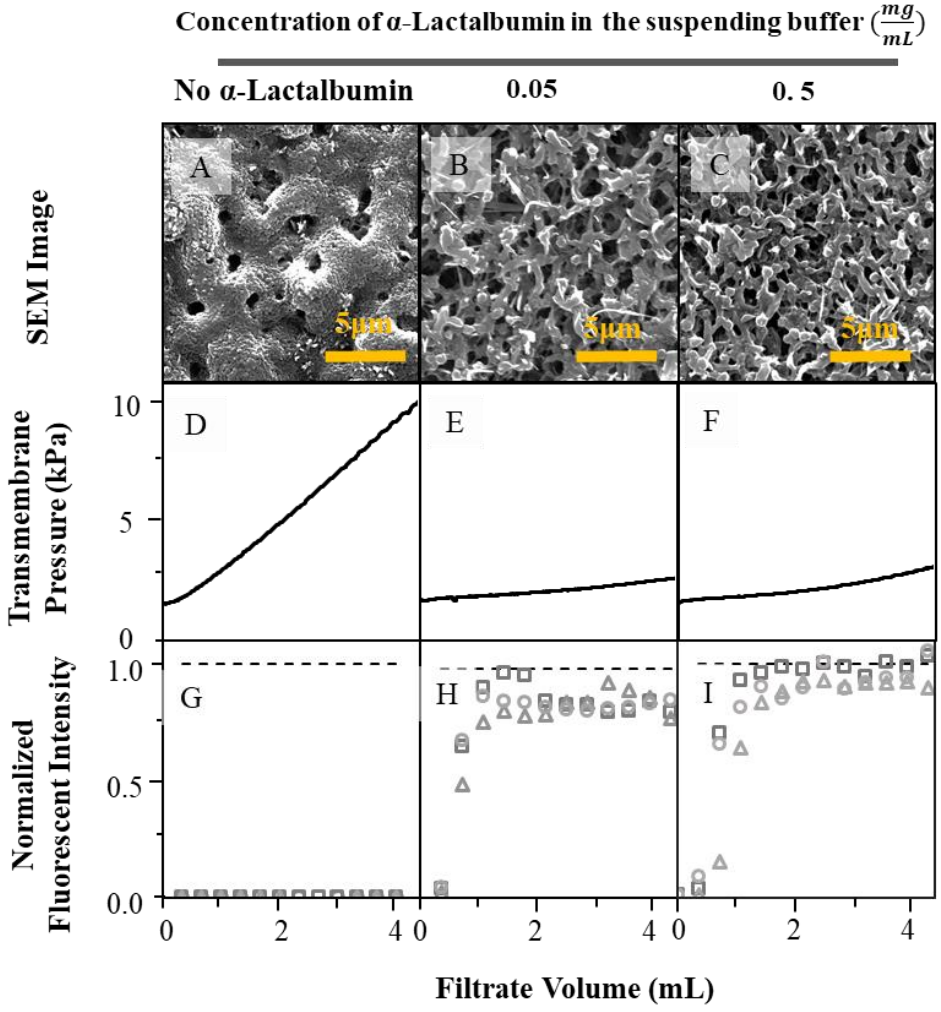

Figure 3.14 Panel (A) to (C): SEM images; Panel (D) to (F): TMP profile; Panel (G) to (I): normalized fluorescent intensity profiles, for filtrate samples collected during constant-flux filtration tests of 189 nm PNPs suspended in different buffer composition by changing the concentration of α-Lactalbumin from 0 to 0.5 mg/mL. The profiles in each panel are from the three separate trials that were conducted at each experimental condition are displayed by △,□, and ○ in each panel.

Permeability measurement of the PNP filtration experiments with α-Lactalbumin was also similar to permeability results collected for the BSA. Figure 3.15 clearly shows how permeability of the membrane declined after filtration of PNPs suspended in no α-Lactalbumin in the suspending solution. It should be noted again, the strategy of repeatedly washing the membrane with a micropipette to remove any unbound PNPs from the surface and within the pore structure makes it difficult to characterize the exact nature (i.e. reversible vs irreversible) of the membrane fouling.

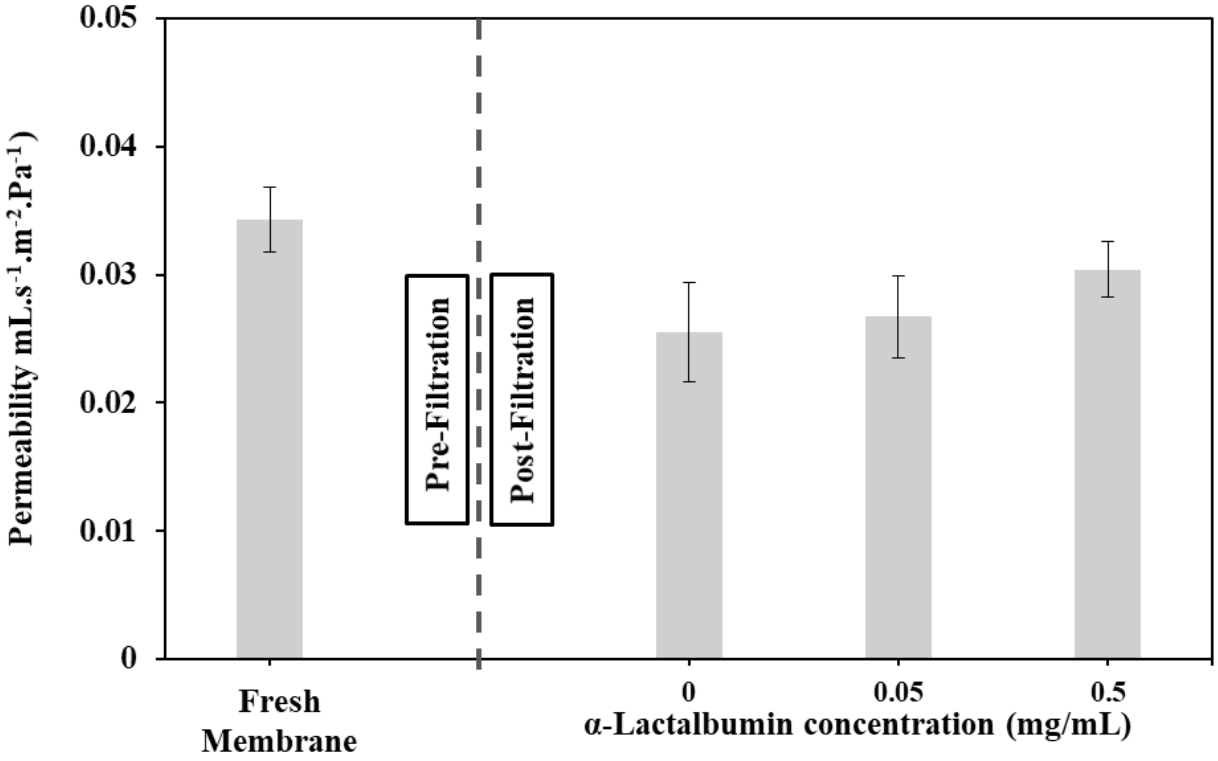

Figure 3.15 Comparison of hydraulic permeability measurements of the PVDF membranes pre- and post-filtration of 0.01% w/v of PNPs in three buffers with different α-Lactalbumin concentrations. The value for each post-filtration vertical bar is the average of the measurements from the triplicate tests for each condition, while the one vertical bar for pre-filtration permeability is the average of fifteen permeability measurements of fresh membranes before the filtration experiments at different α-Lactalbumin concentration. The error bars are the standard deviation calculated for these experiments.

3.4. Conclusion

The results demonstrated in this study clearly shows that surface properties of PNPs (protein-coated) suspended in a solution has a significant effect on their transmission through sterile filtration membranes. Similar findings have been reported on transportation of protein-coated PNPs in chromatography systems and porous media [44,45,140]. It is believed that fouling and rejection of colloidal solutions, either biological (i.e. pathogenic viruses) or non-biological (e.g. PNPs), in filtration studies can be easily controlled by changing the surface properties of the particles. In this study, the differences between the results acquired during filtration of unmodified and surface modified PNPs clearly show that virus surrogates studies should be performed with great consideration in terms of surface properties in order to be able to correlate the filtration results to actual virus particles. Protein-coated PNPs could provide new insights for studying the transport of therapeutic viruses in sterile filtration studies.

Since the solution conditions (e.g. salt concentration, pH) in which the PNPs were suspended were completely different than the solution conditions of the media of therapeutic viruses, theoretical conclusions cannot be drawn regarding the reliability of using PNPs as virus surrogates. Nonetheless, the current study still offers a very simple model for the sterile filtration of spherical viruses with dimensions that are close to the PNPs used in this work. The results of this study could be able to answer some fundamental questions about pathogen transport through sterile filtration membranes. These fundamental aspects will later allow us to expand further researches and studies to have a better model of pathogen transport in different applications, especially separation processes, to be tested and developed.

The HTAF setup was a proof of concept in sterile filtration experiments in order to be able to run more experiments at the same time. The HTAF system that has been developed in this work

allows us to increase the capacity of filtration tests from one experiment (in the second chapter) at a time to three simultaneous experiments (in this chapter) and can potentially be used for many more parallel experiments. This new modification helps us to speed up the filtration experiment along reducing the load of the researcher's work. Also by using a reduced membrane area in a reusable polycarbonate filter holders, the number of materials needed for an experiment, especially PNP stock, significantly decreased and can be a proof of concept for miniaturization of such studies. However, the key feature of the current filtration setup is the automated sampling ability which has been achieved by the aid of a modified 3D printer. To the best of the author's knowledge, this is the first study that has used a 3D printer in order to make an automated sampling device for filtration experiments. Although commercial linear actuator exists in the market that can move the 96-well microplates on a moving stage to collect filtrate samples in different wells during the filtration experiment, these linear actuators are very expensive (in the order of thousands of dollars) and they are limited in their direction of movement However, the 3D printer gave us the ability to precisely collect filtrate samples from tubings branched out from the bottom of the filter holder and attached to the 3D printer's nozzle, in three different directions. Interestingly, the prices for these 3D printers are in the order of hundreds of dollars.

In the second chapter, the author raised the concern regarding the pore-size measurement and characterizations that currently exist for determination of membrane's specifications used by different manufacturers. It is believed that since membrane manufacturing companies use different techniques, which they do not disclose to the public, the outcome of filtration experiment might vary from one another. Since there is no way in which the number of pores characterizing a filter, especially phase inversion membranes, can be ascertained, it is assumed that membrane manufacturers use techniques that are fundamentally based on a multitude of assumptions. It is

clearly obvious from SEM images of the membrane's top surface that a wide distribution of pore sizes exists in the membrane's structure. Pores with dimensions significantly greater than 0.22 μm were also observed, which increases the probability of particles larger than 0.22 μm passing through the membrane. The SEM image of the membranes along full transmission of coated PNPs with the size (i.e. 206 ± 7 nm) of slightly smaller than the pore size rating of the membranes (0.22 μm) is a big concern us that the reliability of such membranes as a sterilizing grade membrane can be questioned.

Chapter 4: Conclusions and recommendations

4.1. Conclusions

With regards to the importance of studies in the field of therapeutic viruses, this study focused on the basic concepts of filtration of OVs through sterile filtration membranes by using fluorescently labeled PNPs as surrogates due to difficulties associated with running actual VF studies at this stage. This strategy also provides us many advantages in terms of our understandings on basic variables that affect the transmission of virus-sized particles through sterilizing grade membrane filters and will be helpful in future studies when the actual VF needs to take place. In this thesis, different factors such as membrane material, particle size, the chemical composition of suspending buffer and surface properties of particles were investigated in order to study how these parameters can affect their transmission through a sterile filtration process. Some of the important key findings and conclusions of this thesis will be mentioned below:

I. This study shows that addition of surfactant (i.e. nonionic Tween 20) to a PNP solution will cause a shift from full transmission to complete retention of the PNPs during the dead-end MF. This is an important finding since Tween 20 is a relatively nontoxic chemical compound that is allowed to be used up to a certain amount in pharmaceutical products. Indeed, currently, Tween 20 is being used as an excipient in pharmaceutical applications to stabilize emulsions and suspensions, especially vaccine manufacturing. For example, Flublok® and Flublok® Quad are two vaccines for preventing infection by influenza virus which both contains ≤27.5 mcg Tween 20 in their final formulation solution [153].

II. PNPs were successfully coated with protein molecules in order to have a better resemblance of virus particles in this study. The results clearly show that surface properties of PNPs

suspended in a solution has a significant effect on their transmission through sterile filtration membranes. It is believed that fouling and rejection of colloidal solutions, either biological (i.e. pathogenic viruses) or non-biological (e.g. PNPs), in filtration studies can be easily controlled by changing the surface properties of any particle.

III. It has been shown that even a small change in the chemical composition of certain chemicals or substances (i.e. surfactant and protein) can entirely change the outcome of any filtration results. Therefore, this brings a lot of controversy and confusion in terms of the accuracy of the previous PNP filtration studies, especially for studies that not used surfactants in their suspending buffer [49,52,63].

IV. It has also been shown that membrane chemistry and morphology can significantly influence the transmission behavior of any particle, regardless of its nature (e.g. biological or non-biological). Moreover, pore-size measurement and characterization seem to be a big challenge in membrane-based separation and purification studies and scientific works, since manufacturers determine membrane's specifications using different techniques, which they do not disclose to the public. One possibility is that the inconsistencies between the results of same membrane materials from different manufacturers are due to different characterization techniques that these producers are using hence, it is important to develop a universal method for determining membrane pore size measurements.

V. This study is the first to use fluorescently labeled PNPs as therapeutic virus surrogates (not an impurity to capture by VF membranes) in order to obtain quantitative data for the fouling propensity of membranes (pore sizes ~ 0.2–0.22 μm). However, the solution conditions (e.g. salt concentration, pH) in which the PNPs in this thesis were suspended were completely different than the solution conditions of biological media in which virus particles are

suspended; as such, these findings do not allow theoretical conclusions to be drawn regarding the reliability of using PNP as virus surrogates for any OVs.

VI. Also, as a proof of concept, it has been successfully shown that employing novel high throughput filtration systems in such experiments can be really beneficial in different ways. With the aid of HTAF system, three simultaneous filtration experiments were been able to be performed. Definitely more parallel experiments can be performed by designing sophisticated modules with novel designs. The HTAF system is also unique in its own and is the first study that has used a 3D printer in order to build an automated sampling device with a very lower cost in comparison to automated sampling machines in the market.

4.2. Recommendations for future works

Although using PNPs as virus surrogates have brought a lot of advantages with regards to better understanding the factors affecting the virus transportation in different media, there is still a big difference between the nature of the virus particles and the media that are suspended in compare to what the PNPs were suspended. Even coating PNPs with proteins to make similar surface properties as virus surrogates, cannot fully be a resemblance of what exactly will happen during filtration of actual virus solutions. Clinical therapeutic virus solutions are very complex solutions that can totally change the transmission behavior of any particle, as the results in this thesis have also proved the effect of different factors. Hence, future works in this field need to consider important factors in order to make a better model of actual therapeutic virus solutions in different applications, especially separation processes. First, virus surrogates should be covered with a proper protein similar to proteins that exist on the surface of virus particles, not only proteins that have similar zero point of charge. Second, making a better resemblance of virus particles should not be limited to just coating the surrogates with protein and other factors need to be added.

For example, biological solutions, including therapeutic virus solutions that currently are being processed for clinical trials, consist of many macromolecules such as proteins, DNA, enzymes and cell debris. Presence of any of these macromolecules can totally change the transportation of any particle (either biological or non-biological) in a media. Last but not least, the pH and salt concentration or in another word, the ionic strength of the surrogate solution should match the pH of the actual biological solution in order to have a better resemblance of the transmission, since physiochemical properties have an important impact on transmission of surrogates through any media.

Although the first motivation of the current thesis was to comprehensively understand different variables that affect the sterile filtration of virus-sized particles, the strategy and approach on studying the transmission of particles through filters can be extended to many other applications which separation of micro and NPs are important. For instance, nowadays, plastic pollutions have turned into a big environmental crisis that is endangering our ecosystem in different ways. Basically, plastic pollution can be defined as the accumulation of plastic objects that are adversely affecting the health of living beings. When plastics are not properly recycled and are carelessly thrown away, over years a portion of these plastics crumbles into small pieces called "Microplastics" [154–156]. Microplastic is a term to define plastic objects in a wide size range of 1 nm to < 5 mm in different shapes (e.g. fiber and sphere) everywhere in soil, river, lakes, oceans and surprisingly drinking water. The broadness of the presence of microplastics can extend to our food chain by nourishing the seafood that contains these microplastics in their tissue as a result of penetration in the marine environment or digested by fishes [157]. Moreover, these microplastics are good chemical adsorbents as they decrease in size (properties of micro and nano-scale materials) and many toxic chemical compounds in water and soil can easily adsorb on their

surfaces. Penetration of these microplastics covered with toxic chemicals into the food chain is dangerous to the entire health of animals and humans [158]. The accumulation of these microplastics in the body of sea creatures can cause deficiency in the activity of their internal organs which leads to their death. Although the effect of these microplastics on human health has not been studied comprehensively yet, certainly the goal is to avoid the transportation of these microplastics in the food chain, including humans by controlling their production and spread from its source and discharge point.

Interestingly one of the major sources of production of microplastics comes from our clothing materials in the washing machine. Physical movement of clothes, along with detergents and chemicals that are used to clean the clothes in the washing machine accelerate the production of a large number of microplastics that will be discharged to water treatment facilities and nature. One of the solutions for preventing this from happening or reducing the number of microplastics spreading all over the places is to use filters on the water discharge pipe to collect the particles and stop their transportation and penetration to the environment. Many research groups all around the world are currently working on studying different negative aspects of microplastics in the environment and investigating how to control the production and their spread into nature.

It is believed that the concept of this thesis can also be applied to study the transportation of microplastics in different porous media and how to collect and capture them in its first place when they are produced. Therefore, there is a great opportunity to comprehensively study the transmission behavior of microplastics in different media and investigate the most efficient way to capture these floating practices by the means of separation techniques, especially filtration processes. Undoubtedly, the knowledge that has been acquired on factors affecting the particle's transmission during sterile filtration of PNP solutions in this project can be employed into

investigating the proper approach to capture these microplastics. It is believed that there is a great potential to better understand basic concepts of these microplastics in terms of their capturing process and their penetration to food chain with the aid of NPs (or microparticles). Hopefully with the advances in the production of colloidal solutions, nowadays NPs are produced by specific detecting properties (i.e. fluorescent) that allows us to quantify them accurately by specific instruments. Also employing novel and more sophisticated high throughput systems such as the HTAF system that has been introduced in this thesis in chapter three (see section 3.2.3) can be helpful in order to ease the difficulties of experimental work, in terms of expenses, time and load of work by performing simultaneous parallel experiments.

Appendices

Appendix A

The information in this sections is related to chapter two.

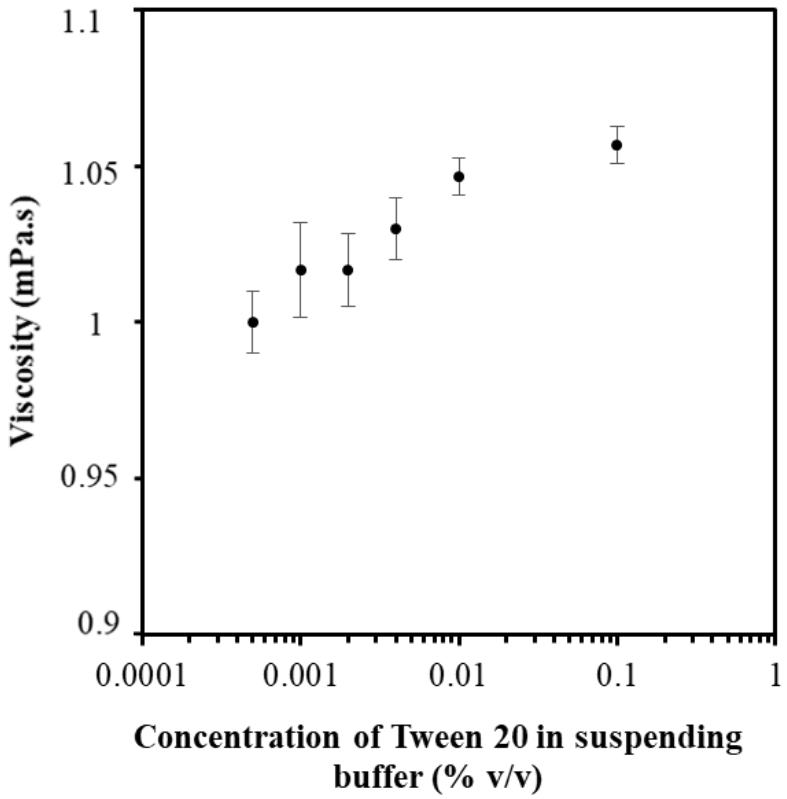

Figure A1 Effect of Tween 20 concentration on the viscosity of 0.1 M carbonate buffer solution containing 0.1% (w/v) sodium azide. The data points correspond to the average value of the measurements made on triplicate samples of the six different solutions. The error bars correspond to the standard deviation of the triplicate measurements

SEM images of each PNP solution prepared with the suspending buffer containing 0.1% Tween 20 were obtained using a (FEI) Magellan 400 SEM microscope. For this purpose, a small amount (~5 µL) of the PNP solution was inoculated on a clean flat substrate. After allowing the sample to dry, the substrate was mounted on a SEM specimen carrier and then gold sputtered for 1.5 minutes at a current of 20 mA under vacuum.

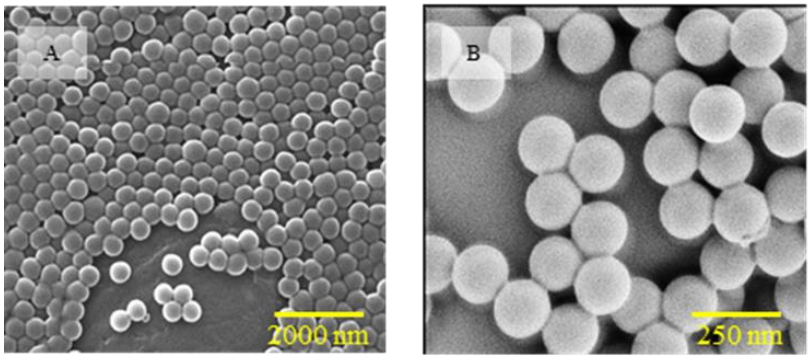

Figure A2 SEM images of the 'sky-blue' PNPs (490 nm) in panel A (25,000× magnification), 'yellow' PNPs (188 nm) in panel B (200,000× magnification).

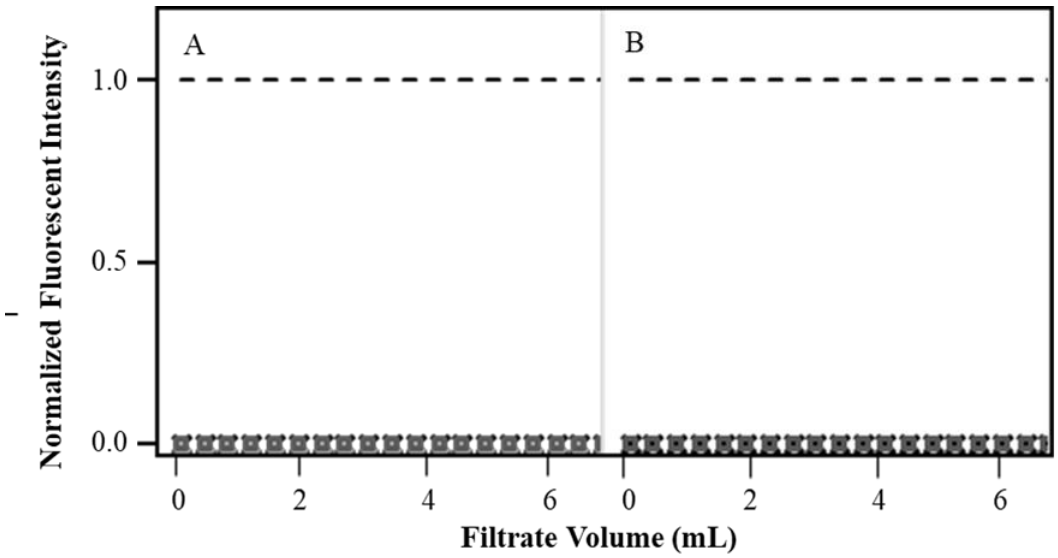

Figure A3 Normalized fluorescent intensity profile of filtrate fractions collected during filtration. The performance of Durapore PVDF (panel A) and MiniSart PES (panel B) on the transmission of PNPs has been challenged using 490 nm PNPs suspended in buffer containing 0.1% v/v Tween 20. All combination of PNP-membrane were done in three separate trials marked by ▲, ◘ and ✖.

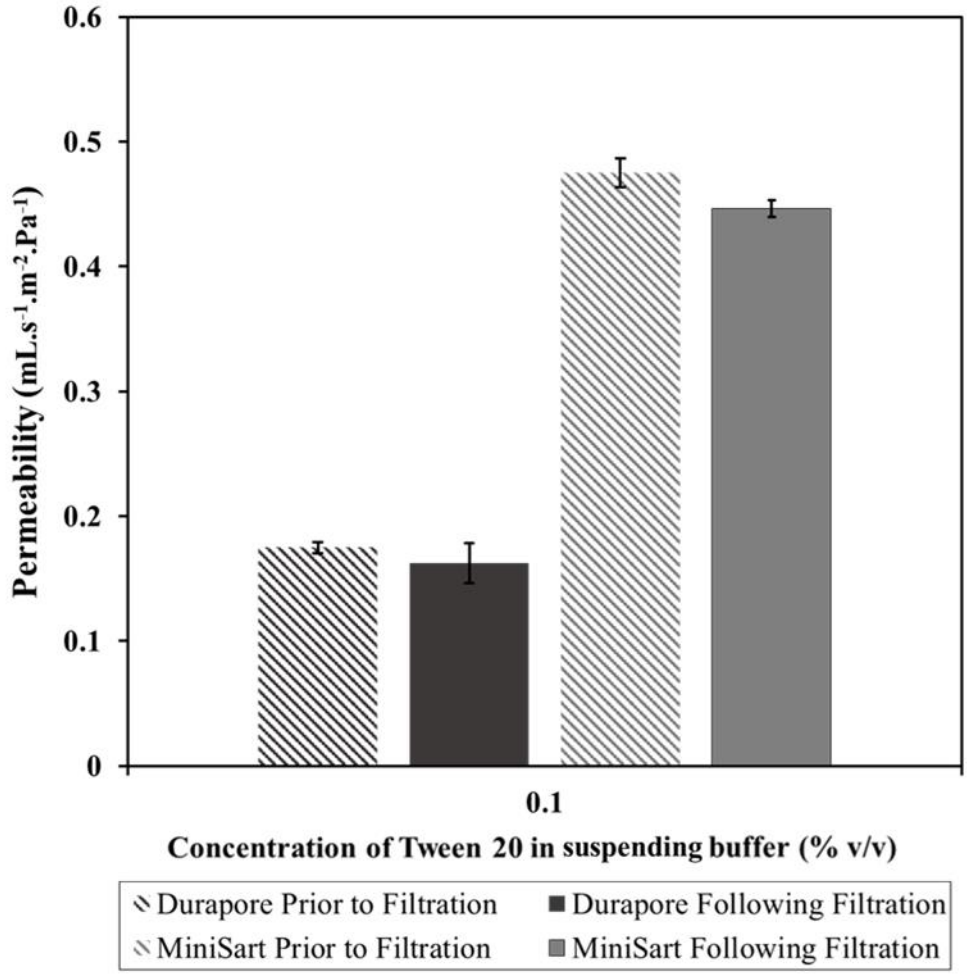

Figure A4 Permeability measurement of Durapore PVDF and MiniSart PES membrane prior and following filtration of 0.01% w/v of 490 nm PNPs suspended in buffer containing 0.1% v/v Tween 20. Each column is the average of three separate permeability measurement for three trials of filtration and error bars are the standard deviation calculated according to the repeats

.

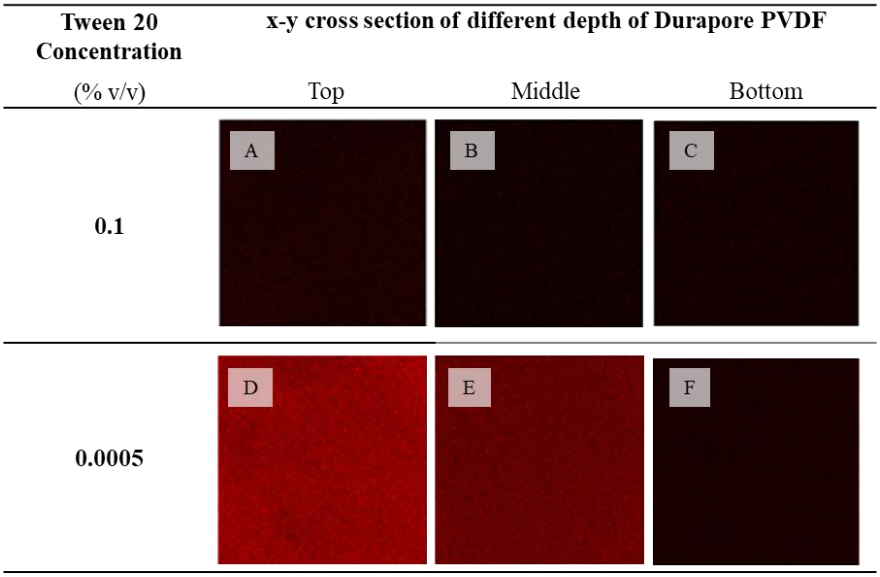

Figure A5 CLSM images of the Durapore PVDF membrane after filtering 0.01% w/v of 188 nm PNPs suspended in buffers containing two different Tween 20 concentrations (i.e. 0.1 and 0.0005% v/v). Panels (A) and (D) are the images obtained at the membrane surface (i.e. 'top'). Panels (B) and (E) are the images obtained at a depth of approximately 50 microns from the top of the membrane (i.e. 'middle'). Panels (C) and (F) are the images obtained at a depth of approximately 120 microns from the top of the membrane (i.e. 'bottom').

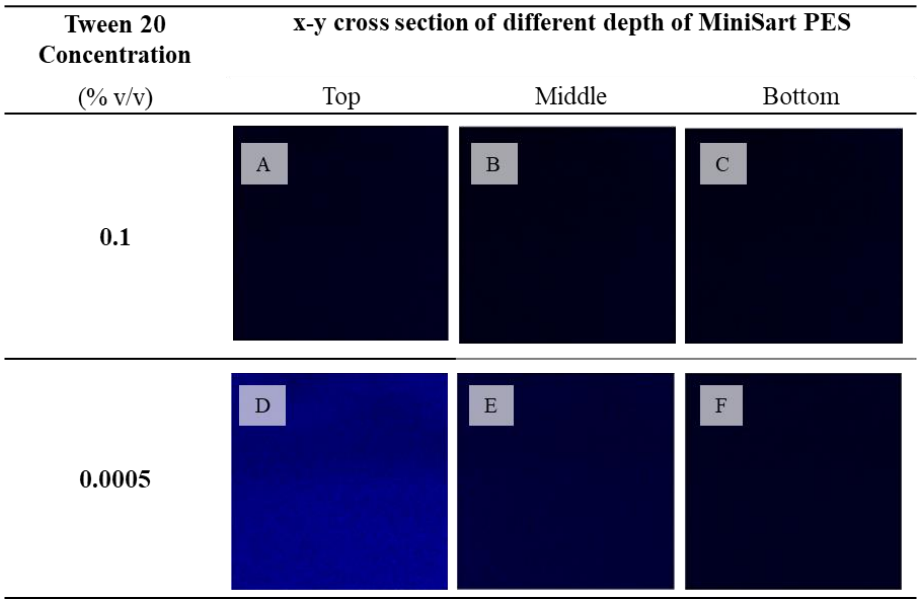

Figure A6 CLSM images of the MiniSart PES membrane after filtering 0.01% w/v of 59 nm PNPs suspended in buffers containing two different Tween 20 concentrations (i.e. 0.1 and 0.0005% v/v). Panels (A) and (D) are the images obtained at the membrane surface (i.e. 'top'). Panels (B) and (E) are the images obtained at a depth of approximately 50 microns from the top of the membrane (i.e. 'middle'). Panels (C) and (F) are the images obtained at a depth of approximately 120 microns from the top of the membrane (i.e. 'bottom').

Appendix B

The information in this sections is related to chapter three.

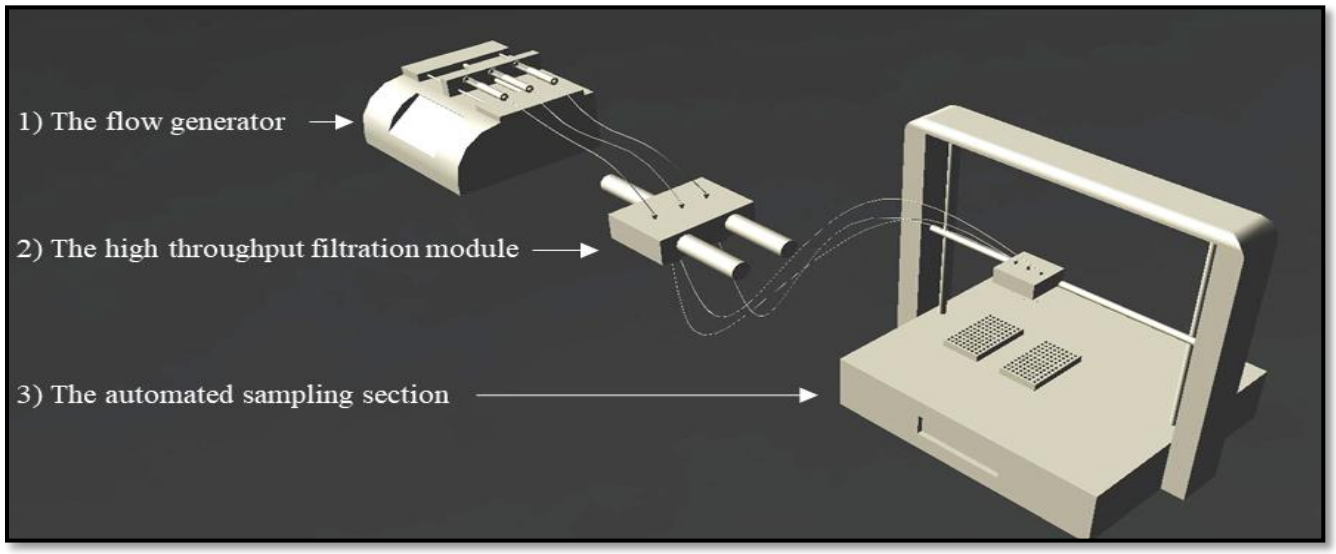

Figure B1 The 3D design of the HTAF setup (sketched using AutoCAD)

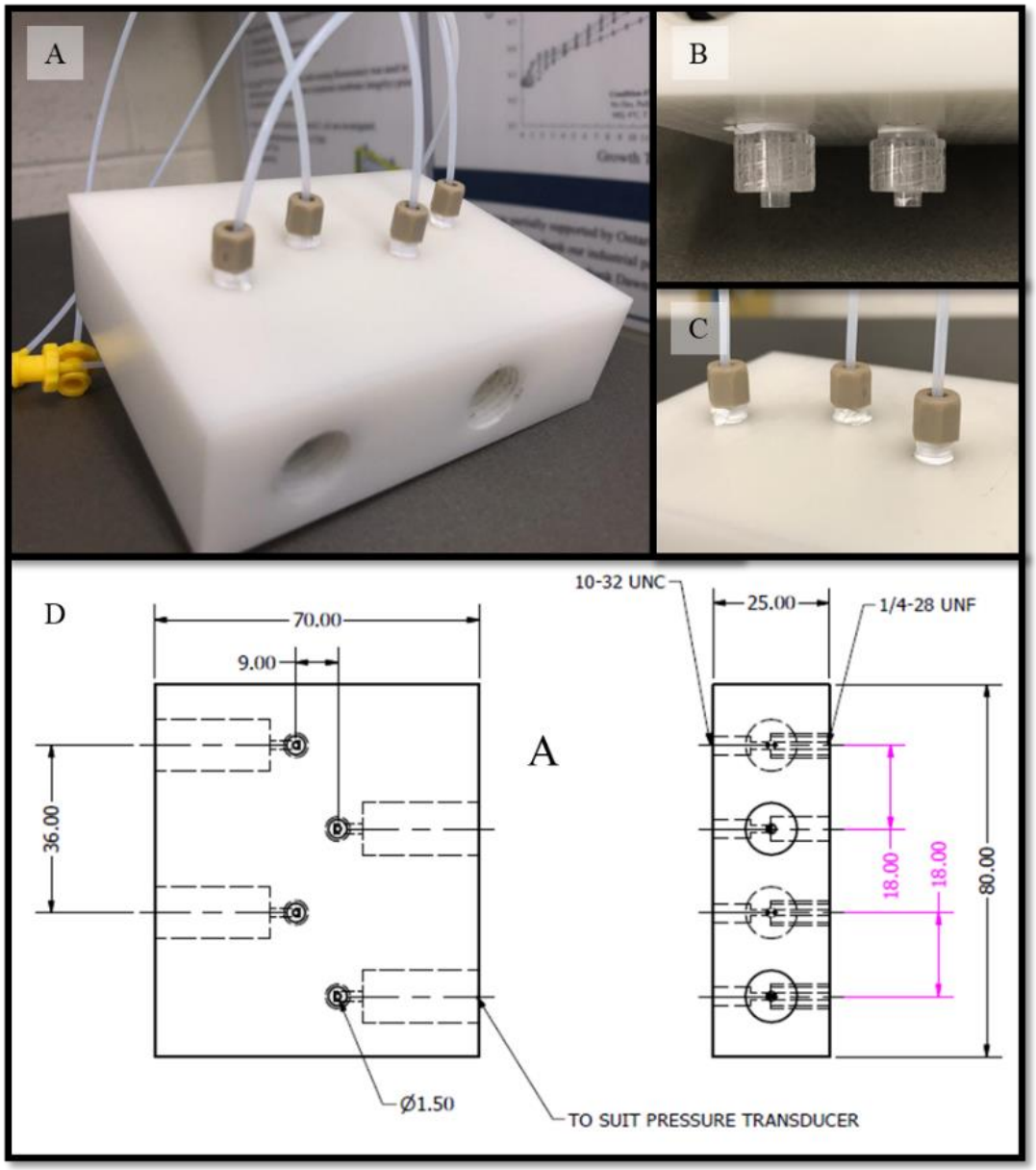

Figure B2 Panel A: picture demonstration of the high throughput module. Panel (B) and (C): proper fluidic connectors at bottom and top of the module respectively. Panel (D): technical drawing of the high throughput module. Note that the preliminary design was for performing four parallel filtration experiments. Only three of the channels were used in the study conducted in the third chapter.

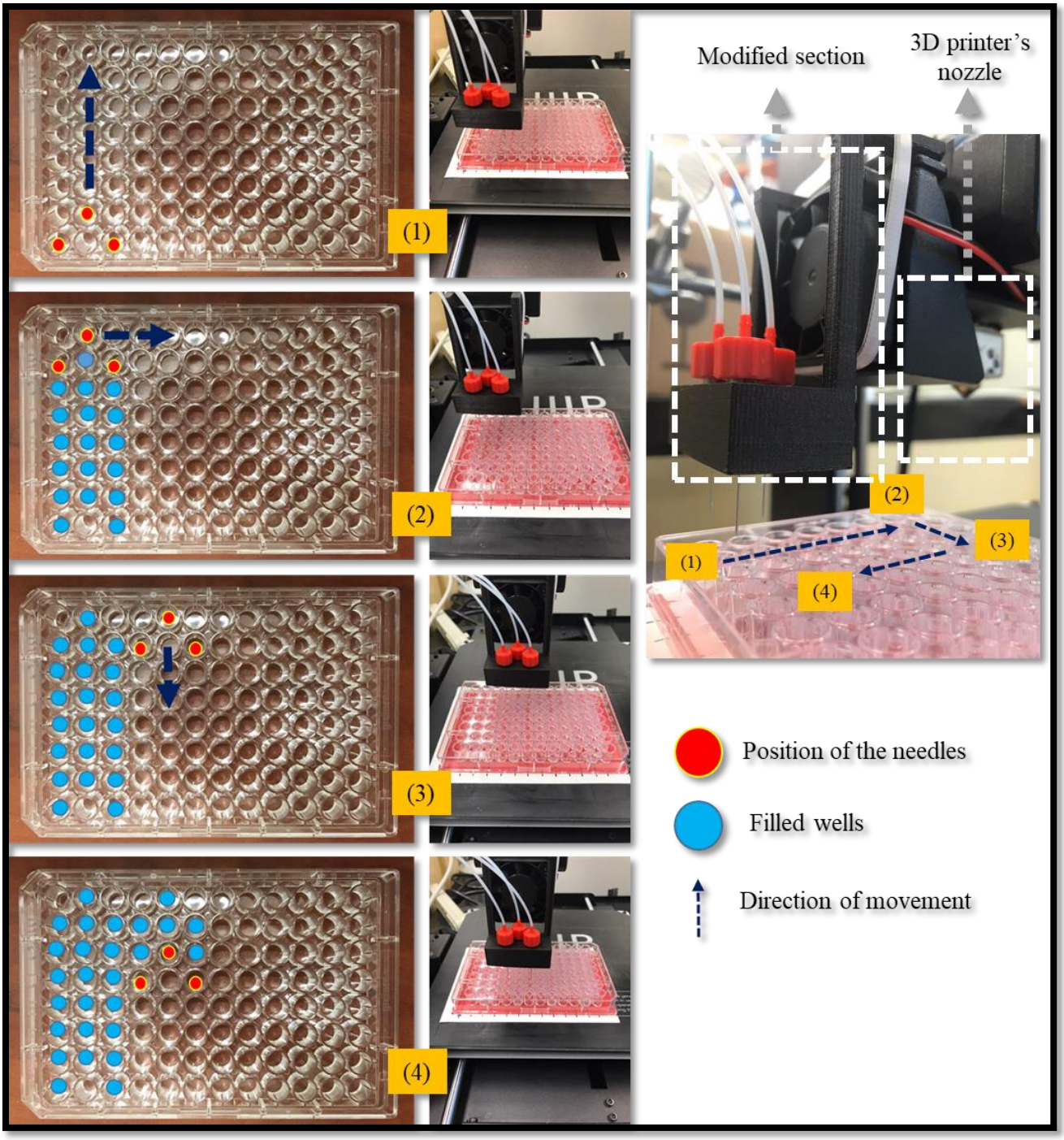

Figure B3 Picture demonstration of the position of the dispensing needles and the pattern on the movement of the modified nozzle in order to fill the 96-well microplate (Greiner Bio-One) with filtrate samples collected from the bottom of filtration unit via Teflon tubings during three simultaneous parallel filtration experiment.

Actual G-code used for programming the 3D printer's nozzle to follow the pattern shown in Figure B3

G90 ; Use absolute coordinates
G92
G1 F1200n ; mm/min (The desired speed for movement from one well to another)
G1 X0 Y0 Z46.11; (Bringing the nozzle up to the desired height)
G1 X37 Y108.36 Z45.11 ; (Moving the nozzle closer to the edge of the microplate on the stage from the zero set point, considering offset 80mm in Y direction due to attachment of the modified section)
G1 F1 ; mm/min (Tricking the 3D Printer to stay still by lowering the speed 1mm/min in the Z direction)
G1 X37 Y108.36 Z44.11; (Moving 1 mm up and in next line moving 1mm down with 1mm/min speed while the printer is moving in Z direction with the low speed, the 96 well plate is filling in 2 minutes)
G1 X37 Y108.36 Z45.11 ; (This line and the previous line is for making the stage stay still for 2minutes without changing in X and Y direction)
G1 X37 Y108.36 Z44.11 ;
G1 X37 Y108.36 Z45.11 ; G1 X37 Y108.36 Z44.11 ; G1 X37 Y108.36 Z44.11 ;G1 X37 Y108.36 Z45.11 ;
G1 X37 Y108.36 Z44.11 ;G1 X37 Y108.36 Z45.11 ;G1 X37 Y108.36 Z44.11 ;G1 X37 Y108.36 Z45.11 ;
G1 X37 Y108.36 Z44.11 ;G1 F1200 ; mm/min (Back to the regular speed, because the first three wells are filled and a higher speed is needed to move to the next three wells)
G1 X37 Y117.36 Z46.11 ; (Moving the stage for 9 mm (distance between the middle of each well) in the X-direction to fill the next well and repeat it for other wells)
G1 F1 ; mm/min
G1 X37 Y117.36 Z45.11; G1 X37 Y117.36 Z44.11 ; G1 X37 Y117.36 Z45.11 ;G1 X37 Y117.36 Z45.11 ;
G1 X37 Y117.36 Z44.11 ;G1 X37 Y117.36 Z44.11 ;G1 X37 Y117.36 Z45.11 ;G1 X37 Y117.36 Z44.11 ;
G1 X37 Y117.36 Z45.11 ;G1 X37 Y117.36 Z44.11 ;G1 X37 Y117.36 Z45.11 ;G1 X37 Y117.36 Z44.11 ;
G1 F1200 ; mm/min
G1 X37 Y126.36 Z46.11 ;
G1 F1 ; mm/min
G1 X37 Y126.36 Z44.11; G1 X37 Y126.36 Z45.11 ;G1 X37 Y126.36 Z44.11 ;G1 X37 Y126.36 Z45.11 ;
G1 X37 Y126.36 Z44.11 ;G1 X37 Y126.36 Z44.11 ;G1 X37 Y126.36 Z45.11 ;G1 X37 Y126.36 Z44.11 ;
G1 X37 Y126.36 Z45.11 ;G1 X37 Y126.36 Z44.11 ;G1 X37 Y126.36 Z45.11 ;G1 X37 Y126.36 Z44.11 ;
G1 F1200 ; mm/min
G1 X37 Y135.36 Z46.11 ;
G1 F1 ; mm/min
G1 X37 Y135.36 Z44.11; G1 X37 Y135.36 Z45.11 ;G1 X37 Y135.36 Z44.11 ;G1 X37 Y135.36 Z45.11 ;
G1 X37 Y135.36 Z44.11 ;G1 X37 Y135.36 Z44.11 ;G1 X37 Y135.36 Z45.11 ;G1 X37 Y135.36 Z44.11 ;
G1 X37 Y135.36 Z45.11 ;G1 X37 Y135.36 Z44.11 ;G1 X37 Y135.36 Z45.11 ;G1 X37 Y135.36 Z44.11 ;
G1 F1200 ; mm/min
G1 X37 Y144.36 Z46.11 ;
G1 F1 ; mm/min
G1 X37 Y144.36 Z44.11; G1 X37 Y144.36 Z45.11 ;G1 X37 Y144.36 Z44.11 ;G1 X37 Y144.36 Z45.11 ;
G1 X37 Y144.36 Z44.11 ;G1 X37 Y144.36 Z44.11 ;G1 X37 Y144.36 Z45.11 ;G1 X37 Y144.36 Z44.11 ;
G1 X37 Y144.36 Z45.11 ;G1 X37 Y144.36 Z44.11 ;G1 X37 Y144.36 Z45.11 ;G1 X37 Y144.36 Z44.11 ;
G1 F1200 ; mm/min
G1 X37 Y153.36 Z46.11 ;
G1 F1 ; mm/min
G1 X37 Y153.36 Z44.11; G1 X37 Y153.36 Z45.11 ;G1 X37 Y153.36 Z44.11 ;G1 X37 Y153.36 Z45.11 ;
G1 X37 Y153.36 Z44.11 ;G1 X37 Y153.36 Z44.11 ;G1 X37 Y153.36 Z45.11 ;G1 X37 Y153.36 Z44.11 ;
G1 X37 Y153.36 Z45.11 ;G1 X37 Y153.36 Z44.11 ;G1 X37 Y153.36 Z45.11 ;G1 X37 Y153.36 Z44.11 ;
G1 F1200 ; mm/min
G1 X37 Y162.36 Z46.11 ;
G1 F1 ; mm/min spot 7
G1 X37 Y162.36 Z44.11; G1 X37 Y162.36 Z45.11 ;G1 X37 Y162.36 Z44.11 ;G1 X37 Y162.36 Z45.11 ;
G1 X37 Y162.36 Z44.11 ;G1 X37 Y162.36 Z44.11 ;G1 X37 Y162.36 Z45.11 ;G1 X37 Y162.36 Z44.11 ;
G1 X37 Y162.36 Z45.11 ;G1 X37 Y162.36 Z44.11 ;G1 X37 Y162.36 Z45.11 ;G1 X37 Y162.36 Z44.11 ;

```
G1 F1200 ; mm/min
G1 X37 Y171.36 Z46.11 ;G1 X64 Y171.36 Z46.11 ; G1 X64 Y162.36 Z46.11 ;
G1 F1 ; mm/min 8
G1 X64 Y162.36 Z44.11; G1 X64 Y162.36 Z45.11 ;G1 X64 Y162.36 Z44.11 ;G1 X64 Y162.36 Z45.11 ;
G1 X64 Y162.36 Z44.11 ;G1 X64 Y162.36 Z44.11 ;G1 X64 Y162.36 Z45.11 ;G1 X64 Y162.36 Z44.11 ;
G1 X64 Y162.36 Z45.11 ;G1 X64 Y162.36 Z44.11 ;G1 X64 Y162.36 Z45.11 ;G1 X64 Y162.36 Z44.11 ;
G1 F1200 ; mm/min
G1 X64 Y153.36 Z46.11 ;
G1 F1 ; mm/min 9
G1 X64 Y153.36 Z44.11; G1 X64 Y153.36 Z45.11 ;G1 X64 Y153.36 Z44.11 ;G1 X64 Y153.36 Z45.11 ;
G1 X64 Y153.36 Z44.11 ;G1 X64 Y153.36 Z44.11 ;G1 X64 Y153.36 Z45.11 ;G1 X64 Y153.36 Z44.11 ;
G1 X64 Y153.36 Z45.11 ;G1 X64 Y153.36 Z44.11 ;G1 X64 Y153.36 Z45.11 ;G1 X64 Y153.36 Z44.11 ;
G1 F1200 ; mm/min
G1 X64 Y144.36 Z46.11 ;
G1 F1 ; mm/min 10
G1 X64 Y144.36 Z44.11; G1 X64 Y144.36 Z45.11 ;G1 X64 Y144.36 Z44.11 ;G1 X64 Y144.36 Z45.11 ;
G1 X64 Y144.36 Z44.11 ;G1 X64 Y144.36 Z44.11 ;G1 X64 Y144.36 Z45.11 ;G1 X64 Y144.36 Z44.11 ;
G1 X64 Y144.36 Z45.11 ;G1 X64 Y144.36 Z44.11 ;G1 X64 Y144.36 Z45.11 ;G1 X64 Y144.36 Z44.11 ;
G1 F1200 ; mm/min
G1 X64 Y135.36 Z46.11 ;
G1 F1 ; mm/min 11
G1 X64 Y135.36 Z44.11; G1 X64 Y135.36 Z45.11 ;G1 X64 Y135.36 Z44.11 ;G1 X64 Y135.36 Z45.11 ;
G1 X64 Y135.36 Z44.11 ;G1 X64 Y135.36 Z44.11 ;G1 X64 Y135.36 Z45.11 ;G1 X64 Y135.36 Z44.11 ;
G1 X64 Y135.36 Z45.11 ;G1 X64 Y135.36 Z44.11 ;G1 X64 Y135.36 Z45.11 ;G1 X64 Y135.36 Z44.11 ;
G1 F1200 ; mm/min
G1 X64 Y126.36 Z46.11 ;
G1 F1 ; mm/min 11
G1 X64 Y126.36 Z44.11; G1 X64 Y126.36 Z45.11 ;G1 X64 Y126.36 Z44.11 ;G1 X64 Y126.36 Z45.11 ;
G1 X64 Y126.36 Z44.11 ;G1 X64 Y126.36 Z44.11 ;G1 X64 Y126.36 Z45.11 ;G1 X64 Y126.36 Z44.11 ;
G1 X64 Y126.36 Z45.11 ;G1 X64 Y126.36 Z44.11 ;G1 X64 Y126.36 Z45.11 ;G1 X64 Y126.36 Z44.11 ;
G1 F1200 ; mm/min
G1 X0 Y0 Z50.11 ;
G92
M84     ; Disable motors
```

References

[1] IUPAC, Compendium of Chemical Terminology-Gold Book, 2014. doi:10.1351/goldbook.I03352.

[2] C.P. Poole, F.J. Owens, Introduction To Nanotechnology - Poole , Owens, 2003. doi:10.1300/J105v21n01_01.

[3] M. Faraday, The Bakerian Lecture: Experimental Relations of Gold (and Other Metals) to Light, Philos. Trans. R. Soc. London. (1857). doi:10.1098/rstl.1857.0011.

[4] R.P. Feynman, There's plenty of room at the bottom: An invitation to enter a new field of physics, in: Caltech's Eng Sci, 1960. doi:10.1007/s12045-011-0109-x.

[5] B. Khodashenas, H.R. Ghorbani, Synthesis of silver nanoparticles with different shapes, Arab. J. Chem. (2015). doi:10.1016/j.arabjc.2014.12.014.

[6] B.P. Khanal, E.R. Zubarev, Purification of high aspect ratio gold nanorods: Complete removal of platelets, J. Am. Chem. Soc. 130 (2008) 12634–12635. doi:10.1021/ja806043p.

[7] E. Martis, R. Badve, M. Degwekar, Nanotechnology based devices and applications in medicine: An overview, Chronicles Young Sci. (2012). doi:10.4103/2229-5186.94320.

[8] R. Singh, J.W. Lillard, Nanoparticle-based targeted drug delivery, Exp. Mol. Pathol. (2009). doi:10.1016/j.yexmp.2008.12.004.

[9] A. Loureiro, N. G. Azoia, A. C. Gomes, A. Cavaco-Paulo, Albumin-Based Nanodevices as Drug Carriers, Curr. Pharm. Des. (2016). doi:10.2174/1381612822666160125114900.

[10] D. Klemm, F. Kramer, S. Moritz, T. Lindström, M. Ankerfors, D. Gray, A. Dorris, Nanocelluloses: A new family of nature-based materials, Angew. Chemie - Int. Ed. (2011). doi:10.1002/anie.201001273.

[11] P. Cavaliere, Mechanical Properties of Nanocrystalline Materials, in: Handb. Mech. Nanostructuring, 2015. doi:10.1002/9783527674947.ch1.

[12] R. Portela, M.D. Hernández-Alonso, Environmental applications of photocatalysis, Green Energy Technol. (2013). doi:10.1007/978-1-4471-5061-9_3.

[13] J. Kim, B. Van Der Bruggen, The use of nanoparticles in polymeric and ceramic membrane structures: Review of manufacturing procedures and performance improvement for water treatment, Environ. Pollut. (2010). doi:10.1016/j.envpol.2010.03.024.

[14] W.X. Zhang, Nanoscale iron particles for environmental remediation: An overview, J. Nanoparticle Res. (2003). doi:10.1023/A:1025520116015.

[15] A. Kamyshny, S. Magdassi, Conductive nanomaterials for printed electronics, Small. (2014). doi:10.1002/smll.201303000.

[16] V. Abhinav K, V.K. Rao R, P.S. Karthik, S.P. Singh, Copper conductive inks: Synthesis and utilization in flexible electronics, RSC Adv. (2015). doi:10.1039/c5ra08205f.

[17] Y. Lee, J.R. Choi, K.J. Lee, N.E. Stott, D. Kim, Large-scale synthesis of copper

nanoparticles by chemically controlled reduction for applications of inkjet-printed electronics, Nanotechnology. (2008). doi:10.1088/0957-4484/19/41/415604.

[18] V. In, A. Palacios, Energy harvesting, in: Underst. Complex Syst., 2018. doi:10.1007/978-3-662-55545-3_8.

[19] P. V. Kamat, Photophysical, photochemical and photocatalytic aspects of metal nanoparticles, J. Phys. Chem. B. (2002). doi:10.1021/jp0209289.

[20] S.S. Kim, S.I. Na, J. Jo, D.Y. Kim, Y.C. Nah, Plasmon enhanced performance of organic solar cells using electrodeposited Ag nanoparticles, Appl. Phys. Lett. (2008). doi:10.1063/1.2967471.

[21] C.M.J. Hu, R.H. Fang, B.T. Luk, K.N.H. Chen, C. Carpenter, W. Gao, K. Zhang, L. Zhang, 'Marker-of-self' functionalization of nanoscale particles through a top-down cellular membrane coating approach, Nanoscale. (2013). doi:10.1039/c3nr00015j.

[22] A. Akthakul, A.I. Hochbaum, F. Stellacci, A.M. Mayes, Size fractionation of metal nanoparticles by membrane filtration, Adv. Mater. (2005). doi:10.1002/adma.200400636.

[23] V. Moghimifar, A. Raisi, A. Aroujalian, Surface modification of polyethersulfone ultrafiltration membranes by corona plasma-assisted coating TiO2 nanoparticles, J. Memb. Sci. (2014). doi:10.1016/j.memsci.2014.02.012.

[24] T. Sun, Y.S. Zhang, B. Pang, D.C. Hyun, M. Yang, Y. Xia, Engineered nanoparticles for drug delivery in cancer therapy, Angew. Chemie - Int. Ed. (2014). doi:10.1002/anie.201403036.

[25] Y. Hua, S. Chang, D. Huang, X. Zhou, X. Zhu, J. Zhao, T. Chen, W.Y. Wong, W.K. Wong, Significant improvement of dye-sensitized solar cell performance using simple phenothiazine-based dyes, Chem. Mater. 25 (2013) 2146–2153. doi:10.1021/cm400800h.

[26] S. Hao, Y. Shang, D. Li, H. Ågren, C. Yang, G. Chen, Enhancing dye-sensitized solar cell efficiency through broadband near-infrared upconverting nanoparticles, Nanoscale. 9 (2017) 6711–6715. doi:10.1039/c7nr01008g.

[27] M.J. Lee, J.Y. Park, C.S. Kim, K. Okuyama, S.E. Lee, T.O. Kim, Improvement of light scattering capacity in dye-sensitized solar cells by doping with SiO2nanoparticles, J. Power Sources. 327 (2016) 96–103. doi:10.1016/j.jpowsour.2016.07.032.

[28] S. Ananthakumar, J. Ramkumar, S.M. Babu, Semiconductor nanoparticles sensitized TiO2 nanotubes for high efficiency solar cell devices, Renew. Sustain. Energy Rev. 57 (2016) 1307–1321. doi:10.1016/j.rser.2015.12.129.

[29] B. Kumar, K. Jalodia, P. Kumar, H.K. Gautam, Recent advances in nanoparticle-mediated drug delivery, J. Drug Deliv. Sci. Technol. 41 (2017) 260–268. doi:10.1016/j.jddst.2017.07.019.

[30] Y. Barenholz, Doxil® - The first FDA-approved nano-drug: Lessons learned, J. Control. Release. (2012). doi:10.1016/j.jconrel.2012.03.020.

[31] D. Bobo, K.J. Robinson, J. Islam, K.J. Thurecht, S.R. Corrie, Nanoparticle-Based Medicines: A Review of FDA-Approved Materials and Clinical Trials to Date, Pharm. Res. (2016). doi:10.1007/s11095-016-1958-5.

[32] A. Sparreboom, C.D. Scripture, V. Trieu, P.J. Williams, T. De, A. Yang, B. Beals, W.D. Figg, M. Hawkins, N. Desai, Comparative preclinical and clinical pharmacokinetics of a Cremophor-free, nanoparticle albumin-bound paclitaxel (ABI-007) and paclitaxel formulated in cremophor (Taxol), Clin. Cancer Res. (2005). doi:10.1158/1078-0432.CCR-04-2291.

[33] T. Tsuzuki, Commercial scale production of inorganic nanoparticles, Int. J. Nanotechnol. (2009). doi:10.1504/IJNT.2009.024647.

[34] Y. Huang, A.A. Keller, Magnetic nanoparticle adsorbents for emerging organic contaminants, ACS Sustain. Chem. Eng. (2013). doi:10.1021/sc400047q.

[35] S.C.N. Tang, I.M.C. Lo, Magnetic nanoparticles: Essential factors for sustainable environmental applications, Water Res. (2013). doi:10.1016/j.watres.2013.02.039.

[36] F. Perreault, A. Fonseca De Faria, M. Elimelech, Environmental applications of graphene-based nanomaterials, Chem. Soc. Rev. (2015). doi:10.1039/c5cs00021a.

[37] S. Dutz, S. Wojahn, C. Gräfe, A. Weidner, J.H. Clement, Influence of Sterilization and Preservation Procedures on the Integrity of Serum Protein-Coated Magnetic Nanoparticles, (2017). doi:10.3390/nano7120453.

[38] L.M. Jin, S.L. Yu, W.X. Shi, X.S. Yi, N. Sun, Y.L. Ge, C. Ma, Synthesis of a novel composite nanofiltration membrane incorporated SiO2nanoparticles for oily wastewater desalination, Polymer (Guildf). (2012). doi:10.1016/j.polymer.2012.09.014.

[39] Q. Zhao, N. Chen, D. Zhao, X. Lu, Thermoresponsive magnetic nanoparticles for seawater desalination, ACS Appl. Mater. Interfaces. (2013). doi:10.1021/am403719s.

[40] P. Lipp, U. Müller, B. Hetzer, T. Wagner, Characterization of nanoparticulate fouling and breakthrough during low-pressure membrane filtration, Desalin. Water Treat. 9 (2009) 234–240. doi:10.5004/dwt.2009.812.

[41] H.S. Lee, S.J. Im, J.H. Kim, H.J. Kim, J.P. Kim, B.R. Min, Polyamide thin-film nanofiltration membranes containing TiO2nanoparticles, Desalination. 219 (2008) 48–56. doi:10.1016/j.desal.2007.06.003.

[42] G.-T. Wei, F.-K. Liu, Separation of nanometer gold particles by size exclusion chromatography, J. Chromatogr. A. 836 (1999) 253–260. doi:10.1016/S0021-9673(99)00069-2.

[43] F.-K. Liu, G.-T. Wei, Effect of Mobile-Phase Additives on Separation of Gold Nanoparticles by Size-Exclusion Chromatography, Chromatographia. 59 (2003) 115–119. doi:10.1365/S10337-003-0135-2.

[44] G. Iyer, S. Ramaswamy, D. Asher, U. Mehta, A. Leahy, F. Chung, K.S. Cheng, Reduced surface area chromatography for flow-through purification of viruses and virus like particles, J. Chromatogr. A. 1218 (2011) 3973–3981. doi:10.1016/j.chroma.2011.04.086.

[45] L. Pang, K. Farkas, G. Bennett, A. Varsani, R. Easingwood, R. Tilley, U. Nowostawska, S. Lin, Mimicking filtration and transport of rotavirus and adenovirus in sand media using DNA-labeled, protein-coated silica nanoparticles, Water Res. 62 (2014). doi:10.1016/j.watres.2014.05.055.

[46] J.A. Simonetti, H.G. Schroeder, Particle Retention of Submicrometer Membranes, in: P. R. Johnston, H. G. Schroeder Fluid Filtr. Liq. Vol. II, American Society for Testing and Materials, Philadelphia, 1986: pp. 37–50.

[47] D.C. Grant, B.Y.H. Liu, Sieving Capture of Liquidborne Particles by microporous membrane filtration media, Part. Part. Syst. Charact. 8 (1991) 142–150. doi:10.1002/ppsc.19910080126.

[48] J.K. Lee, B.Y.H. Liu, K.I. Rubow, Latex sphere retention by microporous membranes in liquid filtration. Part 2, Environ. Eng. 5 (1992) 22–23.

[49] F.W. Pontius, G.L. Amy, M.T. Hernandez, Fluorescent microspheres as virion surrogates in low-pressure membrane studies, J. Memb. Sci. 335 (2009) 43–50. doi:10.1016/j.memsci.2009.02.026.

[50] K.W. Trzaskus, W.M. de Vos, A. Kemperman, K. Nijmeijer, Towards controlled fouling and rejection in dead-end microfiltration of nanoparticles - Role of electrostatic interactions, J. Memb. Sci. 496 (2015) 174–184. doi:10.1016/j.memsci.2015.06.047.

[51] D. Breite, M. Went, I. Thomas, A. Prager, A. Schulze, Particle adsorption on a polyether sulfone membrane: How electrostatic interactions dominate membrane fouling, RSC Adv. 6 (2016) 65383–65391. doi:10.1039/c6ra13787c.

[52] K. Trzaskus, M. Elshof, A. Kemperman, K. Nijmeijer, Understanding the role of nanoparticle size and polydispersity in fouling development during dead-end microfiltration, J. Memb. Sci. 516 (2016) 152–161. doi:10.1016/j.memsci.2016.05.043.

[53] A. Helling, A. Kubicka, I.A.T. Schaap, M. Polakovic, B. Hansmann, H. Thiess, J. Strube, V. Thom, Passage of soft pathogens through microfiltration membranes scales with transmembrane pressure, J. Memb. Sci. 522 (2017) 292–302. doi:10.1016/j.memsci.2016.08.016.

[54] T. Tsurumi, N. Osawa, T. Hirasaki, K. Yamaguchi, Mechanism of removing monodisperse gold particles from a suspension using cuprammonium regenerated cellulose hollow fiber (BMM hollow fiber), Polym. J. 22 (1990) 304–311. doi:10.1295/polymj.22.304.

[55] A. Duek, E. Arkhangelsky, R. Krush, A. Brenner, V. Gitis, New and conventional pore size tests in virus-removing membranes, Water Res. 46 (2012) 2505–2514. doi:10.1016/j.watres.2011.12.058.

[56] F. Springer, S. Laborie, C. Guigui, Removal of SiO2nanoparticles from industry wastewaters and subsurface waters by ultrafiltration: Investigation of process efficiency, deposit properties and fouling mechanism, Sep. Purif. Technol. 108 (2013) 6–14. doi:10.1016/j.seppur.2013.01.043.

[57] A. Antony, J. Blackbeard, M. Angles, G. Leslie, Non-microbial indicators for monitoring virus removal by ultrafiltration membranes, J. Memb. Sci. 454 (2014) 193–199. doi:10.1016/j.memsci.2013.11.052.

[58] S.C. Chen, D. Segets, T.Y. Ling, W. Peukert, D.Y.H. Pui, An experimental study of ultrafiltration for sub-10nm quantum dots and sub-150 nm nanoparticles through PTFE membrane and Nuclepore filters, J. Memb. Sci. 497 (2016).

doi:10.1016/j.memsci.2015.09.022.

[59] P.L. Roberts, P. Feldman, D. Crombie, C. Walker, K. Lowery, Virus removal from factor IX by filtration: Validation of the integrity test and effect of manufacturing process conditions, Biologicals. 38 (2010) 303–310. doi:10.1016/j.biologicals.2009.12.006.

[60] S. Sekine, M. Komuro, T. Sohka, T. Sato, Integrity testing of Planova™ BioEX virus removal filters used in the manufacture of biological products, Biologicals. 43 (2015) 186–194. doi:10.1016/j.biologicals.2015.02.003.

[61] P. Kosiol, B. Hansmann, M. Ulbricht, V. Thom, Determination of pore size distributions of virus filtration membranes using gold nanoparticles and their correlation with virus retention, J. Memb. Sci. 533 (2017) 289–301. doi:10.1016/j.memsci.2017.03.043.

[62] F. Fallahianbijan, S. Giglia, C. Carbrello, A.L. Zydney, Use of fluorescently-labeled nanoparticles to study pore morphology and virus capture in virus filtration membranes, J. Memb. Sci. 536 (2017) 52–58. doi:10.1016/J.MEMSCI.2017.04.066.

[63] H. Nazem-Bokaee, F. Fallahianbijan, D. Chen, S.M. O'Donnell, C. Carbrello, S. Giglia, D. Bell, A.L. Zydney, Probing pore structure of virus filters using scanning electron microscopy with gold nanoparticles, J. Memb. Sci. 552 (2018) 144–152. doi:10.1016/j.memsci.2018.01.069.

[64] P. Kosiol, M. Theres, B. Schneider, B. Hansmann, V. Thom, M. Ulbricht, Determination of pore size gradients of virus fi ltration membranes using gold nanoparticles and their relation to fouling with protein containing feed streams, J. Memb. Sci. 548 (2018) 598–608. doi:10.1016/j.memsci.2017.11.048.

[65] M. Kitis, J.C. Lozier, J.H. Kim, B. Mi, B.J. Mari??as, Microbial removal and integrity monitoring of RO and NF membranes, J. / Am. Water Work. Assoc. 95 (2003).

[66] M.L. Pype, M.G. Lawrence, J. Keller, W. Gernjak, Reverse osmosis integrity monitoring in water reuse: The challenge to verify virus removal - A review, Water Res. 98 (2016) 384–395. doi:10.1016/j.watres.2016.04.040.

[67] R.E. Baltus, A.R. Badireddy, W. Xu, S. Chellam, Analysis of configurational effects on hindered convection of nonspherical bacteria and viruses across microfiltration membranes, Ind. Eng. Chem. Res. 48 (2009) 2404–2413. doi:10.1021/ie800579e.

[68] B. Agasanapura, R.E. Baltus, C.T. Tanneru, S. Chellam, Effect of electrostatic interactions on rejection of capsular and spherical particles from porous membranes: Theory and experiment, J. Colloid Interface Sci. 448 (2015) 492–500. doi:10.1016/j.jcis.2015.02.016.

[69] R.G. Sinclair, J.B. Rose, S.A. Hashsham, C.P. Gerba, C.N. Haas, Criteria for Selection of Surrogates Used To Study the Fate and Control of Pathogens in the Environment, (2012) 1969–1977. doi:10.1128/AEM.06582-11.

[70] G. Sofer, Preparative chromatographic separations in pharmaceutical, diagnostic, and biotechnology industries: current and future trends, J. Chromatogr. A. 707 (1995) 23–28. doi:10.1016/0021-9673(95)00155-G.

[71] K. Tiede, A.B.A. Boxall, X. Wang, D. Gore, D. Tiede, M. Baxter, H. David, S.P. Tear, J. Lewis, Application of hydrodynamic chromatography-ICP-MS to investigate the fate of silver nanoparticles in activated sludge, J. Anal. At. Spectrom. 25 (2010) 1149–1154.

doi:10.1039/b926029c.

[72] M. Li, Y.X. Qiu, A review on current downstream bio-processing technology of vaccine products, Vaccine. 31 (2013) 1264–1267. doi:10.1016/j.vaccine.2012.12.056.

[73] A.F. Jozala, D.C. Geraldes, L.L. Tundisi, V. de A. Feitosa, C.A. Breyer, S.L. Cardoso, P.G. Mazzola, L. de Oliveira-Nascimento, C. de O. Rangel-Yagui, P. de O. Magalhães, M.A. de Oliveira, A. Pessoa, Biopharmaceuticals from microorganisms: from production to purification, Brazilian J. Microbiol. 47 (2016) 51–63. doi:10.1016/j.bjm.2016.10.007.

[74] T.A. Grein, Z. Kovacs, M. Ebrahimi, R. Michalsky, Membrane Supported Virus Separation from Biological Solutions, (2013) 1183–1192. doi:10.1002/cite.201200241.

[75] L. Besnard, V. Fabre, M. Fettig, E. Gousseinov, Y. Kawakami, N. Laroudie, C. Scanlan, P. Pattnaik, Clarification of vaccines: An overview of filter based technology trends and best practices, Biotechnol. Adv. 34 (2016) 1–13. doi:10.1016/j.biotechadv.2015.11.005.

[76] G. Ungerechts, S. Bossow, B. Leuchs, P.S. Holm, J. Rommelaere, M. Coffey, R. Coffin, J. Bell, D.M. Nettelbeck, Moving oncolytic viruses into the clinic: clinical-grade production, purification, and characterization of diverse oncolytic viruses, Mol. Ther. - Methods Clin. Dev. 3 (2016) 16018. doi:10.1038/mtm.2016.18.

[77] D. Vincent, P. Kramberger, R. Hudej, A. Štrancar, Y. Wang, Y. Zhou, A. Velayudhan, The development of a monolith-based purification process for Orthopoxvirus vaccinia virus Lister strain, J. Chromatogr. A. 1524 (2017) 87–100. doi:10.1016/j.chroma.2017.09.003.

[78] N. Itoh, T. Santa, M. Kato, Rapid evaluation of the quantity of drugs encapsulated within nanoparticles by high-performance liquid chromatography in a monolithic silica column, Anal. Bioanal. Chem. 407 (2015) 6429–6434. doi:10.1007/s00216-015-8805-0.

[79] M.E. Laska, R.P. Brooks, M. Gayton, N.S. Pujar, Robust scale-up of dead end filtration: Impact of filter fouling mechanisms and flow distribution, Biotechnol. Bioeng. (2005). doi:10.1002/bit.20587.

[80] R.W. Baker, Membrane Technology and Applications, 2012. doi:10.1016/S0958-2118(96)90133-0.

[81] R. Radcliff and A. Zarnadze, Application of Membrane Technology to the Production of Drinking Water, Water Cond. Purif. Mag. (2004) 23–25. http://www.wcponline.com/2004/08/14/application-membrane-technology-production-drinking-water/.

[82] L.J. Zeman, A.L. Zydney, Microfiltration and ultrafiltration: Principles and applications, 2017. doi:10.1201/9780203747223.

[83] ASTM F838 - 15ae1, Standard Test Method for Determining Bacterial Retention of Membrane Filters Utilized for Liquid Filtration, in: ASTM International, West Conshohocken, 2015. doi:10.1520/F0838-15AE01.

[84] C.M. Bondy, C. Santeufemio, Analysis of fouling within microporous membranes in biopharmaceutical applications using latex microsphere suspensions, 349 (2010) 12–24. doi:10.1016/j.memsci.2009.11.005.

[85] A. Abdelrasoul, H. Doan, A. Lohi, C.H. Cheng, The influence of aggregation of latex particles on membrane fouling attachments & ultrafiltration performance in ultrafiltration of latex contaminated water and wastewater, J. Environ. Sci. (China). (2017). doi:10.1016/j.jes.2016.03.023.

[86] A. Abdelrasoul, H. Doan, A. Lohi, A mechanistic model for ultrafiltration membrane fouling by latex, J. Memb. Sci. (2013). doi:10.1016/j.memsci.2013.01.003.

[87] G. Miesegaes, S. Lute, K. Brorson, Analysis of viral clearance unit operations for monoclonal antibodies, Biotechnol. Bioeng. (2010). doi:10.1002/bit.22662.

[88] P. Nestola, R.J.S. Silva, C. Peixoto, P.M. Alves, M.J.T. Carrondo, J.P.B. Mota, Adenovirus purification by two-column, size-exclusion, simulated countercurrent chromatography, J. Chromatogr. A. 1347 (2014) 111–121. doi:10.1016/j.chroma.2014.04.079.

[89] M.E. Verbyla, J.R. Mihelcic, A review of virus removal in wastewater treatment pond systems, Water Res. (2015). doi:10.1016/j.watres.2014.12.031.

[90] M. Amarasiri, M. Kitajima, T.H. Nguyen, S. Okabe, D. Sano, Bacteriophage removal efficiency as a validation and operational monitoring tool for virus reduction in wastewater reclamation: Review, Water Res. (2017). doi:10.1016/j.watres.2017.05.035.

[91] H. Rehman, A.W. Silk, M.P. Kane, H.L. Kaufman, Into the clinic: Talimogene laherparepvec (T-VEC), a first-in-class intratumoral oncolytic viral therapy, J. Immunother. Cancer. 4 (2016). doi:10.1186/s40425-016-0158-5.

[92] S.E. Lawler, M.C. Speranza, C.F. Cho, E.A. Chiocca, Oncolytic viruses in cancer treatment a review, JAMA Oncol. (2017). doi:10.1001/jamaoncol.2016.2064.

[93] D. Mahalingam, S. Patel, G. Nuovo, G. Gill, G. Selvaggi, M. Coffey, S.T. Nawrocki, The combination of intravenous Reolysin and gemcitabine induces reovirus replication and endoplasmic reticular stress in a patient with KRAS-activated pancreatic cancer, BMC Cancer. 15 (2015). doi:10.1186/s12885-015-1518-0.

[94] K. Rajani, C. Parrish, T. Kottke, J. Thompson, S. Zaidi, L. Ilett, K.G. Shim, R.M. Diaz, H. Pandha, K. Harrington, M. Coffey, A. Melcher, R. Vile, Combination therapy with reovirus and Anti-PD-1 blockade controls tumor growth through innate and adaptive immune responses, Mol. Ther. 24 (2016) 166–174. doi:10.1038/mt.2015.156.

[95] J. Heo, C.J. Breitbach, A. Moon, C.W. Kim, R. Patt, M.K. Kim, Y.K. Lee, S.Y. Oh, H.Y. Woo, K. Parato, J. Rintoul, T. Falls, T. Hickman, B.G. Rhee, J.C. Bell, D.H. Kirn, T.H. Hwang, Sequential therapy with JX-594, a targeted oncolytic poxvirus, followed by sorafenib in hepatocellular carcinoma: Preclinical and clinical demonstration of combination efficacy, Mol. Ther. 19 (2011) 1170–1179. doi:10.1038/mt.2011.39.

[96] J. Zhang, L.H. Tai, C.S. Ilkow, A.A. Alkayyal, A.A. Ananth, C.T. De Souza, J. Wang, S. Sahi, L. Ly, C. Lefebvre, T.J. Falls, K.B. Stephenson, A.B. Mahmoud, A.P. Makrigiannis, B.D. Lichty, J.C. Bell, D.F. Stojdl, R.C. Auer, Maraba MG1 virus enhances natural killer cell function via conventional dendritic cells to reduce postoperative metastatic disease, in: Mol. Ther., 2014: pp. 1320–1332. doi:10.1038/mt.2014.60.

[97] P. Singh, S.K. Pal, A. Alex, N. Agarwal, Development of PROSTVAC immunotherapy in

prostate cancer, Futur. Oncol. (2015). doi:10.2217/fon.15.120.

[98] J. Stoeckel, J.G. Hay, Drug evaluation: Reolysin--wild-type reovirus as a cancer therapeutic, Curr.Opin.Mol.Ther. (2006).

[99] S.-G. Kim, H.K. Ha, S. Lim, N.S. De Silva, A. Pelusio, J.H. Mun, R.H. Patt, C.J. Breitbach, J.M. Burke, Phase II trial of pexa-vec (pexastimogene devacirepvec; JX-594), an oncolytic and immunotherapeutic vaccinia virus, in patients with metastatic, refractory renal cell carcinoma (RCC)., J. Clin. Oncol. (2018). doi:10.1200/JCO.2018.36.6_suppl.671.

[100] R.H.I. Andtbacka, H.L. Kaufman, F. Collichio, T. Amatruda, N. Senzer, J. Chesney, K.A. Delman, L.E. Spitler, I. Puzanov, S.S. Agarwala, M. Milhem, L. Cranmer, B. Curti, K. Lewis, M. Ross, T. Guthrie, G.P. Linette, G.A. Daniels, K. Harrington, M.R. Middleton, W.H. Miller, J.S. Zager, Y. Ye, B. Yao, A. Li, S. Doleman, A. Van Der Walde, J. Gansert, R.S. Coffin, Talimogene laherparepvec improves durable response rate in patients with advanced melanoma, J. Clin. Oncol. (2015). doi:10.1200/JCO.2014.58.3377.

[101] S.D. Products, C. Good, M. Practice, Sterile Drug Products Current Good Manufacturing Practice Guidance for Industry, (2004).

[102] T.P. Pato, M.C.O. Souza, A.N.M.R. Silva, R.C. Pereira, M. V. Silva, E. Caride, L.P. Gaspar, M.S. Freire, L.R. Castilho, Development of a membrane adsorber based capture step for the purification of yellow fever virus, Vaccine. 32 (2014) 2789–2793. doi:10.1016/j.vaccine.2014.02.036.

[103] N. Kawabata, I. Ujino, Removal of virus from air by filtration using a composite microporous membrane made of crosslinked poly(N-benzyl-4-vinylpyridinium chloride), React. Funct. Polym. 37 (1998) 213–218. doi:10.1016/S1381-5148(97)00133-8.

[104] R. Lu, Q. Li, T.H. Nguyen, Random sequential adsorption of human adenovirus 2 onto polyvinylidene fluoride surface influenced by extracellular polymeric substances, J. Colloid Interface Sci. 466 (2016) 120–127. doi:10.1016/j.jcis.2015.12.017.

[105] M. Bakhshayeshi, N. Jackson, R. Kuriyel, A. Mehta, R. van Reis, A.L. Zydney, Use of confocal scanning laser microscopy to study virus retention during virus filtration, J. Memb. Sci. 379 (2011) 260–267. doi:10.1016/j.memsci.2011.05.069.

[106] S. Shoaebargh, I. Gough, M. Fe Medina, A. Smith, J. van der Heijden, B.D. Lichty, J.C. Bell, D.R. Latulippe, Sterile filtration of oncolytic viruses: An analysis of effects of membrane morphology on fouling and product recovery, J. Memb. Sci. 548 (2018) 239–246. doi:10.1016/j.memsci.2017.11.022.

[107] Canadian Cancer Statistics Advisory Committee, Canadian Cancer Statistics 2018 Special report on cancer incidence by stage, 2018. doi:10.1080/0141861021000039455.

[108] B.S. Olo, I. Microbiology, F.A. June, Isoeleetrie Foeusin 9 of Herpes Simplex Virus By, 98 (1975) 93–98.

[109] G. OSTER, The isoelectric points of some strains of tobacco mosaic virus., J. Biol. Chem. (1951).

[110] B.P. Khanal, E.R. Zubarev, Purification of High Aspect Ratio Gold Nanorods: Complete Removal of Platelets Bishnu P. Khanal and Eugene R. Zubarev*, J. Am. Chem. Soc. 130

(2010) 1–7. doi:Doi 10.1021/Ja806043p.

[111] B. Xiong, J. Cheng, Y. Qiao, R. Zhou, Y. He, E.S. Yeung, Separation of nanorods by density gradient centrifugation, J. Chromatogr. A. 1218 (2011) 3823–3829. doi:10.1016/j.chroma.2011.04.038.

[112] A. Delavari, B. Agasanapura, R.E. Baltus, The effect of particle rotation on the motion and rejection of capsular particles in slit pores, AIChE J. (2018). doi:10.1002/aic.16132.

[113] D. Bourcier, J.P. Féraud, D. Colson, K. Mandrick, D. Ode, E. Brackx, F. Puel, Influence of particle size and shape properties on cake resistance and compressibility during pressure filtration, Chem. Eng. Sci. 144 (2016) 176–187. doi:10.1016/j.ces.2016.01.023.

[114] J.D. Winans, K.J.P. Smith, T.R. Gaborski, J.A. Roussie, J.L. McGrath, Membrane capacity and fouling mechanisms for ultrathin nanomembranes in dead-end filtration, J. Memb. Sci. 499 (2016) 282–289. doi:10.1016/j.memsci.2015.10.053.

[115] S. Sekiguchi, K. Ito, M. Kobayashi, H. Ikeda, S. Manabe, T. Tsurumi, G. Ishikawa, M. Satani, K. Yamaguchi, An attempt to prepare Hepatitis B Virus (HBV)-free plasma by ultrafiltration using Microporous regenerated cellulose hollow fiber, Transfus. Sci. 11 (1990) 211–216. doi:10.1016/0955-3886(90)90097-3.

[116] D.B. Pall, E.A. Kirnbauer, B.T. Allen, Particulate retention by bacteria retentive membrane filters, Colloids and Surfaces. 1 (1980) 235–256. doi:10.1016/0166-6622(80)80015-1.

[117] S.E. Lawler, M.-C. Speranza, C.-F. Cho, E.A. Chiocca, Oncolytic Viruses in Cancer Treatment, JAMA Oncol. 3 (2017) 841. doi:10.1001/jamaoncol.2016.2064.

[118] U.S. Food and Drug Administration, Flublok Quadrivalent, (2018). https://www.fda.gov/biologicsbloodvaccines/vaccines/approvedproducts/ucm524660.htm.

[119] T.F. Tadros, Stabilization and Destabilization of Suspensions Using Polymeric Surfactants and the Theory of Steric Stabilization, in: Dispers. Powders Liq. Stab. Suspens., 2012: pp. 131–149.

[120] T.H. Meltzer, Modus of Filtration, in: Maik W. Jornitz (Ed.), Sterile Filtr., Springer-Verlag Berlin Heidelberg, 2006: pp. 27–71. doi:10.1007/b101405.

[121] T.H. Meltzer, M.W. Jornitz, The sterilizing filter and its pore size rating, Am. Pharm. Rev. 6 (2003) 44–52.

[122] C.D. Lytle, L.B. Routson, Minimized virus binding for tests of barrier materials, Appl. Environ. Microbiol. 61 (1995) 643–649.

[123] S.K. Dishari, A. Venkiteshwaran, A.L. Zydney, Probing effects of pressure release on virus capture during virus filtration using confocal microscopy, Biotechnol. Bioeng. 112 (2015) 2115–2122. doi:10.1002/bit.25614.

[124] F. Fallahianbijan, S. Giglia, C. Carbrello, A.L. Zydney, Use of fluorescently-labeled nanoparticles to study pore morphology and virus capture in virus filtration membranes, J. Memb. Sci. 536 (2017) 52–58. doi:10.1016/j.memsci.2017.04.066.

[125] S. Chaurasiya, N.G. Chen, Y. Fong, Oncolytic viruses and immunity, Curr. Opin. Immunol. 51 (2018) 83–90. doi:10.1016/j.coi.2018.03.008.

[126] L.K. Hawkins, N.R. Lemoine, D. Kirn, Oncolytic biotherapy: A novel therapeutic platform, Lancet Oncol. 3 (2002) 17–26. doi:10.1016/S1470-2045(01)00618-0.

[127] J.G. Pol, L. Zhang, B.W. Bridle, K.B. Stephenson, J. Rességuier, S. Hanson, L. Chen, N. Kazdhan, J.L. Bramson, D.F. Stojdl, Y. Wan, B.D. Lichty, Maraba virus as a potent oncolytic vaccine vector, Mol. Ther. 22 (2014) 420–429. doi:10.1038/mt.2013.249.

[128] D.O. Cliver, Factors in the membrane filtration of enteroviruses, Appl. Microbiol. 13 (1965) 417–31. http://www.pubmedcentral.nih.gov/articlerender.fcgi?artid=1058265&tool=pmcentrez&rendertype=abstract.

[129] K.D. Kostenbader, D.O. Cliver, Membrane filter evaluations using poliovirus, J. Virol. Methods. 7 (1983) 253–257. doi:10.1016/0166-0934(83)90076-9.

[130] D.O. Cliver, Virus interactions with membrane filters, Biotechnol. Bioeng. 10 (1968) 877–889. doi:10.1002/bit.260100612.

[131] W.J. Weiss, E.J. Bouwer, R. Aboytes, M.W. LeChevallier, C.R. O'Melia, B.T. Le, K.J. Schwab, Riverbank filtration for control of microorganisms: Results from field monitoring, Water Res. 39 (2005) 1990–2001. doi:10.1016/j.watres.2005.03.018.

[132] V. Gitis, A. Adin, A. Nasser, J. Gun, O. Lev, Fluorescent dye labeled bacteriophages - A new tracer for the investigation of viral transport in porous media: 1. Introduction and characterization, Water Res. 36 (2002) 4227–4234. doi:10.1016/S0043-1354(02)00163-X.

[133] V.B. Rajal, B.S. McSwain, D.E. Thompson, C.M. Leutenegger, B.J. Kildare, S. Wuertz, Validation of hollow fiber ultrafiltration and real-time PCR using bacteriophage PP7 as surrogate for the quantification of viruses from water samples, Water Res. 41 (2007) 1411–1422. doi:10.1016/j.watres.2006.12.034.

[134] M.A. Woods, A.L. Zydney, Effects of a pressure release on virus retention with the Ultipor DV20 membrane, Biotechnol. Bioeng. 111 (2014) 545–551. doi:10.1002/bit.25112.

[135] T. Iskra, A. Sacramo, C. Gallo, R. Godavarti, S. Chen, S. Lute, K. Brorson, Development of a modular virus clearance package for anion exchange chromatography operated in weak partitioning mode, Biotechnol. Prog. (2015). doi:10.1002/btpr.2080.

[136] P. Kosiol, B. Hansmann, M. Ulbricht, V. Thom, Determination of pore size distributions of virus filtration membranes using gold nanoparticles and their correlation with virus retention, J. Memb. Sci. 533 (2017) 289–301. doi:10.1016/j.memsci.2017.03.043.

[137] P. Kosiol, M. Theres, B. Schneider, B. Hansmann, V. Thom, M. Ulbricht, Determination of pore size gradients of virus fi ltration membranes using gold nanoparticles and their relation to fouling with protein containing feed streams, J. Memb. Sci. 548 (2018) 598–608. doi:10.1016/j.memsci.2017.11.048.

[138] F. Fallahianbijan, S. Giglia, C. Carbrello, A.L. Zydney, virus capture in virus fi ltration membranes, J. Memb. Sci. 536 (2017) 52–58. doi:10.1016/j.memsci.2017.04.066.

[139] R.W. Harvey, L.H. George, R.L. Smith, D.R. LeBlanc, Transport of Microspheres and Indigenous Bacteria through a Sandy Aquifer: Results of Natural and Forced-Gradient Tracer Experiments, Environ. Sci. Technol. (1989). doi:10.1021/es00178a005.

[140] L. Pang, U. Nowostawska, J.N. Ryan, W.M. Williamson, G. Walshe, K.A. Hunter, Modifying the Surface Charge of Pathogen-Sized Microspheres for Studying Pathogen Transport in Groundwater, (2009) 2210–2217. doi:10.2134/jeq2008.0451.

[141] L. Pang, U. Nowostawska, L. Weaver, G. Ho, A. Karmacharya, A. Skinner, N. Karki, Biotin- and Glycoprotein-Coated Microspheres : Potential Surrogates for Studying Filtration of Cryptosporidium parvum in Porous Media, (2012). doi:10.1021/es302555n.

[142] F. Betton, A. Theretz, A. Elaissari, C. Pichot, Adsorption of bovine serum albumin onto amphiphilic acrylic acid copolymer-stabilized polystyrene latex particles, Colloids Surfaces B Biointerfaces. (1993). doi:10.1016/0927-7765(93)80040-6.

[143] P.A.C. Arriere, J.A.R. Evilla, A.B.E. Lai, Adsorption of Bovine Serum Albumin onto Polystyrene Latex Particles Bearing Saccharidic Moieties, 412 (1996) 405–412.

[144] B. Jachimska, K. Tokarczyk, M. Łapcz Nska, A. Puciul-Malinowska, S. Zapotoczny, J. Haber, Structure of bovine serum albumin adsorbed on silica investigated by quartz crystal microbalance, Colloids Surfaces A Physicochem. Eng. Asp. (2016). doi:10.1016/j.colsurfa.2015.10.033.

[145] B. Jachimska, M. Łapczyńska, S. Zapotoczny, Reversible swelling process of sixth-generation poly(amido amine) dendrimers molecule as determined by quartz crystal microbalance technique, J. Phys. Chem. C. (2013). doi:10.1021/jp307832p.

[146] B. Jachimska, A. Pajor, Physico-chemical characterization of bovine serum albumin in solution and as deposited on surfaces, Bioelectrochemistry. (2012). doi:10.1016/j.bioelechem.2011.09.004.

[147] B. Jachimska, K. Tokarczyk, M. Łapczyńska, A. Puciul-Malinowska, S. Zapotoczny, Structure of bovine serum albumin adsorbed on silica investigated by quartz crystal microbalance, Colloids Surfaces A Physicochem. Eng. Asp. (2016). doi:10.1016/j.colsurfa.2015.10.033.

[148] C. Abad?Zapatero, C.T. Lin, Statistical descriptors for the size and shape of globular proteins, Biopolymers. (1990). doi:10.1002/bip.360291407.

[149] S. Akiyama, Quality control of protein standards for molecular mass determinations by small-angle X-ray scattering, J. Appl. Crystallogr. (2010). doi:10.1107/S002188981000138X.

[150] E.W. Weisstein, Circle Packing, MathWorld--A Wolfram Web Resour. (n.d.). http://mathworld.wolfram.com/CirclePacking.html.

[151] C.C. Ho, A.L. Zydney, Transmembrane pressure profiles during constant flux microfiltration of bovine serum albumin, J. Memb. Sci. (2002). doi:10.1016/S0376-7388(02)00282-X.

[152] X. Sun, D.M. Kanani, R. Ghosh, Characterization and theoretical analysis of protein fouling of cellulose acetate membrane during constant flux dead-end microfiltration, J. Memb. Sci. (2008). doi:10.1016/j.memsci.2008.04.017.

[153] R. Baxter, N. Hastings, A. Law, E.J.. Glass, Flublok Quadrivalent Medication Package Insert (V3.0), Anim. Genet. (2018).

[154] J.P. McDevitt, C.S. Criddle, M. Morse, R.C. Hale, C.B. Bott, C.M. Rochman, Addressing the Issue of Microplastics in the Wake of the Microbead-Free Waters Act - A New Standard Can Facilitate Improved Policy, Environ. Sci. Technol. (2017). doi:10.1021/acs.est.6b05812.

[155] J.C. Anderson, B.J. Park, V.P. Palace, Microplastics in aquatic environments: Implications for Canadian ecosystems, Environ. Pollut. (2016). doi:10.1016/j.envpol.2016.06.074.

[156] D. Eerkes-Medrano, R.C. Thompson, D.C. Aldridge, Microplastics in freshwater systems: A review of the emerging threats, identification of knowledge gaps and prioritisation of research needs, Water Res. (2015). doi:10.1016/j.watres.2015.02.012.

[157] C.M. Rochman, J.M. Parnis, M.A. Browne, S. Serrato, E.J. Reiner, M. Robson, T. Young, M.L. Diamond, S.J. Teh, Direct and indirect effects of different types of microplastics on freshwater prey (Corbicula fluminea) and their predator (Acipenser transmontanus), PLoS One. (2017). doi:10.1371/journal.pone.0187664.

[158] C.M. Rochman, The complex mixture, fate and toxicity of chemicals associated with plastic debris in the marine environment, in: Mar. Anthropog. Litter, 2015. doi:10.1007/978-3-319-16510-3_5.